La collana della Scuola di Alta Formazione Dottorale accoglie le migliori tesi di dottorato dell'Università degli Studi di Bergamo, insignite della dignità di stampa e sottoposte a procedura di *blind peer review*.

The development of patient-specific digital twins is transforming orthopedic care by enabling personalized prevention, diagnosis, treatment, and long-term management of musculoskeletal disorders. This work presents a modular framework integrating medical imaging, motion analysis, and computational modeling to generate patient-specific digital twins tailored to different clinical needs. Depending on the application, the framework supports the assessment of anatomy, function, biomechanical behavior, and disease progression, enabling personalized clinical decision-making. Its versatility is demonstrated through applications including automated knee cartilage analysis, gait assessment after hip surgery, biomechanical evaluation of meniscal lesions, and customized knee implant design, advancing precision orthopedic care.

Anna Ghidotti earned her PhD in Technology, Innovation and Management (37th cycle) at the University of Bergamo and University of Naples Federico II. Currently, she is assistant professor at the University of Bergamo. Her research focuses on biomedical engineering, with particular emphasis on collaborations with hospitals to address clinical needs through advanced engineering tools. Her work includes the use of deep learning for automatic image segmentation and morphological analysis of medical data. She also applies computer-aided design techniques for the development of customized prostheses and uses motion capture systems to support rehabilitation assessment and monitoring.

ISBN: 978-88-97253-45-7
DOI: 10.13122/978-88-97253-45-7

Anna Ghidotti
A PATIENT DIGITAL TWIN IN ORTHOPEDICS
90

Collana della Scuola di Alta Formazione Dottorale
- 90 -

Anna Ghidotti

A PATIENT DIGITAL TWIN IN ORTHOPEDICS

UNIVERSITÀ DEGLI STUDI DI BERGAMO

2026

Collana della Scuola di Alta Formazione Dottorale

Diretta da Paolo Cesaretti

Ogni volume è sottoposto a *blind peer review*.

ISSN: 2611-9927

Sito web: https://aisberg.unibg.it/handle/10446/130100

Anna Ghidotti

A PATIENT DIGITAL TWIN IN ORTHOPEDICS
A Framework for Patient-Specific Care

Università degli Studi di Bergamo

2026

Shaping A Patient Digital Twin in Orthopedics. A Framework
for Patient-Specific Care.
/ Anna Ghidotti. – Bergamo :
Università degli Studi di Bergamo, 2026.
(Collana della Scuola di Alta Formazione Dottorale; 90)

ISBN: 978-88-97253-45-7
DOI: 10.13122/978-88-97253-45-7

Progetto grafico: Servizi Editoriali – Università degli Studi di Bergamo

via Salvecchio, 19
24129 Bergamo
Cod. Fiscale 80004350163
P. IVA 01612800167

https://aisberg.unibg.it/handle/10446/330672

Table of contents

Introduction

Context

In recent years, orthopaedics has been significantly impacted by various technological advancements, leading to a transformation in patient care and treatment. One of the most promising innovations in this field is the concept of the patient digital twin. A patient digital twin is a virtual representation of an individual's anatomy and physiology, created using a combination of advanced technologies to simulate and predict the outcomes of various treatments and interventions [1].

To construct a patient digital twin, several key technologies are employed, including 3D modelling and motion capture (MoCap) data.

3D modeling plays a critical role in the development of patient digital twins. This process begins with the acquisition of detailed imaging data through techniques such as Computed Tomography (CT) and Magnetic Resonance (MR) scans. These scans are then processed using segmentation techniques to create accurate and detailed 3D models of the patient's anatomy [2]. The advent of deep learning (DL) has further revolutionized this process by enabling automatic segmentation of medical images, producing precise 3D models in few seconds [3]. These models allow for in-depth morphological analysis of anatomical variations, deformities, and injuries, facilitating precise diagnosis, surgical planning, and execution. 3D modeling is particularly valuable in creating patient-specific instruments and anatomical models for preoperative planning and education, enhancing the precision and customization of orthopaedic care.

Motion capture (MoCap) technology is another essential component in building patient digital twins. MoCap systems capture detailed, real-time data on a patient's movements, providing invaluable insights into their biomechanical function and dysfunction [4]. This technology enables orthopedic specialists to analyze gait patterns, joint kinematics, and overall movement mechanics with high precision. The data collected through MoCap is crucial for designing effective treatment plans, whether they involve physical therapy or surgical procedures.

By integrating 3D modeling and MoCap data, advanced computational modeling techniques can create comprehensive patient digital twins. These digital twins simulate biomechanical behaviours, predict joint stresses, and forecast surgical outcomes, providing a powerful tool for personalized patient care. Through this integration, healthcare providers can explore the effects of different treatment options, optimize surgical planning, and ultimately improve patient outcomes.

Aim

The aim of this research is to develop a patient digital twin to enhance orthopedic care, through the integration of key technologies, including 3D modelling and MoCap data. This innovative approach seeks to enhance the precision, customization, and effectiveness of orthopedic care, ultimately leading to improved patient outcomes

The following key areas of research have been examined:

- **Integration of DL for Fast and Accurate 3D Modeling**
  The research will focus on integrating DL algorithms to achieve rapid and precise segmentation of medical images obtained from DICOM. By automating the segmentation process, DL enhances the efficiency and accuracy of creating detailed 3D models of anatomical structures. These models will serve as the foundation for comprehensive morphological analysis.
- **Risk Factor Identification for Pathology Development**
  This work aims to identify and analyze risk factors associated with musculoskeletal pathologies using a data-driven approach. By leveraging on morphological analysis, the research will seek to establish correlations between specific risk factors and the development of orthopedic conditions. This investigation will contribute to a deeper understanding of disease progression and inform preventive measures and personalized treatment strategies.
- **Pathology Identification and Diagnosis**
  Building on the foundation of accurate 3D models and MoCap data, the thes will focus on enhancing the capability to identify and diagnose orthopedic pathologies. Through detailed morphological analysis, gait analysis and comparison with healthy ranges from the literature, the methodology will facilitate early detection and precise characterization of conditions such as osteoarthritis, ligament tears, and degenerative joint diseases. This diagnostic precision will support timely interventions and optimize treatment planning tailored to individual patient needs.
- **Pathology Impact Assessment**
  The research will investigate the impact of identified pathologies on patient health and functional outcomes. By accurately simulating these biomechanical changes, this work aims to provide orthopedic specialists with valuable insights into the mechanical consequences of pathologies. This knowledge will inform personalized treatment planning, surgical decision-making, and the development of innovative orthopedic interventions tailored to enhance patient-specific outcomes and improve quality of care.

- **Personalized Treatment Impact**

  An essential focus of this work is to develop methodologies for personalized treatment planning based on individualized pathology assessments. By integrating patient-specific anatomical data into the analysis, the research aims to enhance the customization of orthopedic interventions, particularly in the design of customized prostheses and implants. This innovative approach seeks to improve the fit, functionality, and comfort of orthopedic devices by ensuring they align perfectly with each patient's unique anatomy.
- **Treatment impact**

  The aim includes evaluating treatment impact through gait analysis. By comparing pre- and post-treatment gait data, the research aims to assess improvements in gait efficiency, stability, and overall function. This comparative analysis helps quantify the success of surgical procedures, identify any residual impairments, and guide postoperative rehabilitation strategies. Ultimately, the goal is to leverage comprehensive biomechanical analyses to validate treatment efficacy, enhance patient mobility, and refine orthopedic care practices for improved patient outcomes.

Structure

The structure of this work is organized to provide a comprehensive exploration of the development and application of patient digital twins in orthopedic care.

The first chapter presents the scientific background necessary for understanding patient digital twins. It covers the fundamentals of the key technologies, including 3D modeling and MoCap. Additionally, it provides an overview of the anatomy and pathology of the main joints, such as the knee, shoulder, and hip, which are crucial for contextualizing the subsequent chapters.

The second chapter outlines the architecture of the present study, detailing the integrated approach developed to construct orthopedic patient digital twins. It introduces the 3D modeling module, describing the process of automating image segmentation to generate accurate 3D anatomical models. The MoCap module is then discussed, highlighting how motion capture data is used to analyze human movement and identify pathologies. This chapter explains the integration of these modules into the digital twin framework, emphasizing the importance of morphological analysis and MoCap data analysis in creating functional and precise digital twins.

The third chapter presents detailed case studies and clinical applications of the patient digital twin framework. They include comprehensive assessments of patient care, from risk factor identification and pathology diagnosis to treatment planning and evaluation. The chapter covers a range of applications, such as the development of customized knee implants, the analysis of gait in patients with hip replacements, and the diagnosis of shoulder disorders. Each case study underscores the versatility and robustness of the methodology, showcasing its potential to improve patient outcomes in various orthopedic contexts.

The final chapter draws conclusions from the research findings, summarizing the key contributions and implications of the developed patient digital twin framework. It discusses the advantages of integrating 3D modeling and MoCap technologies in orthopedic care, highlighting the improved accuracy and personalization of diagnoses and treatments. The chapter also addresses the limitations of the study and proposes potential future directions for research, such as further refining the digital twin models and expanding their application to other medical fields.

Chapter 1. Scientific Background

1.1 Patient Digital Twin

In recent years, the concept of Patient Digital Twin (PDT) has emerged as a promising frontier in healthcare innovation, offering a paradigm shift towards personalized and precision medicine. PDT represents virtual model that simulate an individual's physiological and pathological characteristics using real-time data and advanced computational techniques [1].

PDT involves the integration and analysis of vast amounts of heterogeneous data, as shown in Figure 1. Electronic health records serve as foundational repositories of medical history, providing a chronological record of diagnoses, treatments, and patient outcomes. Genomic data offers insights into genetic predispositions and pharmacogenomics, aiding in personalized treatment strategies [1]. Wearable devices continuously monitor physiological parameters and activities, contributing real-time data crucial for monitoring health trends and predicting disease risks. Imaging technologies provide detailed anatomical and functional information, enhancing the accuracy of digital twin models. Integration of these diverse data streams requires robust interoperability standards and advanced computational infrastructure capable of processing and analyzing complex datasets [5].

The potential applications of PDT span across various domains of healthcare delivery and management. In clinical practice, PDT facilitates personalized medicine by tailoring treatment plans based on individual patient profiles. Clinicians can leverage predictive analytics derived from PDT to anticipate disease progression, identify early warning signs, and optimize therapeutic interventions. PDT also supports clinical decision-making by providing comprehensive patient insights, enhancing diagnostic accuracy, and enabling proactive healthcare management strategies [6].

PDT offers significant benefits to both patients and healthcare systems. By aligning interventions with a patient's particular health profile, personalized healthcare can enhance treatment efficacy and patient outcomes. Early detection of health risks and proactive management of chronic conditions contribute to reducing healthcare costs associated with preventable hospitalizations and complications. Moreover, PDT empowers patients by fostering greater engagement in their healthcare decisions, promoting adherence to treatment regimens, and supporting lifestyle modifications conducive to better health outcomes [1] .

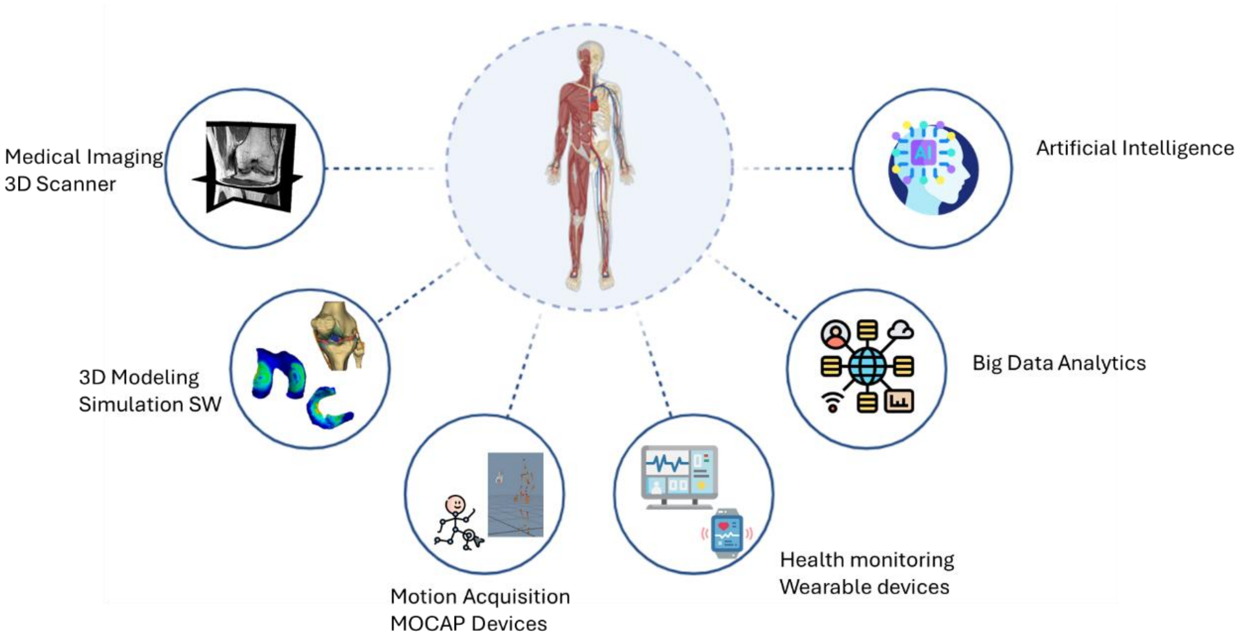

Figure 1: Patient Digital Twin requires the integration and analysis of several and heterogeneous data.

1.1.1 Patient Digital Twin in Orthopedic Care

In orthopedic practice, PDT serves as virtual replica that simulate a patient's musculoskeletal system and biomechanics. This digital twin can be constructed using a combination of patient-specific data sources such as medical imaging (X-rays, CT scans, MRI), biomechanical measurements, clinical assessments, and patient-reported outcomes. By integrating these data points, orthopedic surgeons and healthcare teams can gain a comprehensive understanding of a patient's anatomical structure, joint function, range of motion, and physiological conditions affecting orthopedic health.

The development of PDT for orthopedic care begins with the collection and integration of diverse data sources. Medical imaging and 3D modeling play a crucial role in creating detailed anatomical models, providing insights into bone structure, joint morphology, and soft tissue conditions [7]. Biomechanical data from gait analysis, motion capture systems, and wearable sensors contribute real-time information on joint movements, muscle activation patterns, and dynamic loading during physical activities.

Advanced computational modeling techniques, including finite element analysis (FEA) and machine learning algorithms, process these datasets or this data to simulate biomechanical behaviors, predict joint stresses, and simulate surgical outcomes. These simulations enable orthopedic surgeons to perform virtual surgeries, optimize surgical plans, and anticipate post-operative recovery trajectories tailored to each patient's unique anatomy and biomechanics.

The integration of patient digital twins in orthopedics may revolutionize the field by enhancing the identification and management of risk factors, improving diagnostic accuracy, assessing the full impact of pathologies, personalizing treatments, and predicting treatment outcomes. Algorithms can analyze patterns in the data to predict the likelihood of developing certain conditions. Early identification of risk factors allows healthcare providers to implement preventive measures, such as lifestyle changes, or targeted exercises, to reduce the risk of disease progression or injury. Furthermore, patient digital twins may enhance the accuracy and speed of diagnosing musculoskeletal disorders by combining various data sources into a single, coherent model. They can simulate how a condition will evolve over time, helping to predict future complications or the spread of a pathology. Preoperative planning benefits from PDT by allowing surgeons to visualize complex anatomical structures in three dimensions, prepare surgical procedures, and customize implant placement based on individual patient anatomy. Virtual simulations help mitigate surgical risks, optimize implant sizing and alignment, and enhance intraoperative decision-making to achieve optimal functional. Post-operative management is equally enhanced by PDT through continuous monitoring of patient recovery milestones, rehabilitation progress, and functional outcomes. Real-time data analytics facilitate early detection of complications, such as implant loosening or malalignment, prompting timely interventions and personalized rehabilitation strategies tailored to the patient's progress and biomechanical responses.

1.2 Three-dimensional Modeling

3D modeling of human districts is becoming more and more popular, since 3D models provide an accurate and realistic virtual representation, whereas traditional 2D imaging methods do not always allow to fully understand the morphology. Indeed, it could happen that the anatomical district of interest is not entirely visible in a single image, due to the principles of imaging acquisition. 3D computer models could provide consistent references for direct evaluation which are not affected by the location of cross section or flexion angle [2]. The use of 3D models in orthopedics offers a detailed representation of the complex anatomy. Surgeons can use 3D models to visualize patient-specific anatomy, identify pathology, and plan surgical approaches and implant placement. The ability to interact with 3D models allows for better understanding of complex anatomical relationships and facilitates the development of personalized treatment strategies. They have numerous applications in orthopedic surgery, including:

- Preoperative planning: Virtual surgical simulations allow surgeons to practice procedures in a risk-free environment, improving surgical proficiency and reducing operating room time.

- Training: By utilizing 3D models, both trainees and experienced clinicians can gain a more comprehensive understanding of anatomical variations and pathological conditions, enhancing their diagnostic and surgical skills.
- Intraoperative navigation: Real-time navigation systems integrate 3D models with intraoperative imaging data to assist surgeons during procedures. These systems provide guidance for implant placement, accurate bone resection, and soft tissue balancing, improving surgical accuracy and reducing the risk of intraoperative complications.
- Custom implants: Patient-specific implants and prosthetics can be designed using 3D modeling techniques based on individual anatomical variations. These custom devices offer improved fit and function compared to off-the-shelf implants, reducing the risk of complications and enhancing patient outcomes.
- Morphological analysis: to study anatomical differences between ethnics and sex or between healthy and pathological conditions.

3D models can be reconstructed from DICOM images by means of a segmentation process. Image segmentation is a technique in digital image processing and analysis, serving as an essential step for the description, recognition, or classification of image constituents [8]. It involves partitioning an image into meaningful regions to distinguish objects or regions of interest from the background [9]. Segmentation algorithms for grayscale images generally rely on two basic properties: discontinuity and similarity. Discontinuity refers to abrupt changes between objects and the background in an image. This approach involves the detection of points, lines, and edges where significant changes in intensity occur, highlighting boundaries between different regions. Techniques like edge detection and line detection are commonly used here [8]. Similarity, on the other hand, describes the uniformity within a given object or region in an image. A connected set of pixels having more or less the same homogeneous characteristics forms a region. Segmentation methods based on similarity include thresholding, region growing, and region splitting and merging [9]. Thresholding differentiates objects from the background based on intensity or brightness levels. Each pixel is compared to a threshold value: if its intensity is higher than the threshold, the pixel is classified as 'foreground' and set to white; if it is lower or equal, it is classified as 'background' and set to black. The success of thresholding critically depends on the selection of an appropriate threshold, which can be challenging in images with varying intensity levels [9]. Region Growing groups pixels or subregions into larger regions based on predefined criteria and connectivity. The process begins with initial starting points or seed pixels. The region grows by appending neighboring points that have similar properties, such as gray level, texture, or color. The effectiveness of region growing depends on the selection of seed pixels, the criteria for similarity, and the stopping rule that defines when to stop the growth [8]. Instead of starting with seed points, the splitting step successively subdivides the entire image into smaller disjoint regions until each region meets a homogeneity criterion. Merging then combines adjacent regions that satisfy the homogeneity criterion, ensuring that the final regions are uniform. Many segmentation algorithms exist in the literature, classified in various ways, but none can be applied without substantial modifications to specific anatomical areas. Segmentation procedures can be divided into the following categories:

- Manual Segmentation: The operator manually outlines the image portions to be labeled. Currently, it is considered as the ground truth, providing the highest accuracy. However, it is demanding, time-consuming, and expensive. Manual labeling is also subjective, difficult to reproduce, and introduces significant inter-observer variability due to differences in operators' knowledge and experience.
- Automatic Segmentation: Algorithms automatically divide the image into regions with similar characteristics, providing faster results but sometimes lacking accuracy in complex images.
- Semi-automatic Segmentation: This method represents a compromise, combining manual input with automated processes to improve efficiency while maintaining a degree of accuracy [10].

In light of the above mentioned limitations, there is a growing demand for automated segmentation algorithms that can provide accurate and reproducible results in clinical practice. These algorithms aim to reduce the workload on clinicians, increase consistency, and enable more efficient processing of large datasets, ultimately improving diagnostic and therapeutic outcomes [10].

Convolutional Neural Networks (CNNs) are a class of deep learning architectures that have demonstrated remarkable success in various computer vision tasks, including medical image segmentation. CNNs consist of multiple layers of convolutional, pooling, and activation functions, which learn hierarchical representations of input images. For segmentation tasks, CNNs are typically designed as encoder-decoder architectures, where the encoder extracts features from the input image, and the decoder generates pixel-wise segmentation masks.

The U-Net architecture is one of the most widely used CNN architectures for medical image segmentation, introduced by [3]. Its architecture is characterized by a symmetric contracting path (encoder) and an expansive path (decoder), which gives it a U-shaped structure. Skip connections between the contracting and expansive paths are used, which help in recovering the spatial information lost during down-sampling. In the encoder part of the network, convolution layers are used to extract high-level features from the input image. It consists of two 3x3 convolutions followed by a rectified linear unit (ReLU) as an activation function, and then two 2x2 max pooling with a stride size of 2 for downsampling. As a result of the encoder's low-dimensional representation, the decoder produces a segmented output image. In the decoder, a feature map is up sampled followed by a 2x2 convolution, which reduces the number of feature channels while increasing the resolution of the image. This architecture is unique in that it uses skip connections between the encoder and the decoder. By using skip connections, the model concatenates the cropped feature map from the encoder path, preserving spatial information by providing localized context for each pixel. The concatenated feature map is then followed by two 3x3 convolutions, each followed by the ReLU function. In the final layer, each feature vector is mapped to the desired number of classes using a 1x1 convolution [11]. U-Net uses relatively few parameters, making it faster and less memory-intensive.

1.3 Motion Capture

Motion Capture (MoCap) is a technology used to digitally record and analyze the movement of humans. It is widely used in various fields:

- Healthcare field: it is employed in rehabilitation and physical therapy to assess movement impairments, monitor progress, and design personalized exercise programs for patients recovering from injuries or surgeries.
- Sport science: it is used to analyze athlete performance, technique, and injury prevention. They provide objective measurements of movement mechanics, biomechanical efficiency, and joint loading during athletic activities.
- Entertainment and video games field: is extensively used in the entertainment industry for creating realistic character animations in movies, video games, and virtual reality applications. Actors perform movements while wearing motion capture suits equipped with markers, which are then translated into digital animations.

Motion capture systems can be classified in different categories according to the employed technology [12]:

- **Optical:** extrapolate the position of body joints through triangulation of images taken by various cameras [13]. Optical systems can be categorized into marker-based and markerless solutions. Marker-based solutions use active or passive markers placed on the body to track joint positions. In contrast, markerless solutions rely on software that identifies the human figure directly from the captured images, eliminating the need for the subject to wear any equipment.

- **Mechanical:** employ a deformable exoskeleton worn by the person to measure their movements. The exoskeleton consists of segments connected by metal or plastic parts, with goniometers and potentiometers placed on joints that convert joint movements into electrical signals. Data can be transferred to a computer using cables or wireless connections. This technique is suitable for capturing movements in large volumes but limits the actor's movements
- **Inertial:** it utilizes inertial measurement units (IMUs) containing accelerometers, gyroscopes, and magnetometers to track movement. These IMUs are attached to the subject's body and measure acceleration, angular velocity, and orientation. Inertial motion capture systems are portable, allowing for motion capture in outdoor environments and real-world settings.
- **Magnetic:** in these systems, the relative magnetic flux of three orthogonal coils is used to determine position and orientation. This solution is fairly economical but sensor wiring tends to restrict movements. Additionally, metallic objects distort the magnetic field, thereby altering data [14].

In the present research markerless MoCap systems have been employed. The fundamentals of this technique is explained in the following subsection.

1.3.1 Markerless MoCap Systems

Markerless motion capture systems utilize computer vision algorithms and image processing techniques to track movement without the need for physical markers attached to the subject's body. Instead of relying on markers, these systems analyze video of the subject's movement and extract motion data using sophisticated algorithms [15].

Markerless MoCap systems begin by capturing video of the subject's movement using one or more cameras. In case of multiple cameras, they are strategically positioned to provide multiple viewpoints of the subject, allowing for accurate reconstruction of movement in three-dimensional space. The resolution and frame rate of the cameras influence the quality and precision of the captured motion data [16]. Then, computer vision algorithms are employed to detect and track distinctive features in the video, such as keypoints, contours, or anatomical landmarks. These features serve as reference points for analyzing movement patterns and extracting motion data. Once the features are detected and tracked, pose estimation algorithms are applied to reconstruct the subject's body pose and movement in three-dimensional space. Pose estimation involves estimating the spatial configuration and orientation of the subject's body segments, such as limbs and joints, based on the detected features and their spatial relationships. Techniques such as inverse kinematics, model fitting, and optimization algorithms are utilized to infer the subject's pose from the tracked features. With the subject's pose estimated, the markerless motion capture system analyzes the temporal changes in pose over consecutive frames to reconstruct the subject's movement trajectory. Motion analysis algorithms compute key motion parameters such as joint angles, joint velocities, and trajectories of body segments. These parameters provide insights into movement dynamics, biomechanical properties, and kinematic patterns.

Markerless MoCap systems offer several advantages [4]:

- Non-invasive: Markerless motion capture systems do not require subjects to wear physical markers, eliminating the need for attaching markers to the body. This non-invasive nature makes markerless systems more comfortable for subjects and avoids potential discomfort or interference with movement.
- Natural Movement: Markerless systems capture movement in a more naturalistic manner since subjects are not constrained by markers. This allows for the analysis of spontaneous movements and interactions in real-world environments, making markerless motion capture suitable for applications such as sports science, biomechanics, and animation.
- Versatility: Markerless motion capture systems are versatile and adaptable to various environments and scenarios. They can be used indoors or outdoors, in controlled laboratory settings or in the field, making them suitable for a wide range of applications including sports training, clinical rehabilitation, and virtual reality.
- Cost-effective: Markerless motion capture systems may be more cost-effective compared to marker-based systems since they do not require the purchase and maintenance of physical markers. Additionally, markerless systems typically utilize standard cameras, reducing equipment costs compared to specialized motion capture cameras.
- Real-time Tracking: Some markerless motion capture systems offer real-time tracking capabilities, allowing for immediate feedback and analysis of movement during live performances, training sessions, or interactive applications.

However, these systems also present challenges [4]:

- Complexity of Analysis: Markerless motion capture systems rely on sophisticated computer vision algorithms for feature detection, pose estimation, and motion tracking. The complexity of these algorithms may require extensive computational resources and expertise in computer vision and image processing for system setup and calibration.

- Limited Accuracy: Markerless systems may have limitations in accuracy and precision compared to marker-based systems, especially for fine-scale movements or subtle changes in motion. Factors such as lighting conditions, occlusions, and camera calibration errors can affect the accuracy of motion tracking and pose estimation.
- Data Processing Time: The processing time required for analyzing video and extracting motion data in markerless motion capture systems can be significant, particularly for large datasets or real-time applications. This processing time may delay the availability of motion analysis results and limit the system's suitability for time-sensitive applications.
- Dependency on Environmental Conditions: Markerless motion capture systems are sensitive to environmental conditions such as lighting, background clutter, and camera positioning. Changes in lighting conditions or occlusions in the environment can affect the quality and reliability of motion tracking, requiring careful setup and calibration to ensure optimal performance.
- Limited Coverage: Markerless motion capture systems may have limitations in capturing movement from certain viewpoints or perspectives, leading to blind spots or gaps in the motion data. Achieving full-body coverage and accurate tracking from multiple viewpoints may require multiple cameras and careful placement to ensure comprehensive coverage of the subject's movement.

1.4 Anatomy and Pathology of the Main Joints

The human body comprises several major joints that facilitate a wide range of movements and provide structural support. The main joints include the knee, shoulder, hip. In the following sections, we will explore their anatomy and investigate common disorders and pathologies associated with these critical joints.

1.4.1 Knee Joint

The knee is one of the most complex human joints, as depicted in Figure 2. The distal end of the femur, the proximal end of the tibia, and the patella represent the main three bones. They are covered in thick articular cartilage, which ensures that friction is limited. Menisci, which adhere the tibia, absorb the shocks and bear the weight. Several ligaments support the bones. The main roles of the largest joint in the musculoskeletal system are to support the body weight and facilitate locomotion

[2]. However, the knee is often suffers from pathologies, such as osteoarthritis (OA), ligament injuries and meniscus tears [3].

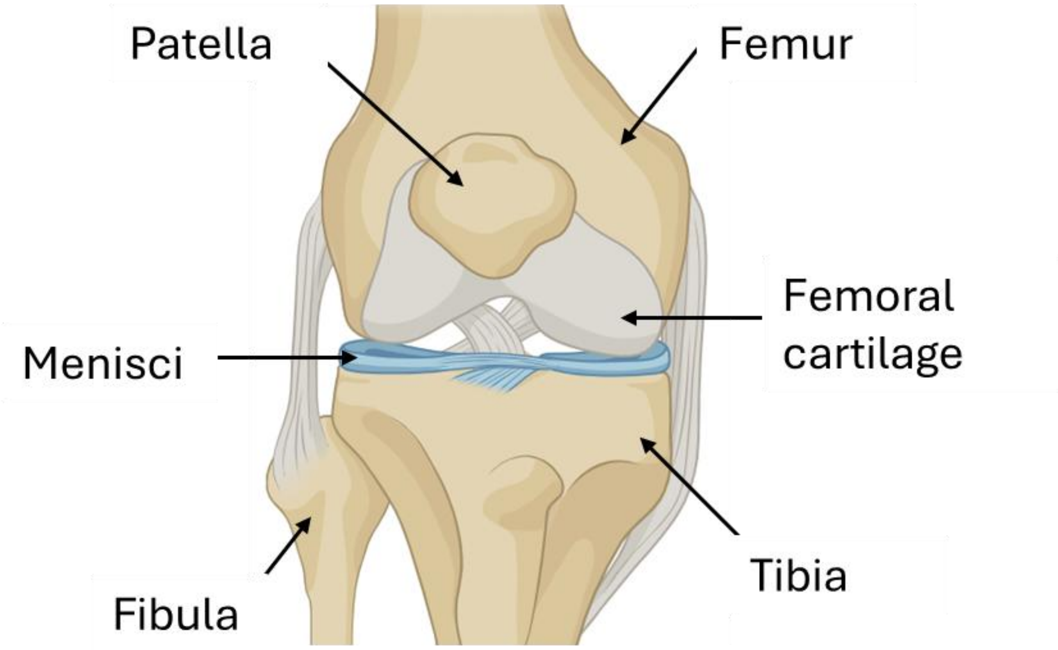

Figure 2: Anatomy of the knee joint. Partially created with BioRender [17].

Osteoarthritis (OA) of the knee is a degenerative joint disease characterized by the progressive breakdown of cartilage, which cushions the ends of bones within the joint [18]. This condition is commonly associated with aging, but other risk factors include obesity, joint injuries, repetitive stress on the knee, genetic predisposition, and certain metabolic disorders. As the cartilage deteriorates, bones begin to rub against each other, leading to pain, swelling, stiffness, and decreased range of motion. Patients often experience worsening symptoms with activity and improvement with rest. Over time, osteoarthritis can cause the formation of bone spurs and a reduction in the joint space, contributing to further discomfort and disability. Treatment focuses on pain management and maintaining joint function through a combination of lifestyle modifications, physical therapy, weight management, and pharmacologic interventions. In advanced cases, total knee replacement may be considered to restore mobility and relieve pain [19].

Ligament injuries, particularly to the anterior cruciate ligament (ACL), are prevalent among athletes [20]. The ACL is a crucial stabilizing ligament in the knee, connecting the femur to the tibia and preventing excessive forward movement of the tibia relative to the femur. Injury to the ACL typically occurs through a non-contact mechanism, often involving a sudden pivot, twist, or awkward landing [21]. Treatment options vary based on the severity of the injury and the patient’s activity level, ranging from conservative management with physical therapy and bracing to surgical reconstruction using grafts from the patient's own tissue, donor tissue or synthetic grafts [22].

Meniscus tears are a frequent concomitant injury in cases of ACL ruptures[23]. The menisci are two crescent-shaped cartilage structures that act as shock absorbers between the femur and tibia, aiding in joint stability and load distribution. When an ACL injury occurs, the rotational force and instability can lead to tears in the meniscus, particularly the medial meniscus, which is more rigidly attached to the tibia and hence more susceptible. These tears exacerbate symptoms such as pain, swelling, and joint locking or catching, and they can accelerate the degenerative process within the knee, increasing the risk of osteoarthritis. Treatment strategies for combined ACL and meniscus injuries typically include surgical intervention [24]. During ACL reconstruction, surgeons often repair or remove the torn meniscal tissue to preserve knee function and prevent further joint deterioration [25].

1.4.2 Shoulder Joint

The shoulder joint, or glenohumeral joint, is a highly mobile and complex articulation between the humerus and the scapula, shown in Figure 3.

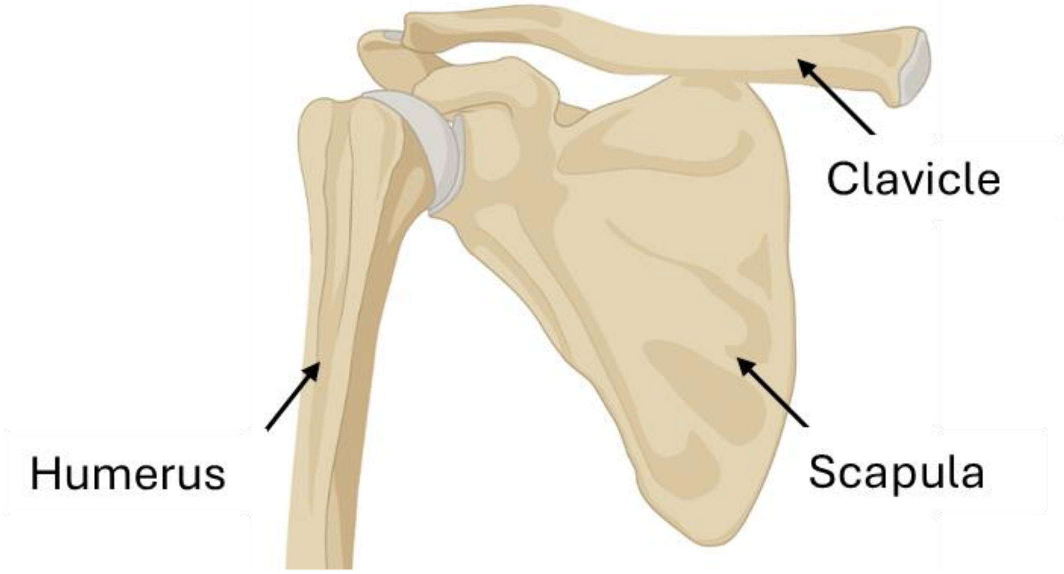

Figure 3: Anatomy of the shoulder joint. Partially created with BioRender [17].

It is a ball-and-socket joint, where the head of the humerus fits into the shallow glenoid cavity of the scapula, allowing for a wide range of motion in multiple planes. This joint is stabilized by a combination of static structures, such as the glenoid labrum (a fibrocartilaginous rim that deepens the socket), and dynamic structures, including the rotator cuff muscles and tendons, which encircle the joint and facilitate movement while maintaining stability. Additionally, the shoulder joint is supported by several ligaments, including the coracoacromial, coracohumeral, and glenohumeral ligaments, and is cushioned by bursae, small fluid-filled sacs that reduce friction between tissues [26]. This intricate anatomy enables the shoulder to perform complex movements like abduction, adduction, flexion, extension, rotation, and circumduction, making it one of the most versatile joints in the human body. Researchers have shown that shoulder pain is classified as the third most common musculoskeletal complaint in primary care. Every year, about 1% of adults visit a primary care practitioner for new shoulder pain [27].

Rotator cuff injuries are the most prevalent source of pain since its tendons are usually under heavy stress as they function in stabilizing the glenohumeral joint. When one or more of the rotator cuff tendons is torn, the tendon no longer fully attaches to the head of the humerus, so that stability is no longer guaranteed. Most tears occur in the supraspinatus tendon, but other parts of the rotator cuff may also be involved. As the damage progresses, the tendon can completely tear. According to the injury extension, it is possible to classify tears [28]. Partial or incomplete tear damages the tendon but does not completely sever it. Whereas, full-thickness or complete tear separates the whole tendon from the bone. Basically, there is a hole in the tendon so that the muscle is no longer attached to the bone. Conservative treatments, such as rest, ice and physical therapy, are sometimes sufficient to recover from a rotator cuff injury. However, if the lesion is severe, surgery is required. Surgeons usually reattach the injured tendon to the bone by means of arthroscopic techniques or through a larger incision. If the torn tendon is too damaged to be reattached to the arm bone, they may decide to use a nearby tendon as a replacement. Furthermore, massive rotator cuff injuries may require shoulder replacement surgery. A standard total shoulder replacement procedure replaces the ball and the socket parts of the shoulder joint with artificial parts. To improve the artificial joint's stability, an innovative procedure (reverse shoulder arthroplasty) installs the ball part of the artificial joint onto the shoulder blade and the socket part onto the arm bone [29]. This technique can be done for many conditions, but it is mainly used when there is a rotator cuff tear in the shoulder with arthritis.

Shoulder arthritis results from gradual wear and tear of the cartilage. It typically develops in stages: firstly, the cartilage gets soft, then it develops cracks in the surface, afterwards it begins to “fibrillate” (deteriorate and flake), and finally it wears away to expose the surface of the bone. As a result, it loses its ability to act as a smooth, gliding surface [29].Hence, part of the original bones are removed and substituted with artificial components.

Traumatic events can cause the shoulder to move beyond its normal range of motion, thus causing shoulder instability. An unstable shoulder can easily lead to a dislocation, which occurs when the humeral head become permanently out of its physiological position, causing pain. If it protrudes anteriorly, an anterior dislocation happens; if it protrudes posteriorly, a posterior dislocation occurs. Anterior dislocation is much more common (95% of the total shoulder dislocation) and often occurs in young patients, and more often in males than in females [3] [4] [5]. The event tends to recur because the structures responsible for glenohumeral stability, the capsule and ligaments, are injured after a dislocation, further reducing the stability of the joint.

1.4.3 Hip Joint

The hip joint is a ball-and-socket synovial joint that plays a critical role in supporting the weight of the body and facilitating a wide range of movements. It is formed by the articulation between the head of the femur and the acetabulum of the pelvis, as depicted in Figure 4.

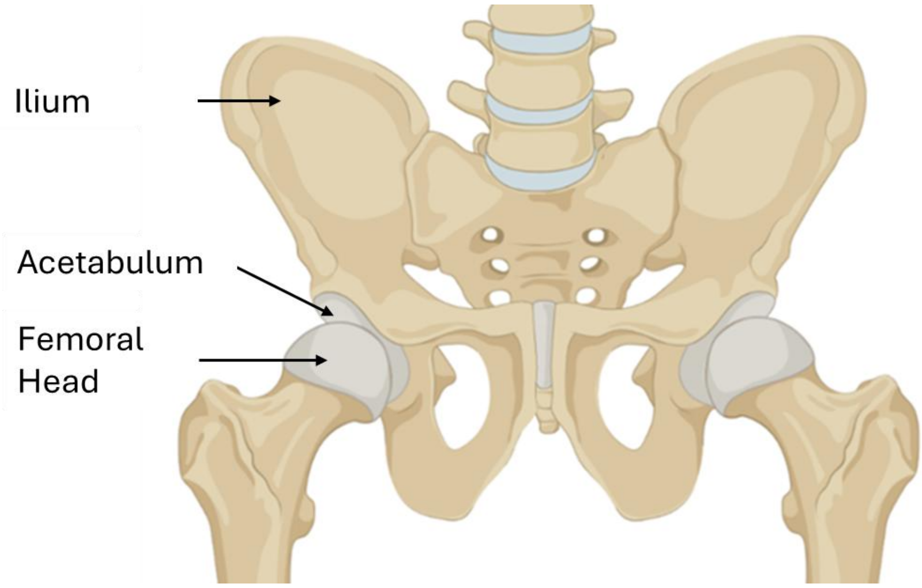

Figure 4: Anatomy of the hip joint. Partially created with BioRender [17].

The acetabulum is a deep, cup-shaped cavity that houses the femoral head, providing a stable yet flexible connection. This joint is encased in a strong, fibrous capsule that is reinforced by several ligaments, including the iliofemoral, pubofemoral, and ischiofemoral ligaments, which contribute to the stability of the hip by limiting excessive movements. Additionally, the ligamentum teres, a small ligament within the joint, provides a blood supply to the femoral head. The articular surfaces of the femur and acetabulum are covered with hyaline cartilage, which reduces friction and absorbs shock. Surrounding muscles, such as the gluteal muscles, iliopsoas, and adductors, further stabilize the joint and facilitate movements like flexion, extension, abduction, adduction, and rotation. The synovial membrane lining the joint capsule produces synovial fluid, which lubricates the joint and nourishes the cartilage. This intricate anatomy allows the hip joint to be both highly mobile and exceptionally strong, essential for activities ranging from walking and running to jumping and climbing [30].

In some cases the hip can suffer from OA. The hip joint, a ball-and-socket joint formed by the femoral head and the acetabulum of the pelvis, relies on smooth cartilage surfaces for pain-free movement and shock absorption. In osteoarthritis, this cartilage deteriorates, leading to the bones rubbing against each other, which causes pain, inflammation, and decreased joint mobility. For patients with severe symptoms unresponsive to conservative measures, surgical options may be considered [31]. Hip arthroscopy can address certain structural issues, while total hip arthroplasty (hip replacement) is highly effective for advanced osteoarthritis, providing significant pain relief and improved function. However, walking abnormalities such as the Trendelenburg gait can be observed after THA [6]. It is caused by weakness of the abductors of the lower limbs, the gluteus medius and gluteus minimus. As the pelvis cannot be kept level by the lesioned abductors, the pelvis drops to the healthy side. In response, the trunk tilts towards the lesioned side in an attempt to maintain balance [7].

Chapter 2. Proposed Architecture

An accurate and customized patient care requires the integration of several types of information from a variety of sources. The developed integrated approach incorporates input from medical professionals, makes use of relevant literature, and utilizes innovative data obtained with the use of advanced technologies. By integrating these various sources, an orthopedic patient’s digital twin is created to gain a more in-depth understanding of the patient's condition, resulting for instance in more informed decision-making by the physician and customized treatment strategies.

The development of patient digital twins relies on several essential technologies. Among the key technologies available, this work focuses on 3D modeling and MoCap data.

The use of 3D modeling is essential for the advancement of patient digital twin technology. Traditional imaging modalities, such as X-rays, CT and MR scans, provide valuable diagnostic information but often lack the spatial resolution and depth required for detailed anatomical assessment. Three-dimensional modeling techniques offer a solution to this challenge by reconstructing patient-specific anatomical structures in three dimensions, enhancing visualization and spatial orientation capabilities. The use of 3D modeling in orthopedics has evolved significantly over the past few decades. Initially, manual methods of 3D reconstruction were employed, requiring tedious segmentation of medical imaging data and manual manipulation to create anatomical models. However, with advancements in computer-aided design (CAD) software and imaging technologies, automated and semi-automated methods of 3D reconstruction have become prevalent. Using deep learning techniques, it is possible to automate image segmentation to generate detailed and accurate 3D models from medical imaging data. Based on the obtained 3D models, the anatomy and morphology of each patient can be studied for a variety of applications, including the identification of pathology and the customization of treatment. Statistical shape modeling (SSM) permits the automation of landmarking and measurements. It helps to automate the process of creating customized prostheses. Furthermore, it permits to study anatomical variations and investigate different morphologies and pathologies. FEA are used to simulate the biomechanics change due to a pathology or to a treatment, compared to the healthy condition.

Motion capture technology is integral to the creation of patient digital twins. Human movement analysis can be an essential tool to identify pathology of the locomotor system, to assess the efficacy of a rehabilitation protocol or a surgery or to follow the evolution of a disease. Comparing the motion parameters before and after the operation allows analyzing the effect of the operation and formulating the treatment plan.

Literature searches in Scopus and PubMed databases enable the identification of relevant parameters and the definition of healthy and pathological ranges. Using these parameters facilitates the investigation of 3D models of patients and the analysis of MoCap data. The parameters obtained from the literature can be utilized to assess and compare the morphology of 3D models representing patients' anatomical structures. By quantifying deviations from established healthy ranges, researchers can identify anomalies or abnormalities in the morphology of these models, providing valuable insight into musculoskeletal conditions or injury. Furthermore, the parameters identified through the literature search provide critical metrics for analyzing data obtained from motion capture systems. MoCap data can be interpreted using parameters derived from literature to determine biomechanical patterns, kinematic relationships, and kinetic characteristics of movement. An analysis of movement patterns is of great importance to researchers, as it provides valuable information for diagnosing, treating, and monitoring musculoskeletal disorders.

By integrating these techniques and diverse sources of information, an orthopedic patient's digital twin is developed, providing a comprehensive and detailed representation of the patient. By analyzing these data, PDTs can predict susceptibility to joint disorders or anatomical abnormalities. This proactive approach enables clinicians to implement preventive strategies and personalized interventions to mitigate risks before they escalate. In diagnostics, PDTs facilitate more accurate and timely assessments of orthopedic conditions. By creating virtual models of joints, bones, and soft tissues based on imaging and biomechanical data, clinicians can visualize anatomical abnormalities, assess disease progression, and identify specific pathologies. PDTs play a crucial role in customizing treatment plans for orthopedic patients. By simulating patient-specific biomechanics and disease progression, PDTs help orthopedic surgeons and multidisciplinary teams optimize treatment strategies tailored to individual anatomical variations and functional requirements. For joint replacements, PDTs assist in selecting optimal implant designs, sizes, and placement based on virtual simulations of joint mechanics and implant kinematics. Post-treatment, PDTs facilitate ongoing monitoring and assessment of treatment outcomes.

Figure 5 depicts the overall platform of the developed system. 3D modeling techniques, domain knowledge and motion capture systems are the input for the creation of the patient digital twin, which permits a comprehensive assessment for patient care, involving:

- Risk factors identification
- Pathology identification and diagnosis
- Pathology impact
- Personalized treatment
- Treatment impact

The methodology presented in this research was developed to address the need for a versatile approach applicable to a wide range of cases in orthopedics. It was designed to accommodate diverse pathologies while maintaining robustness and comprehensibility. A selection of specific orthopedic pathologies was made to demonstrate the adaptability and efficacy of the developed methodology. These pathologies were chosen based on their prevalence, clinical significance, and representation of various anatomical regions and conditions within orthopedics. The three main joints have been investigated. In the knee compartments, pathologies like osteoarthritis (OA) requiring total knee arthroplasty (TKA), anterior cruciate ligament (ACL) injury and concomitant pathologies (meniscal injuries) have been studied. Regarding the shoulder, shoulder instability, rotator cuff injury and OA have been investigated. For the hip, OA requiring Total Hip Arthroplasty (THA) and Trendelenburg gait have been analyzed.

Part of this work was made in collaboration with the orthopedic department of Humanitas Gavazzeni and Castelli, whose expertise and contributions have been invaluable in advancing the integration of patient digital twins in orthopedic care. Their collaboration has provided essential clinical insights and practical applications, ensuring that the technological advancements in 3D modeling and motion capture data are effectively translated into improved diagnostic accuracy, personalized treatment plans, and enhanced patient outcomes. The partnership has also facilitated the continuous refinement of digital twin models, contributing significantly to the overall success and impact of this innovative approach in modern orthopedics.

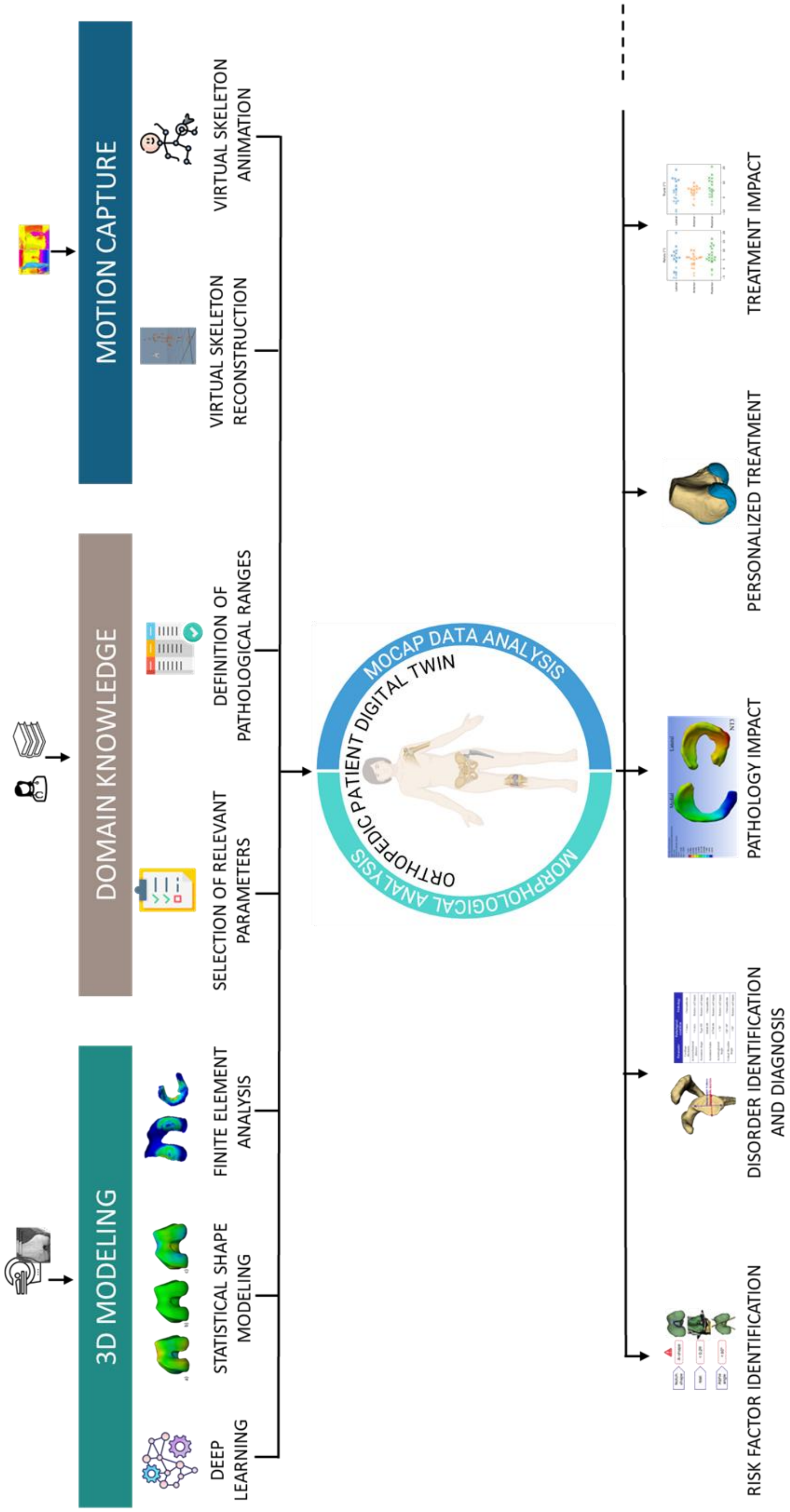

Figure 5: Research proposal architecture.

2.1 Three-Dimensional Modeling Module

The initial module of the proposed architecture is 3D modeling, which encompasses techniques for reconstructing and analyzing 3D models. This module integrates Deep Learning for automatic segmentation, Statistical Shape Modeling and Finite Element Analysis for testing and simulations.

2.1.1 Deep Learning for Automatic Segmentation

DL has revolutionized the field of medical image segmentation, enabling automatic and accurate delineation of structures and tissues from images such as MR and CT. The process can be divided into phases:

1 **Data Preparation**: DL models require a large amount of labeled data for training. In medical imaging, this involves acquiring images along with manually annotated ground truth masks indicating the regions of interest. The manual segmentation involves the contouring of the region of interest in all the slices, as shown in Figure 6. The first image represents the shoulder compartment with the segmented humerus in yellow. The second image depicts the femoral and tibial bone in yellow, the femoral cartilage in green, the tibial cartilage in light blue and the menisci in purple colours.

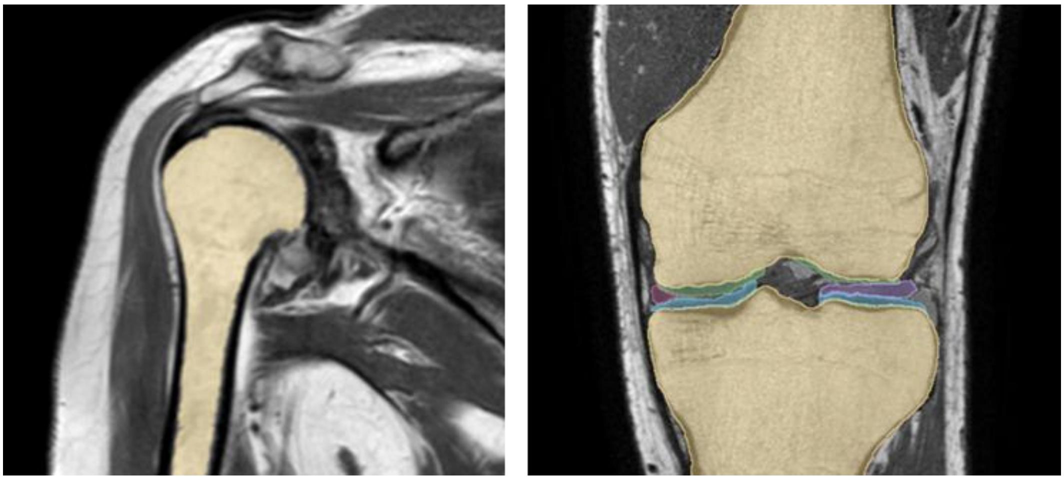

Figure 6. Manual segmentation of shoulder and knee tissues, respectively.

2 **Model Architecture Selection**: The U-Net architecture is one of the most widely used CNN architectures for medical image segmentation, including in orthopedics [3]. It consists of a contracting path, which captures context and spatial information through convolutional and pooling layers (downsampling), followed by an expansive path, which enables precise localization and segmentation through upsampling and concatenation operations. The skip

connections between corresponding layers in the contracting and expansive paths facilitate the fusion of low-level and high-level features, improving segmentation accuracy.

3 **Data Augmentation**: Since labeled medical image datasets are often limited in size, data augmentation techniques such as rotation, flipping, scaling, and elastic deformations are used to artificially increase the size of the training dataset and improve model generalization.

4 **Training**: The selected deep learning model is trained using annotated images and corresponding masks. The model learns to map input images to their corresponding segmented output masks by minimizing a loss function, typically a variant of cross-entropy loss or dice loss. The dataset is divided into three sets for training, validation and testing. A typical division is 75% for training, 20% for validation, and 5% for testing.

5 **Validation and Fine-tuning**: The trained model is evaluated on a separate validation dataset to assess its performance. Fine-tuning may be performed by adjusting hyperparameters, such as learning rate and epochs based on validation results. The learning rate is a parameter that controls the size of weight update steps during training. An appropriate choice of the learning rate is essential to ensure fast and stable convergence during optimization. A learning rate that is too large can cause an optimization error, while a learning rate that is too small can slow down the training process. The epochs represent the number of times the entire training dataset is presented to the model during training. During each epoch, the network weights are updated to improve the model's performance. Increasing the number of epochs can help improve performance to some extent, but can result in overfitting.

6 **Testing**: Once trained and validated, the model can be deployed for automatic segmentation on new, unseen images. To evaluate the accuracy of a neural network, a popular approach is to compare its predicted output with a pre-validated ground truth. When assessing the effectiveness of DL segmentation, the confusion matrix is a useful tool that includes four categories: true positives (TP), false positives (FP), false negatives (FN), and true negatives (TN).

The Dice Similarity Coefficient (DSC) is a measure of the similarity or overlap between two sets. The DSC is often used to quantify the agreement between the predicted segmentation mask and the ground truth. It provides a single scalar value (ranging from 0 to 1) that summarizes the quality of the segmentation results, with higher values indicating better performance. The formula for DSC describes the ratio between two times the intersection of the sets over their sum, as shown in Equation (1):

$$DSC = \frac{2TP}{2TP+FP+FN} \qquad (1)$$

The Hausdorff distance (HD) is another widely used performance measure for evaluating the accuracy of automatic segmentation methods. It measures the maximum distance between two sets of points, where one set represents the ground truth, and the other one represents the segmentation result. The Hausdorff distance is useful for evaluating the accuracy of segmentation methods, as it provides a measure of the maximum error between the ground truth and the segmentation result [32]. The formula for Hausdorff distance is as follows:

$$HD(A,B) = max\ [sup_{a \in A}\ inf_{b \in B}\ d(a,b),\ sup_{b \in B}\ inf_{a \in A}\ d(a,b)] \quad (2)$$

where A and B are two surfaces, *sup* and *inf* denote the least upper bound and greatest lower bound, respectively [33].

This study utilized the Medical Open Network for Artificial Intelligence (MONAI) and the 3D Slicer. MONAI is an open-source framework for DL in healthcare imaging [34]. In particular, MONAI Label [35] is a free open-source tool for image labelling and learning, which allows for the creation of annotated datasets and the development of AI-based annotation models for clinical assessment. The software enables researchers to construct, train, and execute training using labelling applications in a serverless manner. It is feasible to establish a connection between MONAI Label and 3D Slicer, which is an open-source cross-platform software package for biomedical imaging research [36].
The following hardware components are used for training the network: Intel(R) Xeon(R) W-2245 CPU @ 3.90GHz, and GPU NVIDIA RTX A5000.

2.1.2 Statistical Shape Modeling

Statistical Shape Modeling (SSM) is a computational technique used to quantitatively analyze and model the variability of shapes within a population of objects or anatomical structures. It combines principles from geometry, statistics, and machine learning to extract meaningful information about shape variation and its underlying patterns.
To go from a training set of N 3D triangle meshes (shapes) to a statistical shape model, the following steps are followed: vectorization, alignment and principal component analysis.

1 **Vectorization**: In this phase, all shapes are remeshed so that each shape is represented by an equal amount of L corresponding vertices. The result is that each shape is represented by a vector with M=3xL dimensions (x, y, z coordinates of each vertex point).
2 **Alignment**: The shapes are aligned in space in order to eliminate translation and rotation. Two methods are mainly used. The first consists of aligning the shapes according to Generalized Procustes Analysis (GPA). The Procustes distance is a measure of difference between shapes and

is minimized for all shapes by translating and rotating each shape. The second method involves aligning the shapes based on anatomical landmarks.

3 **Principal Component Analysis (PCA)**: It consists of computing the statistically independent eigenvectors and eigenvalues of the data set. The eigenvectors (principal components, PC) show global shape variations, called ‘modes of variation’ in SSM. The associated eigenvalues indicate the amount of shape variance explained by that specific mode of shape variation. The eigenvectors are ordered according to their explained variance; eigenvectors with highest variance are placed first and those with low variance are placed last [37]. The general formula for SSM is

$$y = \bar{x} + \sum_{i=1}^{n} \omega_i p_i \qquad (3)$$

In which y is a random model, $\bar{x}$ is the mean mesh, ω corresponds to the weighting factors and p denotes the mode of variation or PC [38].

The shape characteristics of each principal component can be visualised by plotting the shape corresponding to extreme values. These new meshes were generating setting $w_i = \pm$ 3SD of the scores from the corresponding principal component. All other weighting factors were set to zero.

An assessment of the quality of the SSM was conducted using two measures. First, the compactness of the model was evaluated, which corresponds to the number of PCs required to describe a fixed percentage of variation. Second, the generalization was calculated. It measures the degree to which a random femur can be described with the SSM, based on a comparison of the original femoral mesh and the SSM mesh [7].

Statistical shape models were obtained using modules in two different software: SSM package of Materialise 3-Matic[11] and SlicerMorph module in 3D Slicer.

2.1.3 Finite Element Analysis

Finite Element Analysis (FEA) in the medical field involves using computational techniques to simulate the mechanical behaviour of biological tissues, organs, implants, or medical devices. It can be used to study the effect of a morphological variation, or an injury on biomechanics compared to the physiological condition. It can also be employed to compare different prosthesis design in terms of stress and dislocation. Starting from an anatomical model, Finite Element Analysis (FEA) involves several steps to simulate the mechanical behaviour of tissues or structures:

1 **Mesh Generation:** The 3D anatomical model is converted into a finite element (FE) mesh by discretizing it into smaller, simpler elements. The appropriate element types (e.g., tetrahedral,

hexahedral) and mesh density are chosen based on the geometry and mechanical properties of the tissues.

2 **Material Properties Assignment:** Material properties are assigned to each element based on the mechanical behaviour of the tissues being simulated. They are derived from experimental data, literature, or tissue characterization studies (e.g., Young's modulus, Poisson's ratio).

3 **Boundary Conditions:** They are defined to simulate physiological loading conditions or constraints. Loads such as forces, pressures, or displacements are applied to specific regions of the model to represent external forces or muscle activations. Certain nodes or surfaces are fixed or constrained to simulate constraints or supports.

4 **Formulation of FE Equations:** The FE equations are formulated based on the governing equations of continuum mechanics (e.g., linear elasticity).

5 **Solution of FE Equations:** The FE equations are solved to obtain the nodal displacements, stresses, and strains within the model. Numerical methods such as direct solvers, iterative solvers, or specialized algorithms are employed to solve the system of equations efficiently.

6 **Post-Processing:** The results obtained from the simulation are analyzed to assess the mechanical response of the anatomical model. The distribution of displacements, stresses, strains, or other relevant mechanical parameters within the model can be visualized to better interpret the results. In this way, it is possible to identify regions of interest, potential failure points, or areas of excessive deformation for further analysis.

7 **Validation and Interpretation:** FEA results are validated by comparing them with experimental data, analytical solutions, or clinical observations. The interpretation of the simulation results allows to gain insights into the mechanical behaviour of the anatomical structure under study.

2.2 Motion Capture Module

Motion capture module can be divided into acquisition, virtual skeleton reconstruction and data analysis phases.

1. **Acquisition:**

   Initially, cameras in the capture area are positioned to provide optimal coverage of the subject's movements from multiple angles. It is important to ensure that the cameras are securely mounted and aligned properly to capture the desired field of view without obstruction. Then, calibration phase is required to determine the spatial relationship between the cameras in the capture setup. In markerless MoCap it can be done using either a calibration board or a light-based method.

Finally, the subject's movements are recorded while they perform the desired actions. The subject has to stay within the capture volume.

Figure 7 shows the set up with two Microsoft Kinect version 2 sensors placed opposite to each other and diagonally with respect to the walking path. The patient is asked to walk at his/her preferred speed for 6 meters. A minimum of 2 full gait cycles are recorded.

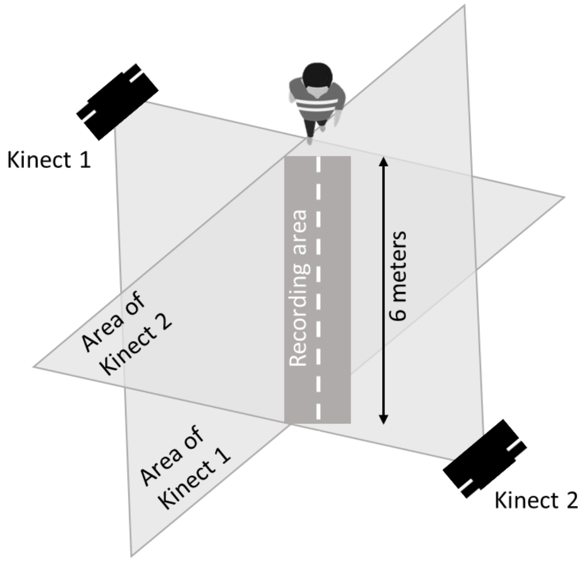

Figure 7. MoCap set up scene.

2. **Virtual Skeleton Reconstruction:**

Initially, the skeletal structure of the subject based on the detected key points or features representing joint locations and anatomical knowledge is defined. These key points are connected to form a virtual skeleton, representing the subject's body structure and articulation. The movement of each skeletal segment, such as limbs and torso, is tracked by analyzing the trajectories of associated key points or features over time. The orientations and positions of these segments are computed. The reconstructed virtual skeleton is mapped onto a digital character or avatar for visualization and analysis purposes.

In the present research, the virtual skeletons of the patients were reconstructed from the acquisition, through iPi Soft software (

Figure 8).

3. **Data Analysis:**

The extracted information is analyzed to study movement, providing valuable insights for fields such as biomechanics and rehabilitation. Kinematic analysis focuses on the kinematics of the captured motion, including joint angles, velocities, accelerations, and trajectories. This can provide insights into the biomechanics and dynamics of the movement. Gait analysis evaluates various gait parameters such as stride length, step width, and gait symmetry to evaluate walking patterns and detect abnormalities. Functional analysis evaluates functional movements such as reaching, grasping, or lifting objects to assess performance and identify areas for improvement. Lastly, statistical analysis allows for an evaluation by applying statistical tests or modeling techniques to compare motion data across different conditions, populations, or interventions and identify significant differences or trends.

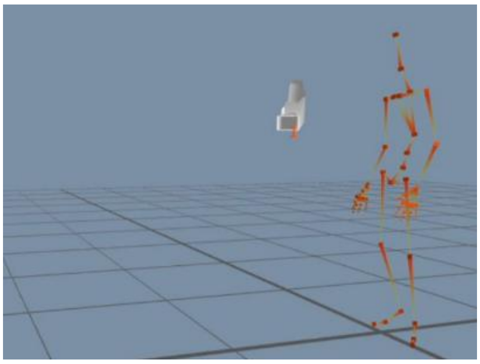

Figure 8. Virtual skeleton reconstruction.

2.3 Orthopedic Patient’s Digital Twin

Integrating data from 3D modeling and MoCap technologies forms the basis for the development of our orthopedic patient digital twin. Advanced computational modeling techniques then synthesize these diverse datasets to create a virtual replica that accurately simulates the patient's biomechanical behavior. This data-rich digital twin can serve as a powerful tool for various clinical applications.

For prevention and diagnostics, the patient’s digital twin allows clinicians to visualize and analyze the patient’s musculoskeletal system in a detailed, interactive 3D environment. Abnormalities such as anatomical variations, gait irregularities, or unusual stress distributions can be identified with high precision. By comparing measured values from these digital twins against established norms and findings documented in the literature, healthcare providers can effectively identify and characterize various pathologies. In addition, clinicians can use this digital twin to simulate the impact of a pathology or a disorder. They can visually and quantitatively assess the extent of the impact, providing clear insights into how much the disorder alters normal biomechanics. In treatment planning, the digital twin can simulate different therapeutic scenarios. By virtually testing surgical procedures, orthopedic implants, or rehabilitation exercises, clinicians can predict their biomechanical impacts and outcomes. This simulation capability helps in selecting the most effective treatment strategy, minimizing the risk of complications, and optimizing the recovery process. For example, in planning a knee replacement surgery, the digital twin can model how different implant designs would affect the patient's joint loading, enabling a tailored approach that maximizes functional recovery. Furthermore, the digital twin can be used to simulate and analyze the impacts of different treatments, providing valuable insights that enhance clinical decision-making and patient outcomes.

Morphological analysis and motion capture (MoCap) data analysis are fundamental components in the development and application of patient digital twins. The developed methodologies are further detailed in the following sub sections.

2.3.1 Morphological Analysis

By using 3D models, it is possible to study the morphology of a specific patients. Anatomic variations within general population may predispose to the development of various injuries, can be an indicator of a pathology, lead the treatment choice or the creation of personalized treatment and solutions and investigate the treatment impact.

To quantitatively assess the morphology of 3D models, manual, semiautomatic or automatic procedure can be employed, according to the operator's involvement.

In a manual procedure, annotations or markings on the 3D model are done entirely by human operators without the aid of automated tools or algorithms. This involves manually identifying specific landmarks, structures, or areas of interest. The operator then places markers directly onto the 3D model using specialized software tools.

In a semi-automatic procedure, the process combines both manual intervention and automated algorithms. Human operators still identify landmarks or points of interest on the 3D model, but specialized software algorithms assist in the measurement process. These algorithms may automatically detect and track features of interest, such as anatomical landmarks or surface contours, and compute relevant morphological measurements based on predefined criteria.

In the automatic procedure, the entire process of morphological measurement is performed by computer algorithms without direct human intervention. Advanced software algorithms analyze the 3D model data, automatically detect relevant landmarks or features, and compute morphological measurements based on predefined algorithms. In the present study, the SSM is employed, since it represents the mean shape of the population. A landmarks template is defined on the SSM according to anatomical references and the desired measurements. The process involves transferring landmarks from the reference model (SSM) to a target model through point cloud alignment and deformable registration. First, the SSM mesh is isotropically scaled to match the target mesh, then a global registration is performed to find a transformation that accurately registers the SSM point cloud to the target. An iterative procedure using the point-to-plane iterative closest point (ICP) algorithm is then used to further refine the alignment of the two point clouds [26]. At each iteration, the squared distance between each SSM point and the tangent plane at its corresponding target point is calculated. The algorithm continues to iterate until the distance between the two point clouds is minimized. The final step is to deform the rigidly aligned SSM point cloud to match the target point cloud using the Coherent Point Drift (CPD) algorithm [25]. CPD is a probabilistic point cloud registration technique that frames the alignment of two point clouds in terms of probability density estimation [26]. This approach facilitates the transfer of landmarks from the SSM reference mesh to the patient's models. In this way, it is possible to automatically detect the desired measurements on the other 3D models.

To perform a morphological analysis, a specific software environment has been developed. It embeds all the main steps of the entire workflow, starting from the medical images load to the creation of a report with an automatic morphological evaluation. It has been built as a scripted extension for 3D Slicer. The 3D modeling capabilities of the Visualization Toolkit (VTK) on an open-source framework uses Python. For computationally demanding features, bindings to optimized C++ code have been used. This choice has enabled rapid development without sacrificing the performance of the tool. The user interface has been developed with the QT framework, allowing the layout of the developed module to be consistent with the 3D Slicer application [36]. The dedicated tool foresees five main phases, as depicted in

Figure 9.

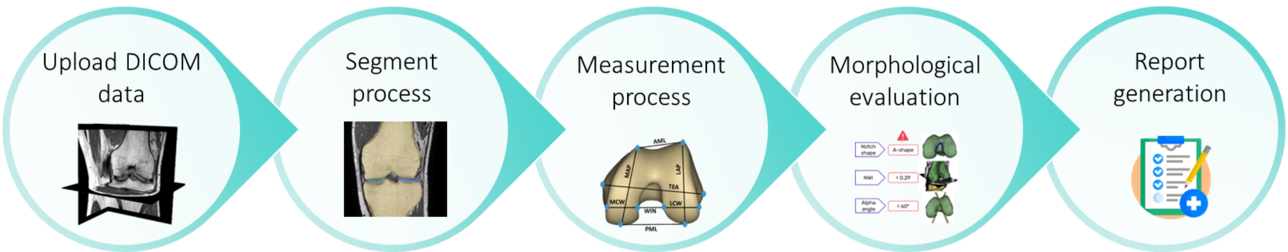

Figure 9: Morphological evaluation tool.

The first one regards the loading of the DICOM data (MR or CT). The second involves segmentation techniques to reconstruct the three-dimensional models. In the third step, the operator is guided through the drawing of a small number of landmarks on the surface of the bones. It is possible to define positions, absolute distances, angles, open and closed curves, and volumes of regions of interest in both 2D and 3D. Landmark points can be used to highlight reference points on the 3D models or in the 2D images, where they can be useful for the registration of medical images obtained with different modalities. Absolute distances can be employed to measure the length and the width of anatomical districts, in order to design medical devices that best fit the patient. Anterior-posterior and medial-lateral length of the femur can be measured to choose the correct size of prosthesis, for example. Angle markups can be employed for the measurement of specific angles, indicators of specific pathologies, such as the sulcus angle for trochlear dysplasia. Curves can be used to define a region of interest, computing its area, useful for studying a lesion, such as a meniscus tear. Thereafter, a specific algorithm exploits the user-defined key points to perform an automatic morphological assessment. Finally, the operator can export the results of the assessment in both CSV and PDF formats.

2.3.1.1 SSM for anatomical variation

To evaluate the changes in shape, SSMs provide a robust framework where parameters taken from literature can be quantitatively measured [5]. These models typically start with a mean shape derived from a cohort of anatomical structures, representing an average or typical form. To ensure uniformity and reduce unwanted variability, the dimensions of the anatomical structures of the sample are standardized. For example, trimming certain dimensions to a specific percentage of the maximum measurement helps maintain consistency across samples. To further ensure uniformity, in case of symmetry, structures from one side of the body can be mirrored to match the other side. This standardization process helps in creating a more reliable SSM. Then, vectorization and alignment are performed. By applying modes of variation extracted from a dataset, such as principal component analysis (PCA), the SSM can generate a range of shapes that encompass anatomical diversity within the population studied. The principal components or modes of variation can be visualized by generating the shape models for ±3 standard deviation (SD) for each mode of variation. Parameters of interest, identified based on clinical or research literature, can then be systematically measured both on the mean shape and across the variations produced by altering specific modes. This comparative analysis allows researchers and clinicians to quantify how anatomical features change across different shapes within the model, providing insights into variations that are relevant for diagnostic, surgical planning, or research purposes.

2.3.1.2 Customized joint prosthesis design

Anatomical variations and detailed morphological analysis are critical factors in the design of customized joint prostheses. By leveraging this anatomical data, it is possible to design prostheses

that are tailored to fit the patient's specific anatomy. A methodology for the automatic creation of customized orthopedic prostheses has been developed (
Figure 10). The procedure is defined based on a SSM and includes several stages from the anatomical study of the affected area to the final creation and validation of the prosthetic component. This procedure is intended for joint replacement surgery, aimed at patients suffering from severe OA or other debilitating joint conditions, which are the most common orthopedic interventions. These surgeries aim to restore joint function and alleviate chronic pain by implanting joint prostheses, which can be partial or total depending on the extent of joint damage. The described method ensures a tailored fit to the patient's anatomy, thereby improving the functionality and comfort of the prosthesis. The first step is the creation of SSM from the cohort of the available 3D models, as described in **Errore. L'origine riferimento non è stata trovata.**, using anatomical landmarks. The obtained SSM is used to design the custom implant. The design process begins with a thorough examination of the target anatomical region. The anatomy of the target bone or joint is studied to understand the usual position and shape of the native cartilage or bone structure. A curve is created following the native morphology of the area. This curve acts as a guide for the subsequent steps. The area within the curve is extruded along normal vectors to restore the volume lost due to damage or degeneration. The thickness of the extrusion is typically set to a standard value and can be adjusted according to the original anatomical structure's characteristics. The extruded area is combined with the bone model using a Boolean union operation to create a single, unified model. A median smoothing operation is applied to achieve a homogeneous surface, which is necessary to remove irregularities such as osteophytes in the case of degenerative conditions. Next, cut planes are created to section the model into the required prosthetic components. Depending on the specific prosthesis, several cut planes are defined to match the required facets of the implant. These planes are positioned based on anatomical landmarks and desired alignment, ensuring minimal bone removal and optimal fit. The 3D model is cut according to the planes, resulting in distinct parts: the sectioned bone and the customized prosthetic component.

During the prosthesis design phase, both clinical and technical parameters are considered to ensure the best possible fit and function. Clinical parameters can be alignment or the number of cut planes, while technical parameters can be the material. To identify the optimal configuration, several models are generated by combining different clinical and technical parameters. Finite Element Analysis are conducted on these models to evaluate their performance. To validate the designed customized implant, the proposed solution is compared to healthy anatomical condition. The customized implant is also compared to virtually implanted off-the-shelf prosthesis through FEA.

Once the procedure has been defined on the SSM, it can be used to automatically design customized implants on the sample. The process involves transferring landmarks from the reference model (SSM) to a target model through point cloud alignment and deformable registration. This approach facilitates the transfer of landmarks and reference planes from the SSM reference mesh to the samples. The area inside the curve is then extruded to a predefined thickness and the planes are used to cut the model to obtain the customized implant. This automated method allows the creation of customized prostheses.

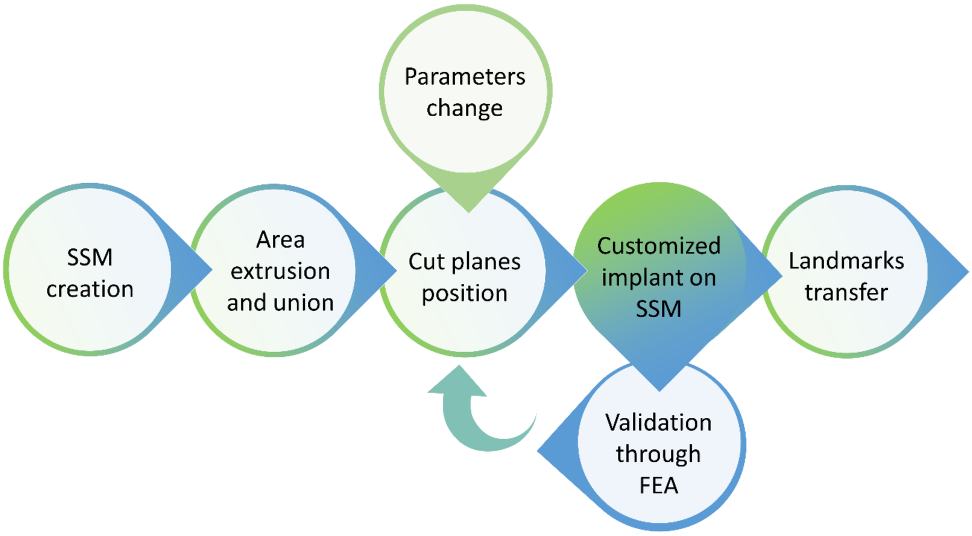

Figure 10: Phases for the creation of customized orthopedic prostheses.

2.3.2 MoCap Data Analysis

For MoCap data analysis, a custom software was developed with Python and the numpy library. The software's workflow followed a systematic approach. Initially, the raw virtual avatar of each patient, acquired as a bvh file from iPi Soft, was imported and parsed within the software. Subsequently, through analysis of the foot joint dynamics, the software automatically detected the foot-floor contact events, allowing for the automatic segmentation of the gait into swing and stance phases. The software then extracted the kinematics of the pelvis and trunk in the coronal plane, considering parameters such as mean angle, maximum angle, range of motion (ROM), peak angular velocity, and peak angular acceleration. The convention adopted in this software was to denote a descent toward the swinging limb with a positive sign and a descent in the opposite direction with a negative sign. The collected information was exported in Excel format for further analysis.

Gait analysis enables the collection of numerous variables, each providing valuable information. However, large dimensionality presents analytical challenges. Interpretation complexity can escalate, and there is an increased risk of Type I error (false positives) due to the higher likelihood of obtaining statistically significant results by chance. To address these challenges, Exploratory Factor Analysis

(EFA) is a valuable technique. EFA groups highly correlated variables into common factors, reducing the dataset's dimensionality to overcome the aforementioned challenges. The statistical analysis comprised three phases: (1) data preprocessing and data quality assessment; (2) EFA for dimensionality reduction and identification of dominant variables; (3) analysis of gait characteristics and gait changes. All computations were performed in Python with the following packages: numpy, pandas, scipy, and factor-analyzer.

Chapter 3. Applications

A selection of specific orthopedic conditions was made to demonstrate the adaptability and efficacy of the developed methodology. This chapter will present clinical case studies utilizing the previously described methods. DL techniques will be employed for the automatic segmentation of knee bones, with a particular focus on the femur [39]. A statistical shape model of ACL-injured femurs will be developed to study anatomical variations under pathological conditions [40]. Comprehensive assessments for patient care will be presented through several clinical cases. Morphological risk factors for ACL injury in the knee compartment [41][42] and instability in the shoulder [43] will be investigated. Furthermore, the methodology will support the diagnosis of shoulder disorders by examining patient morphology [44] and identifying Trendelenburg gait using MoCap systems [45]. The impact of meniscal tears on knee biomechanics will be explored through FE simulations [46]. Personalized treatment approaches for the knee compartment will be studied, including a method for designing and testing customized knee implants [47][48][49][50]. Lastly, the impact of total hip arthroplasty and various surgical approaches will be evaluated using gait analysis comparisons [51].
The following subchapters are structured as follows: first, the scientific background relevant to each specific clinical case is presented. Next, the procedure for each case is detailed, outlining how the previously described general method is adapted to address the specific case study. Finally, the results of these adaptations are presented, followed by a comprehensive discussion of the findings.

3.1 DL Methods for Automated Knee Bone Segmentation

Automated knee segmentation has attracted increasing attention with the diffusion of high-resolution magnetic resonance imaging and the maturation of deep learning techniques [39]. Convolutional neural networks have progressively replaced manual and semi-automatic procedures, offering improved reproducibility and reduced operator dependency.
Early studies frequently adopted hybrid frameworks that combined data-driven learning with explicit anatomical constraints. Approaches integrating convolutional networks with statistical shape models demonstrated improved robustness in the presence of anatomical variability and pathological alterations, particularly when training data were limited or heterogeneous [52]. Subsequent methods enhanced segmentation accuracy by coupling CNNs with probabilistic or deformable models, such as conditional random fields and simplex-based representations, although systematic comparisons with atlas-based techniques and analyses of training data requirements were often lacking [53].

Alternative strategies explored adversarial learning and reduced-dimensional network designs. Adversarially trained three-dimensional networks enabled the incorporation of broader contextual information at the expense of spatial resolution [54], whereas slice-based or 2.5D architectures sought to balance computational efficiency and three-dimensional consistency [55][56]. Comparative evaluations of automatic knee segmentation methods highlighted the strong performance of U-Net-derived architectures, while also revealing the frequent reliance on Dice-based metrics alone, without complementary surface- or volume-based analyses [57].

The availability of larger datasets has further improved segmentation reliability. Fully automated deep learning frameworks trained on extensive MR cohorts have achieved high accuracy and enabled the extraction of imaging biomarkers relevant to osteoarthritis [58]. Other studies have focused on specific anatomical structures, such as the femoral intercondylar notch, to support automated morphometric analysis and injury risk assessment, although population-specific constraints may limit generalizability [59]. CNN-based segmentation has also been applied to broader musculoskeletal visualization and preoperative planning tasks, even when trained on relatively small datasets optimized through dedicated acquisition protocols [33].

Despite the widespread adoption of residual network architectures for knee osteoarthritis detection and grading [60][61][62], their application to direct knee bone segmentation remains comparatively underexplored. SegResNet, originally developed for three-dimensional brain tumor segmentation and validated in the BraTS 2018 challenge [63], has demonstrated strong performance in other volumetric segmentation tasks, including liver and lesion delineation from MR data [64].

Within this context, the present study investigates the use of SegResNet for femoral bone segmentation and compares its performance with the widely adopted U-Net architecture, addressing the ongoing challenge of achieving clinically robust fully automatic segmentation.

The study was based on high-resolution proton density-weighted MR volumes acquired from 50 subjects, each consisting of more than 450 slices with a slice thickness of 0.55 mm. For computational processing, all scans were converted from DICOM to NIfTI format and spatially standardized through cropping and resizing.

Expert-generated three-dimensional femoral segmentations were used as reference annotations. To enhance robustness during training, data augmentation was applied. Automatic femur segmentation was performed using two three-dimensional convolutional architectures, U-Net and SegResNet, both adapted to volumetric data.

The dataset was divided into training, validation, and test subsets (75%, 20%, and 5%, respectively) using identical splits for both models. Network optimization involved exploring different learning rates (10^{-2} to 10^{-8}) and training durations (50-100 epochs), with a batch size of one adopted due to memory constraints. Segmentation accuracy was evaluated using quantitative performance metrics.

SegResNet employs a residual encoder-decoder structure that progressively encodes spatial information into higher-level features and reconstructs the final segmentation through upsampling, supported by skip connections that preserve anatomical detail. The implementation, based on the MONAI framework [34], uses an initial feature depth of eight filters, ReLU activations, batch normalization, and the Adam optimizer. Given the use of a single MR modality, the network input consists of one channel and produces a binary femoral segmentation output.

Segmentation results produced by the two convolutional networks were quantitatively evaluated against the reference models using standard overlap- and distance-based metrics, with particular emphasis on the Dice Similarity Coefficient and the Hausdorff Distance.

For both architectures, multiple training configurations were tested to assess the impact of learning rate and number of epochs on segmentation accuracy. In the case of U-Net, higher and more stable Dice values were generally obtained with lower learning rates, with the best performance observed when training for 100 epochs using a learning rate of 10^{-8}. SegResNet exhibited a stronger dependence on hyperparameter selection, showing reduced accuracy for intermediate learning rates and improved performance when extreme values were used, particularly in shorter training regimes.

Surface-based evaluation using Hausdorff Distance confirmed these trends, with U-Net achieving the lowest average distance values and SegResNet displaying greater variability across configurations. A comparative analysis of Dice distributions indicated that, while U-Net achieved slightly higher average accuracy, SegResNet outperformed U-Net under specific training conditions.

Based on combined Dice and Hausdorff criteria, the optimal configurations were identified for both models. The selected U-Net configuration reached an average Dice score of 0.942 and a Hausdorff Distance of 0.93 mm, whereas the optimal SegResNet configuration achieved a Dice score of 0.938 and a Hausdorff Distance of 1.00 mm (

Figure **11**). Overall, both networks demonstrated a high level of accuracy in femoral segmentation, with Dice values close to 0.94 and submillimetric surface discrepancies. Although U-Net showed greater robustness across training settings, SegResNet proved to be a competitive alternative for automated three-dimensional femoral reconstruction.

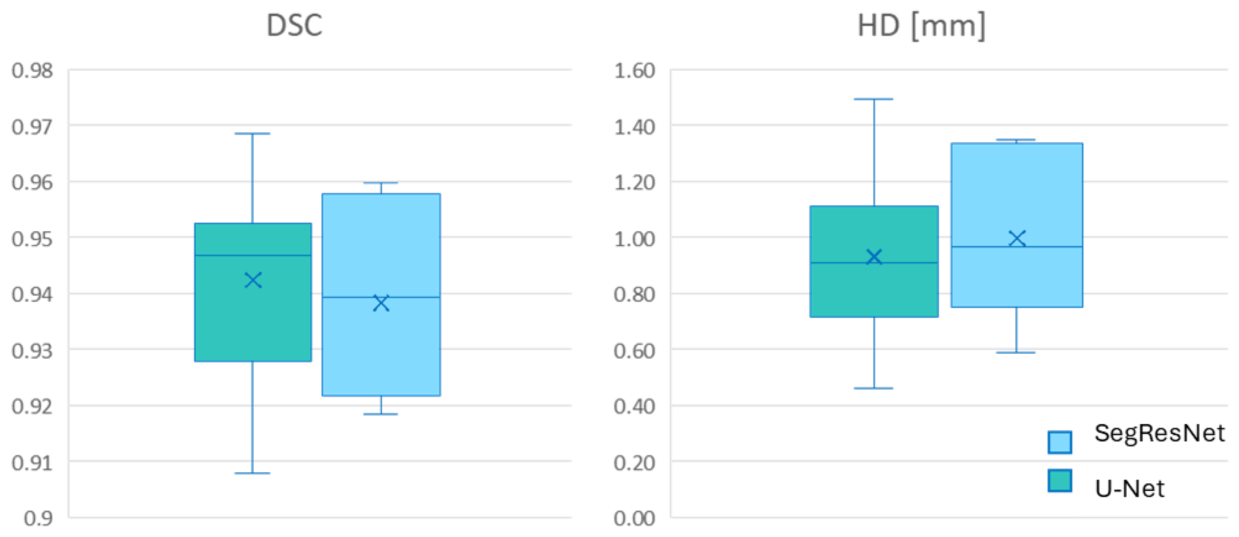

Figure 11: DSC and HD achieved by the best-performing U-Net and SegResNet models on test set.

3.2 Statistical Shape Modeling of ACL-Injured Femurs

Statistical Shape Modeling (SSM) provides a systematic framework to capture anatomical variability, supporting the study of bone morphology and its clinical implications [65] [66]. Applied to ACL-injured femurs, SSM enables quantification of geometric differences that may influence knee mechanics and injury risk.

Previous studies have explored femoral and tibial shape in ACL-injured populations using 2D radiographs or 3D imaging. Notable findings include associations between femoral notch geometry, intercondylar dimensions, and clinical outcomes following ACL rupture [67][68][69][70]. While some studies were limited by image resolution or small sample sizes, they highlight the relevance of bony morphology in ligamentous injuries.

In this work, SSM was constructed from 50 ACL-injured femurs. Volumes were normalized for size and orientation, with right femurs mirrored for uniformity [69]. Standard SSM procedures, vectorization, alignment, and principal component analysis, were applied to generate a population-based model. Ten anatomically relevant parameters of the distal femur, such as transepicondylar axis length, anterior and posterior mediolateral length, medial and lateral anteroposterior height, medial and lateral condylar width, intercondylar notch width, medial and lateral posterior condyle height, were measured on the mean femoral shape as well as on models generated by varying each principal component by ±3 standard deviations [71][72]. This procedure allowed quantification of how each mode of variation affected key distal femur dimensions.

Analysis of shape variation indicated that the first three principal components captured 80% of population variance. The primary mode reflected overall femur size, the second represented intercondylar notch width, and the third captured medial posterior condyle height (

Figure 12). These geometric features align with previously reported risk factors for ACL injury: narrower intercondylar notches and smaller medial condyles are associated with higher susceptibility to ligament rupture [73][74][75][76][77][78].

The identification of key anatomical patterns has practical implications. Knowledge of femoral morphology can guide personalized injury prevention strategies, such as targeted muscle strengthening, and inform surgical planning and rehabilitation tailored to individual anatomy. Integrating SSM-derived morphological insights into clinical practice may therefore enhance both injury mitigation and post-operative outcomes, supporting a more individualized approach to ACL injury management.

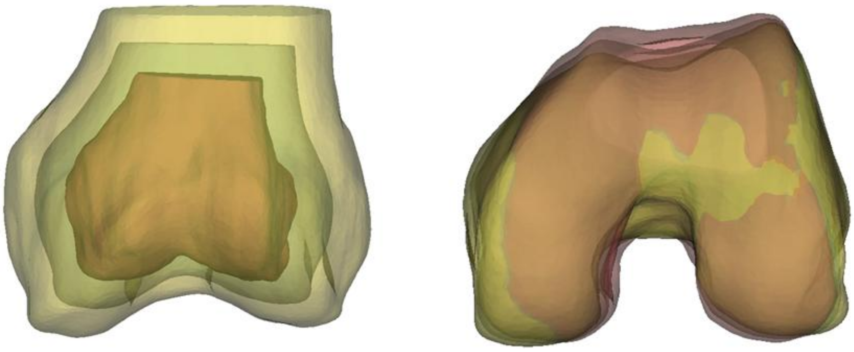

Figure 12: First and second modes of variation. The mean shape is shown in green, -3 SD in red, and +3 SD in yellow.

3.3 Risk factors identification

The identification of risk factors through morphological study involves a detailed analysis of anatomical structures to detect variations and abnormalities that may predispose individuals to certain conditions. This involves identifying key landmarks on the anatomical models and analyzing their spatial relationships. Deviations from the normative range of these morphological parameters can indicate potential risk factors for diseases. This approach allows for the early detection of structural anomalies that could lead to pathological conditions, enabling preventative measures and more personalized healthcare interventions tailored to the individual's specific anatomical risk profile.

Ad hoc packages were developed to assess risk factors, as described in chapter **Errore. L'origine riferimento non è stata trovata.**. The first case study is related to ACL injury [42], the second case study involves shoulder instability [43].

3.3.1 Risk factors for ACL injury

Numerous investigations have explored factors that may increase the likelihood of an anterior cruciate ligament rupture [79][80][81]. Reported contributors include demographic and patient-related characteristics, such as age, body mass index, and sex, as well as anatomical and biomechanical variables. Additional influences may arise from intrinsic elements, including genetic predisposition, and extrinsic conditions related to the sporting environment or training context [82].

Among these aspects, anatomical variability within the general population has received particular attention, as certain skeletal features of the knee may increase susceptibility to ligament injury. Several studies have therefore examined the relationship between ACL rupture and variations in the osseous structures surrounding the knee joint [77]. A detailed understanding of femoral and tibial morphology can improve recognition of individuals who may have a higher predisposition to this type of injury. In this context, the identification of structural risk factors may support the development of screening tools aimed at detecting athletes who could benefit from targeted prevention programs, especially those emphasizing activation and strengthening of the quadriceps, hamstrings, and core musculature [68].

Research examining the association between ACL injury and bone morphology has primarily focused on the structural characteristics of the femoral intercondylar notch and the tibial plateaus [79][80]. The femoral intercondylar notch corresponds to the concave space located between the medial and lateral femoral condyles, while the tibial plateaus represent the medial and lateral portions of the proximal tibial surface. Within this framework, several morphological parameters have been widely investigated in the literature, although the relevance of some additional indicators remains debated. The present work considers five commonly analyzed measures: notch shape, the Notch Width Index (NWI), the beta angle, the alpha angle, and the lateral tibial slope.

The femoral intercondylar notch is of particular relevance because it contains the ACL. Based on morphological appearance, the notch has been categorized into three principal configurations: A-shaped, characterized by a narrow apex; U-shaped, with a broader and more rounded apex; and W-shaped, distinguished by a double-peaked contour. Evidence from previous studies suggests that individuals presenting an A-shaped configuration may have a substantially higher probability of ACL injury compared with those exhibiting U- or W-shaped morphologies [20][81][83][84].

The Notch Width Index is defined as the ratio between the notch width (NW) and the femoral bicondylar width (BCW) [79][85]. This parameter provides a normalized measure of the size of the femoral intercondylar notch relative to the overall distal femoral width and is commonly used to

evaluate anatomical predisposition to injury of the ACL. Values below specific thresholds reported in the literature have been associated with a higher risk of ligament rupture [77][83][86][87][88][89]. Other morphological indicators have also been investigated in relation to ACL injury. One of these is the beta angle, defined as the angle between the femoral longitudinal axis and the Blumensaat line. Larger values of this angle have been proposed as a potential risk factor for ACL rupture [90][91][92]. Another parameter is the alpha angle, also referred to as the notch width angle, which describes the geometric configuration of the intercondylar notch [93][94][95][96][97]. Both angles have been examined in previous studies as potential markers of anatomical susceptibility to ligament injury.
The morphology of the tibial plateau has also been linked to ACL biomechanics. In particular, the lateral tibial slope has been identified in the literature as an important factor, as an increased slope may promote anterior translation of the tibia relative to the femur, thereby increasing mechanical stress on the ACL and potentially contributing to injury [90][98][99][100][101].
To facilitate the evaluation of these anatomical parameters, a dedicated extension for the 3D Slicer platform, was developed for the assessment of ACL injury risk. The tool integrates both two-dimensional and three-dimensional modeling approaches to perform morphological measurements. Three of the analyzed parameters, namely notch shape, alpha angle, and NWI, are evaluated using 3D anatomical models of the knee, since these measures depend on the spatial geometry of the intercondylar notch, as shown in Figure 13.

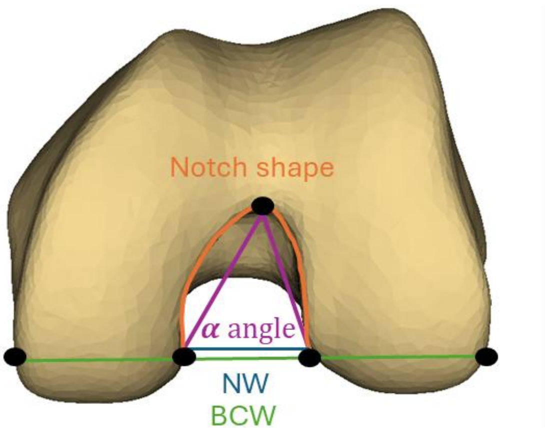

Figure 13: Risk factors for ACL injury measured on 3D models of the femur.

The remaining parameters, beta angle and tibial slope, are determined using a 2D approach because their measurement relies on the identification of specific planar anatomical references, including the Blumensaat line and the peak points of the tibial plateau.
Distance measurements are used to determine the bicondylar width and the notch width, which are required for the calculation of the NWI. Angular measurements are employed to evaluate the alpha

and beta angles as well as the tibial slope. In addition, curves can be drawn along the contour of the intercondylar notch to characterize its shape and to delineate regions of interest, which may also be used for area calculations.

The morphological analysis is supported by a specifically developed algorithm designed to improve the objectivity of notch classification. Computer-assisted classification of the intercondylar notch has been shown to enhance both intra-observer and inter-observer reliability [102]. In this framework, the operator initially traces the contour of the notch, after which the algorithm automatically determines its morphological category. The procedure consists of two main stages. First, the slope of the tangent along the traced curve is analyzed to determine whether the geometry corresponds to a U-shaped configuration. If this condition is not satisfied, the algorithm calculates the ratio between the distance separating the notch walls at the inferior region and the corresponding distance at the mid-portion. When this ratio deviates by more than ±7.5%, the notch is classified as A-shaped; otherwise, it is categorized as U-shaped.

Following the classification step, the software calculates the remaining morphological parameters based on the anatomical landmarks selected by the user. The tibial slope is determined using an approach similar to that proposed in previous studies [103]. The longitudinal tibial axis is identified by connecting the midpoints of the anterior-posterior widths measured at the proximal and distal portions of the tibia. The slope is then measured in the sagittal plane passing through the midpoint of the lateral tibial plateau as the angle between the line perpendicular to the tibial axis and the line connecting the anterior and posterior peak points of the plateau.

Although numerous studies have investigated these morphological parameters, a universal consensus has not yet been reached regarding the precise threshold values that should be considered indicative of increased risk. For this reason, the proposed framework adopts a conservative strategy, selecting the most restrictive thresholds reported in the scientific literature. Each parameter is evaluated against its respective cut-off value: A-shaped notch morphology, NWI lower than 0.29, alpha angle below 60°, beta angle greater than 37.7°, and lateral tibial slope exceeding 7.5°.

A binary scoring system is then applied to summarize the results. Parameters within the physiological range receive a score of 0, whereas those exceeding the defined thresholds are assigned a score of 1. The final risk score corresponds to the sum of these individual values, with higher totals indicating a greater potential predisposition to ACL injury based on the analyzed anatomical characteristics.

3.3.2 Risk factors for shoulder instability

Previous investigations have demonstrated that the risk of shoulder instability is influenced by multiple factors, including age, sex, joint hyperlaxity, soft tissue conditions, and specific bony anatomical characteristics, particularly those related to glenoid morphology [104] [105]. The glenoid plays a crucial role in preserving the stability of the glenohumeral joint. Key structural features of the glenoid include its height, width, depth, orientation, surface area, and overall shape [104].

Quantitative assessment of shoulder morphology, and especially of the glenoid bony structure, may help identify anatomical features associated with an increased susceptibility to anterior shoulder instability. Such evaluations can support the development of preventive strategies by identifying individuals at higher risk and providing tailored recommendations regarding sports participation or occupational activities. In addition, morphological analysis may assist clinicians in determining the most appropriate treatment approach following a first dislocation event by considering the patient's likelihood of recurrence [106].

A number of studies have explored the association between glenoid morphology and shoulder instability in order to better understand the anatomical factors contributing to this condition. Several morphometric parameters have been identified in the literature as particularly relevant for evaluating the risk of instability. For example, analyses based on magnetic resonance imaging in patients with anterior shoulder dislocation have highlighted the potential importance of the glenoid height-to-width ratio as a risk factor in specific populations [107]. Other investigations have suggested that the contribution of osseous and soft tissue factors to joint stability may differ between sexes. In male patients with instability, a reduction in glenoid width and surface area has been observed, along with a relatively smaller glenoid width compared with humeral width, whereas no clear morphological predictors of instability were identified in female patients [105].

Comparative studies between healthy individuals and patients with traumatic glenohumeral instability have also reported notable differences in joint morphology. In particular, the glenoid surface in patients with instability tends to be flatter than in control subjects, both in the anterior–posterior and superior–inferior directions [108]. It has been further hypothesized that a glenoid characterized by greater height, reduced width, and decreased concavity may be associated with a higher likelihood of recurrent instability [109]. Additional parameters that have been proposed as potential risk factors include glenoid shape, depth, the height-to-width ratio, and the maximal area of a circle that can be fitted within the glenoid cavity. Furthermore, increased glenoid anteversion has been reported as another anatomical feature potentially associated with recurrent anterior shoulder dislocation [110][111][112][113].

To facilitate the morphological evaluation of shoulder instability, a dedicated module has been implemented within the 3D Slicer software environment. This tool allows the measurement of several glenoid parameters, including height, width, shape, and version. Glenoid height is defined as the maximum distance between the superior margin of the glenoid at the level of the base of the coracoid process (corresponding to the 12 o'clock position) and the inferior pole (6 o'clock position). Glenoid width is measured along a direction orthogonal to the height and corresponds to the maximum distance between the anterior and posterior rims of the glenoid cavity. The height-to-width ratio is subsequently calculated by dividing these two measurements [114].

The morphology of the glenoid cavity can also be categorized based on the presence and definition of a characteristic notch. Three main configurations have been described: an inverted comma shape, characterized by a distinct notch; a pear-shaped configuration, in which the notch is less clearly defined; and an oval shape, in which no notch is present. These parameters can be evaluated within a three-dimensional environment using reconstructed models of the glenoid after virtual removal of the humeral head in order to isolate the articular surface (
Figure 14).

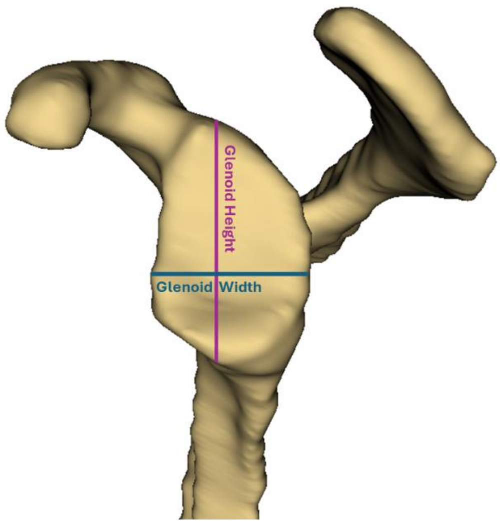

Figure 14: 3D view of a glenoid with displayed height and width.

The articular surface of the glenoid may additionally be described according to its curvature, which can appear concave, flat, or convex. When the surface is concave, the diameter of the concavity is defined by a straight line connecting the two outermost points of the glenoid rim. Glenoid depth is then determined as the perpendicular distance from the deepest point of the concavity to this diameter line [115]. This measurement is typically obtained from computed tomography images.

Another relevant parameter is glenoid version, which describes the orientation of the glenoid cavity relative to the scapular plane. This measurement can be obtained on two-dimensional images by drawing a line tangential to the glenoid articular surface and a second reference line extending from the medial border of the scapula to the center of the glenoid cavity. The angle formed anteromedially between these lines corresponds to glenoid retroversion. In physiologically normal shoulders, glenoid version values generally range from approximately 2° of anteversion to 9° of retroversion [110].
All the parameters described above can be obtained both from two-dimensional medical images and from three-dimensional models of the glenoid. The resulting measurements are then compared with established reference ranges and can be used to estimate an individual's potential risk of developing shoulder instability or experiencing recurrent dislocation.

3.4 Pathology identification and diagnosis

Pathology identification and diagnosis using 3D models and gait analysis provides a sophisticated approach to understand and treat musculoskeletal disorders.
Pathology identification and diagnosis through morphological study involves the precise analysis of anatomical structures to detect deviations from normal anatomical patterns that may indicate the presence of disease. These quantitative assessments provide a robust foundation for diagnosis, enabling clinicians to identify and diagnose pathologies more accurately and at an earlier stage.
By using MoCap data, it is possible to identify abnormal gait patterns associated with specific pathologies. It permits to enhance the diagnostic process and enable personalized therapeutic strategies.
In the following, two study cases are described. The first regards shoulder disorders diagnosis using morphological analysis [44]. The second involves the identification of Trendelenburg gait using MoCap data [45].

3.4.1 Shoulder disorders diagnosis

Morphological analysis of the shoulder can provide important information for the identification of musculoskeletal disorders such as rotator cuff tears and glenohumeral osteoarthritis. Several anatomical parameters described in the literature can be used to support the clinical evaluation of these conditions. For each parameter, physiological and pathological reference ranges have been reported, enabling a quantitative assessment of the patient's morphology and facilitating the interpretation of imaging findings. Among the parameters most frequently considered are cartilage thickness, acromiohumeral distance, acromial morphology, the acromion index, the acromioglenoid angle, and the critical shoulder angle.

Articular cartilage thickness in the shoulder joint is relatively small, with average values typically ranging between approximately 1 and 1.5 mm. This characteristic requires high spatial resolution in imaging techniques as well as accurate digital post-processing to ensure reliable measurements [116]. In the present analysis, cartilage thickness was evaluated using magnetic resonance imaging (
Figure 15). To improve measurement accuracy, three independent measurements were taken at the midportion of the glenoid at different depths, and their mean value was used as a representative estimate of cartilage thickness.

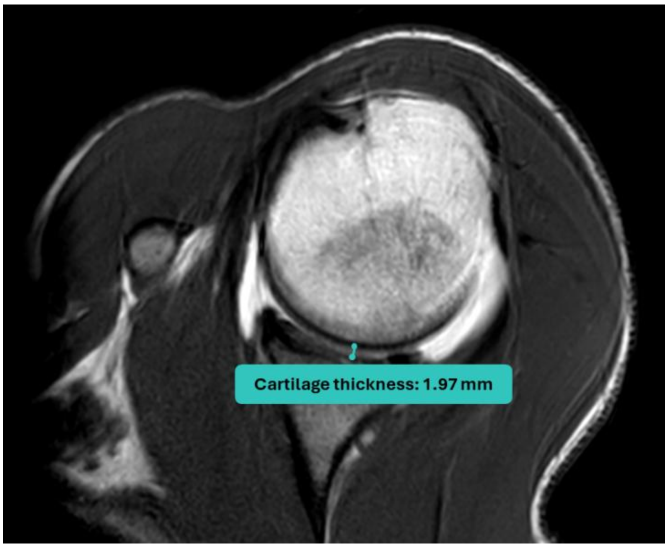

Figure 15: Cartilage thickness measurement.

Another relevant parameter is the acromiohumeral distance, defined as the minimal distance between the inferior surface of the acromion and the superior aspect of the humeral head. Several anatomical structures occupy the space between these two bony landmarks, including the rotator cuff tendons, the long head of the biceps tendon, the subacromial bursa, and the coracoacromial ligament. Alterations in the spatial relationship among these structures may lead to subacromial impingement [117]. In asymptomatic individuals, the acromiohumeral distance generally ranges between 12 mm and 14 mm. Markedly reduced values, particularly those below approximately 6 mm, are commonly associated with full-thickness rotator cuff tears, as shown in Figure 16 [118] [119].

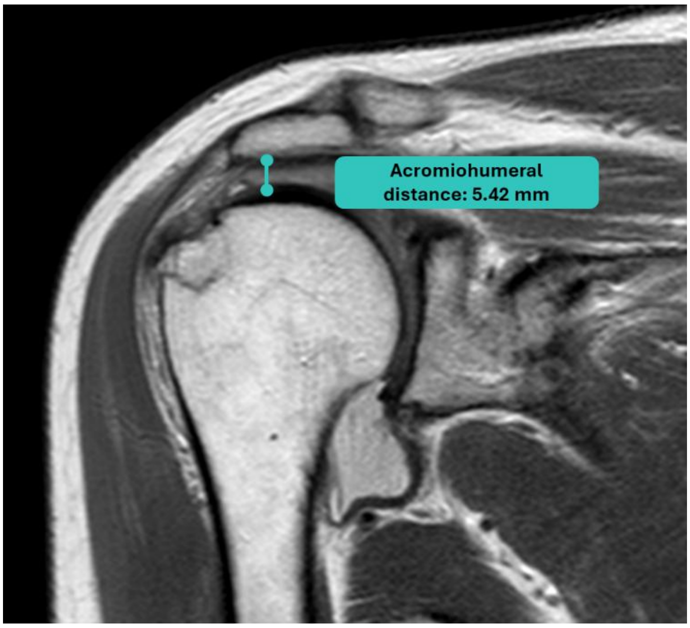

Figure 16: Acromiohumeral distance lower than 6 mm, sign of full thickness rotator cuff tear.

The morphology of the acromion also represents an important anatomical factor influencing shoulder biomechanics. Based on the contour of the acromial undersurface, four principal morphological patterns have been described: flat, curved, hooked, and reverse-curved [120]. The hooked configuration has been reported to show a stronger association with rotator cuff pathology compared with the other morphologies [121]. Consequently, acromial shape can influence both clinical evaluation and surgical decision-making, particularly when considering procedures such as acromioplasty. To reduce subjectivity in classification, quantitative approaches have been proposed. One method relies on identifying three reference points along the acromial undersurface and determining the location of the highest point along the acromial length. If the highest point lies within the middle third of the acromion, the morphology corresponds to a curved configuration, whereas a position within the anterior third is more consistent with a hooked morphology.

Patients affected by rotator cuff tears frequently present with a relatively large lateral extension of the acromion [122]. For this reason, the acromion index (AI) has been introduced as a quantitative descriptor of this anatomical feature. Acromion Index is defined as the ratio between the distance from the glenoid plane to the lateral border of the acromion (GA) and the distance from the glenoid plane to the lateral aspect of the humeral head (GH). Higher AI values (>0.73) indicate a greater lateral projection of the acromion, which has been associated with an increased prevalence of rotator cuff pathology, whereas low values (<0.60) are more commonly observed in shoulders affected by osteoarthritis [123]. Figure 17 show how measurements have been taken on the 3D models and on 2D images, respectively.

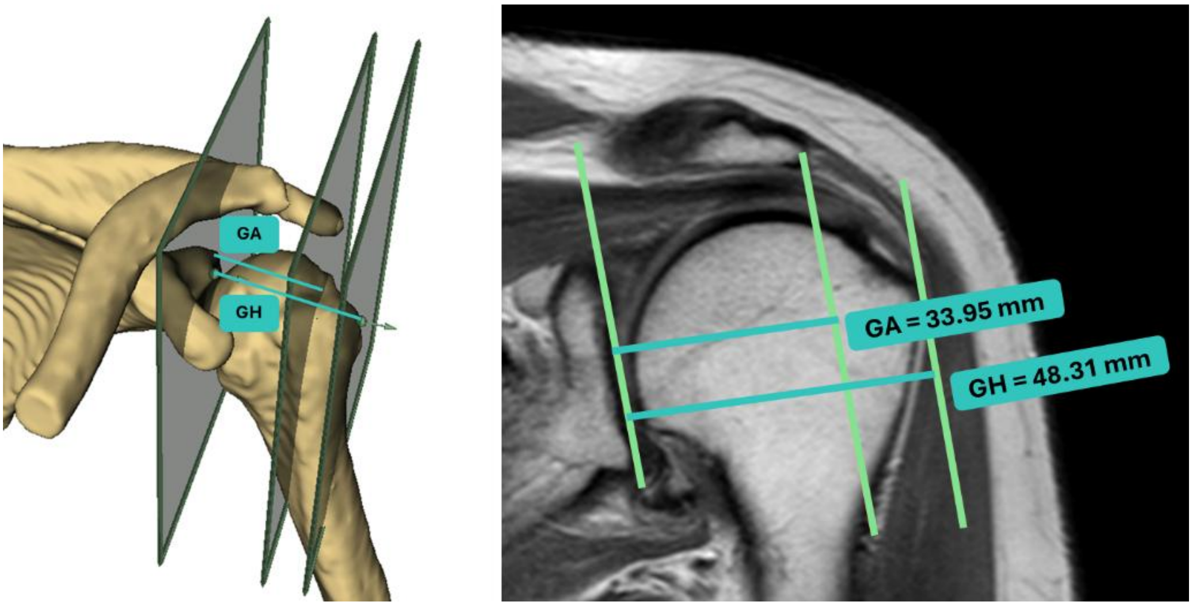

Figure 17: Measurements of glenoid-acromial distance and glenoid-humeral distance.

Another parameter that characterizes the relationship between the acromion and the glenoid is the acromioglenoid angle (AA). This angle is obtained by measuring the intersection between the glenoid reference plane and a line drawn parallel to the inferior surface of the acromion, as shown in Figure 18. Clinical studies have suggested that smaller values of this angle (<70°) may be associated with full-thickness rotator cuff tears, while asymptomatic shoulders generally exhibit larger values (average 80°) [124].

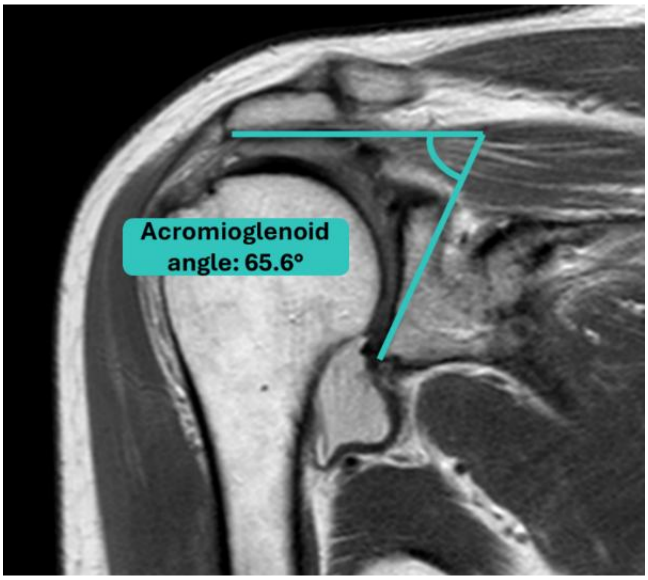

Figure 18: Acromioglenoid angle measurement, sign of rotator cuff tear.

The critical shoulder angle (CSA) is a widely used parameter that incorporates information about both glenoid inclination and the lateral extension of the acromion. It is defined as the angle formed between a line connecting the superior and inferior margins of the glenoid fossa and a second line extending from the inferior glenoid margin to the most lateral point of the acromion (Figure 19).

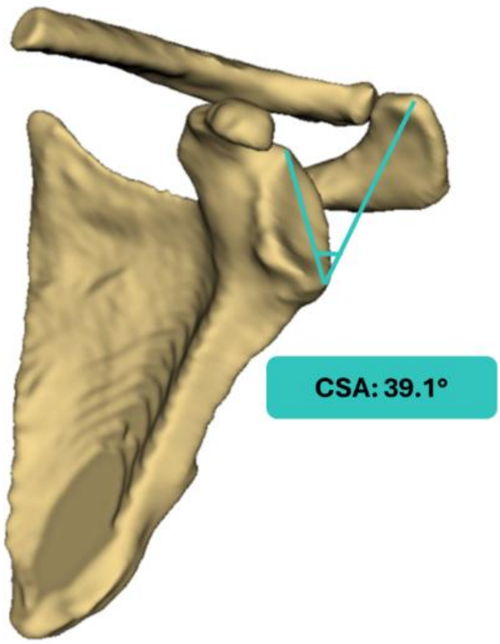

Figure 19: CSA measured on a 3D model highlights a rotator cuff injury.

One advantage of the CSA is that it is relatively independent of arm positioning, the width of the glenohumeral joint space, and the degree of humeral head flattening. Distinct CSA ranges have been associated with different pathological conditions. Lower values (<28°-30°) are typically observed in shoulders affected by primary osteoarthritis, intermediate values (30°-35°) correspond to normal anatomy, and higher values (>35°) are frequently reported in patients with rotator cuff tears [116] [123].

Compared with the acromion index alone, the CSA provides a more comprehensive description of shoulder morphology because it simultaneously reflects the inclination of the glenoid and the lateral extension of the acromion. However, although the CSA incorporates both elements, it does not allow the independent contribution of each factor to be directly distinguished. The angle represents a combined effect in which the individual components remain implicit. Both AI and CSA have demonstrated good predictive value for degenerative rotator cuff tears, whereas CSA appears to be more informative in the context of primary osteoarthritis.

From a biomechanical perspective, CSA can be considered the result of three underlying morphological components: glenoid inclination, lateral acromial extension, and acromial height. Glenoid inclination is traditionally measured using the Friedman method, which relies on identifying the long axis of the scapula and evaluating the orientation of the glenoid relative to this reference [125] [126]. In the present study, three-dimensional models of the shoulder were employed to determine glenoid inclination by measuring the angle between a reference plane and a plane defined by the superior and inferior portions of the glenoid labrum. Lateral acromial extension corresponds to the same measurement used in the numerator of the acromion index and represents the lateral projection of the acromion relative to the glenoid plane. Acromial height is defined as the vertical distance between the inferior margin of the glenoid and the inferior surface of the acromion.

The combined evaluation of these morphological parameters provides a more comprehensive understanding of the structural characteristics of the shoulder joint. Integrating multiple measurements enables the generation of a semi-automated quantitative report that may assist clinicians in interpreting imaging findings and assessing the patient's condition. This approach can serve as a decision-support tool by complementing the physician's clinical judgment with objective anatomical measurements. The proposed methodology was preliminarily tested on a cohort of 18 individuals. In most cases, the conclusions derived from the quantitative analysis were consistent with the diagnoses established by the physician, particularly in the presence of rotator cuff tears or osteoarthritis. In one case, the quantitative parameters remained within normal ranges, whereas the clinical report described suspected early-stage pathology, suggesting that the morphological changes had not yet become sufficiently pronounced to be detected through the evaluated metrics.

These findings highlight the potential value of quantitative morphometric analysis in supporting an evidence-based diagnostic approach. Morphological parameters can provide indications not only of existing pathology but also of a predisposition to future shoulder disorders. Nevertheless, defining universal thresholds remains challenging, as factors such as age, sex, lifestyle, and physical activity may influence anatomical variability and clinical interpretation.

Because the CSA plays a role in predicting both rotator cuff pathology and osteoarthritis, further analysis was conducted to investigate the relative contribution of its underlying components. Although the CSA value summarizes the combined effect of glenoid inclination, lateral acromial extension, and acromial height, the contribution of each individual factor cannot be directly inferred from the angle alone. Understanding the relative influence of these components is particularly important in the context of surgical treatment, where procedures may aim to restore physiological CSA values. Depending on the underlying morphological alteration, surgical correction may involve modifying glenoid inclination, reducing lateral acromial extension, or altering acromial height, and the choice among these strategies can have significant long-term biomechanical consequences.

Previous studies have explored whether glenoid inclination or lateral acromial extension plays a more dominant role in the development of rotator cuff tears and osteoarthritis. Evidence suggests that lateral acromial extension may represent the most influential factor in distinguishing between these two conditions. In particular, shoulders characterized by high CSA values combined with pronounced lateral acromial extension and relatively low glenoid inclination and acromial height appear to be more frequently associated with rotator cuff pathology rather than osteoarthritis.

To further investigate this relationship, a statistical analysis was performed using linear regression to evaluate the influence of glenoid inclination, lateral acromial extension, and acromial height on CSA variability. The results indicated a strong overall correlation, with approximately seventy percent of the variability in CSA explained by the combined contribution of the three parameters. Among them, lateral acromial extension and acromial height showed statistically significant associations with CSA, whereas glenoid inclination exhibited a weaker relationship. Specifically, CSA was found to increase with greater lateral acromial extension and decrease with increasing acromial height.

Overall, the proposed methodology provides a quantitative framework for the morphological evaluation of the shoulder. By integrating multiple anatomical parameters, it enables a comprehensive assessment of joint morphology and may support clinicians in diagnosing shoulder disorders. Although the present study involved a relatively small sample size, the results suggest that this approach may represent a promising tool for assisting clinical decision-making.

3.4.2 Trendelenburg gait identification

The Trendelenburg gait is commonly evaluated by asking the patient to stand on the limb suspected to be affected for approximately 30 seconds. When body weight is supported by that limb, a positive Trendelenburg sign is indicated by elevation of the pelvis on the same side. This alteration typically becomes more evident during walking [127][128]. A comprehensive evaluation should therefore integrate both static and dynamic assessments [129]. For this reason, gait analysis can be incorporated to objectively quantify locomotor alterations in individuals following total hip arthroplasty (THA). During the dynamic assessment, patients are instructed to walk over a short distance in order to observe the presence of the sign during locomotion.

The study involved fifteen individuals who had undergone THA. For each participant, two complete gait cycles were analyzed, resulting in a total of sixty swing phases. Each step was classified as exhibiting a Trendelenburg pattern according to criteria described in the literature [130]: pelvic tilt exceeding 4° relative to the swinging limb and trunk inclination greater than 5° relative to the pelvis. Based on the pelvic tilt threshold, thirty-seven steps met the criterion for a positive Trendelenburg pattern. When considering the trunk inclination criterion, twenty-four steps were classified as positive. Overall, approximately two thirds of the analyzed swing phases met at least one of the two criteria associated with the Trendelenburg gait pattern.

The investigation was subsequently extended to include additional information on pelvic and trunk kinematics. Alongside the maximum values of pelvic drop and trunk inclination, further parameters were evaluated, including mean angles, range of motion (ROM), angular velocity, and angular acceleration of the relevant segments. Statistical analysis using the Kruskal-Wallis test revealed significant differences between surgical approaches. In particular, individuals treated using the posterior surgical approach exhibited greater ROM, higher peak angular velocities, and higher peak angular accelerations in both trunk and pelvic movements, which may indicate increased instability during walking.

In this study, both pelvic drop and trunk inclination dynamics were incorporated into the identification of the Trendelenburg gait pattern [130]. A dedicated software tool was developed to automatically calculate these variables from a reconstructed virtual skeletal model. The resulting parameters were exported in spreadsheet format to allow further quantitative processing. Mean and peak values of pelvic and trunk angles were calculated in the frontal plane in accordance with previous biomechanical research. ROM values were determined for both trunk and pelvis segments. Additionally, kinematic descriptors such as peak velocity and peak acceleration were analyzed to investigate movement variability and postural stability during gait. Acceleration-based metrics derived from trunk and pelvic motion are known to be particularly sensitive indicators of balance deficits and locomotor instability [131].

3.5 Pathology impact

The impact of pathology on anatomical structures can be assessed using FEA. This allows for detailed analysis of stress distribution, strain, and deformation within the affected area. For instance, in the case of osteoarthritis, FEA can demonstrate how cartilage degeneration alters load-bearing patterns in the knee, leading to increased stress on subchondral bone and further joint degeneration. Similarly, for an ACL injury, FEA can show the altered biomechanics of the knee joint, illustrating how the absence of ligament support affects stability and load distribution during movement. By providing a quantitative and visual representation of these biomechanical changes, FEA helps in understanding

the extent and implications of the pathology, guiding clinicians in designing targeted interventions and optimizing treatment strategies to mitigate the adverse effects on the patient's biomechanics.
In the following, a case study involving menisci is reported [46]. The impact of different types of meniscal tears on knee biomechanics is investigated using FEA.

3.5.1 The impact of meniscal tears on knee biomechanics

Meniscal injuries are commonly classified according to the orientation of the tear, with the most frequent patterns being radial, longitudinal, and horizontal [24]. Radial tears extend from the inner free edge of the meniscus toward the peripheral attachment and disrupt the circumferential fiber architecture responsible for transmitting hoop stresses. This structural disruption compromises the ability of the meniscus to distribute loads effectively and may also lead to meniscal extrusion. Longitudinal tears run parallel to the circumferential fibers and divide the meniscus into inner and outer segments, whereas horizontal tears propagate parallel to the tibial plateau, separating the tissue into superior and inferior layers [132].
The menisci perform several essential biomechanical functions in the knee joint, including load transmission, shock absorption, joint stabilization, lubrication, and proprioception [133]. Among these roles, load distribution is particularly important, as the menisci are responsible for transmitting a substantial portion of the compressive forces acting across the knee [134]. Their circumferential fiber structure converts axial compression into tensile hoop stresses, allowing loads to be distributed over a wider contact area and improving joint congruity between the femoral condyles and tibial plateau [135]. Damage to the meniscus can therefore significantly alter knee biomechanics and impair the ability of the joint to dissipate mechanical loads [136].
Meniscal biomechanics has been widely investigated using both experimental and computational approaches. Early studies relied mainly on cadaveric specimens to examine mechanical behavior under controlled loading conditions. Although these experiments have provided valuable insights, they are limited by specimen availability and by the difficulty of reproducing the complex loading conditions experienced during daily activities. For this reason, finite element analysis has increasingly been used to investigate the biomechanical consequences of meniscal injuries. Computational models allow detailed evaluation of stress distribution, contact pressure, and tissue deformation within the knee joint [134][137][138].
Previous numerical investigations have shown that different tear configurations influence joint mechanics in distinct ways [138]. Radial lesions generally produce the most severe biomechanical alterations because they interrupt the circumferential fiber network responsible for transmitting hoop

stresses. As a consequence, they are associated with increased compressive and shear stresses within the joint and with greater alterations in load distribution [139]. Longitudinal tears may also modify stress patterns, particularly when they involve the anterior or posterior horns of the meniscus, while horizontal tears often lead to moderate but still clinically relevant biomechanical changes [134] [140]. Many computational studies have generated meniscal lesions artificially within models derived from a single healthy knee. Although this approach allows controlled comparisons between conditions, it may not fully reproduce the complex morphology of real pathological tears. Moreover, meniscal injuries frequently coexist with other joint abnormalities, such as ligament damage, cartilage degeneration, or meniscal displacement, which may further influence joint mechanics. Another limitation of several previous investigations is the use of a single model, which restricts the possibility of performing statistical analyses.

To address these limitations, the present study analyzes patient-specific finite element models derived from medical imaging data that include naturally occurring meniscal lesions. Subjects were grouped according to tear type, including radial, longitudinal, and horizontal lesions, together with a control group without meniscal injury. For each case, three-dimensional geometries of the distal femur, proximal tibia, articular cartilage, and menisci were reconstructed and used to develop computational models of the knee joint. The simulations aimed to evaluate the influence of different tear patterns on contact pressure at the tibiofemoral interface, internal stress within the meniscus, and the magnitude of meniscal extrusion. Figure 20 shows the main steps of the procedure.

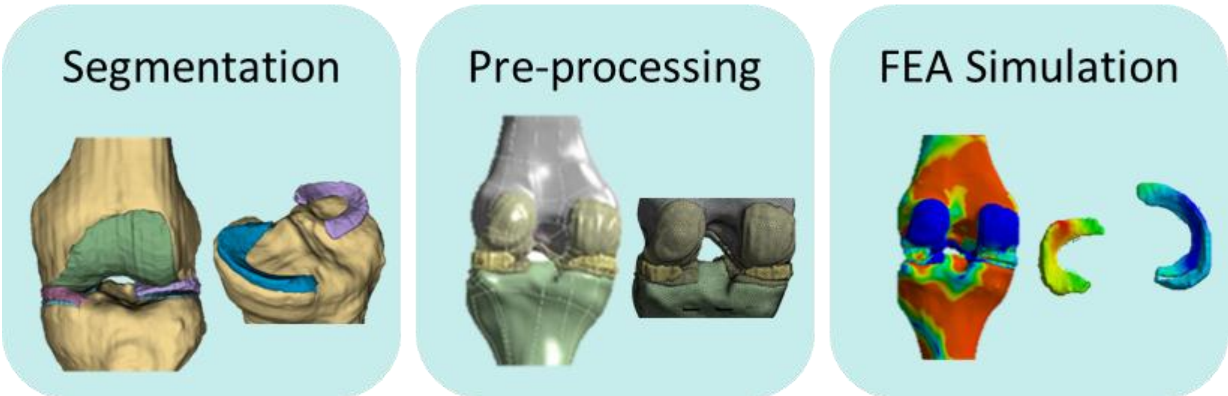

Figure 20: Procedure to study the impact of meniscal tears through FEA.

Under compressive loading conditions representative of physiological weight bearing (1150N), the models without meniscal injury showed higher contact pressures in the lateral compartment than in the medial compartment, which is consistent with previously reported biomechanical observations. When meniscal lesions were present, increases in contact pressure were generally observed in the compartment affected by the tear. Radial tears produced the most pronounced alterations, leading to substantial increases in local contact pressure (with a peak contact pressure reaching 6.65 MPa in a lateral radial tear).

Longitudinal tears involving the posterior horn of the medial meniscus also increased contact pressure within the medial compartment with a maximum value of 4.61 MPa. In some cases, separation of the torn segments resulted in distinct deformation patterns that may contribute to the progression of the lesion. Horizontal tears produced smaller changes in contact pressure but still altered the distribution of loads across the joint surface.

The analysis of internal stresses revealed similar trends. In intact knees, higher shear stresses were typically observed in the lateral meniscus, reflecting the greater load-bearing role of this compartment. Radial tears generated the highest stress concentrations (max shear stress = 6.25 MPa), particularly near the lesion margins, indicating that disruption of the circumferential fibers substantially increases mechanical loading within the tissue. Longitudinal and horizontal tears also produced elevated stress levels in the affected compartment, although their effect was less pronounced than that associated with radial lesions (
Figure 21).

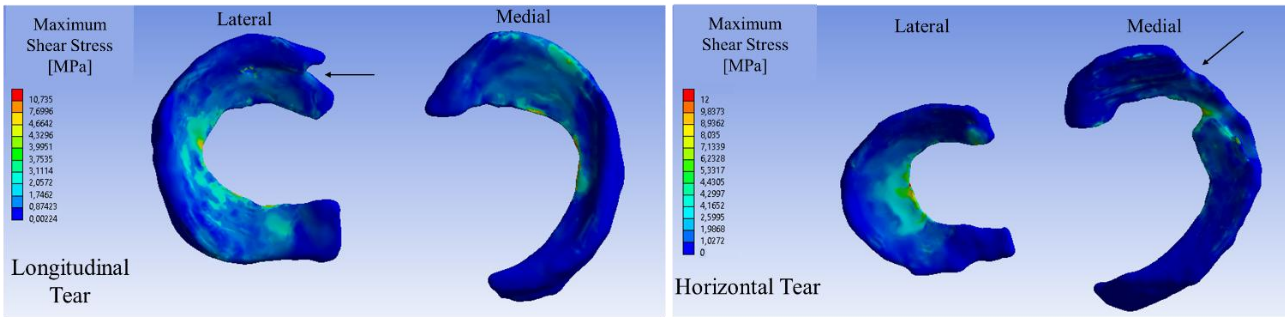

Figure 21. Maximum shear stress on menisci with longitudinal tear and horizontal tear, respectively.

Meniscal extrusion was also evaluated as an indicator of meniscal stability. Extrusion reduces the functional contact area between the meniscus and the articular cartilage and limits the ability of the tissue to transmit hoop stresses [134]. The simulations indicated that radial tears resulted in the greatest extrusion values (max meniscal extrusion = 2.26 mm), while longitudinal and horizontal tears produced more moderate displacement (<1.5 mm). Although the observed extrusion values remained within the range generally considered physiological [141], increased displacement may still compromise the mechanical function of the meniscus and contribute to progressive cartilage degeneration.

Overall, the results suggest that radial tears have the most detrimental biomechanical impact on the knee joint because they interrupt the structural continuity of the meniscus. By increasing contact pressure, elevating internal stresses, and promoting meniscal extrusion, these lesions can significantly alter joint mechanics and may accelerate degenerative processes. The use of patient-specific finite element models derived from real clinical cases provides a more realistic representation of pathological conditions and may offer valuable information for understanding the biomechanical consequences of meniscal injuries and supporting clinical decision-making.

3.6 Personalized treatment

Personalized treatment involves tailoring medical interventions to the unique anatomical and physiological characteristics of each patient, ensuring that therapeutic strategies are optimally suited to their specific needs. By leveraging detailed morphological data obtained through imaging techniques and Statistical Shape Modeling, it is possible to design customized prosthetics, implants, and orthotics that precisely fit the patient’s anatomy. In orthopedic surgery, personalized implants can be created to match the exact contours of a patient's bone structure, improving fit and functionality while reducing the risk of complications. Additionally, personalized treatment plans can incorporate insights from biomechanical analyses, FEA, to predict how a patient’s body will respond to different interventions. By focusing on the patient’s unique anatomical and biomechanical profile, personalized treatment enhances the effectiveness of medical care, promotes faster recovery, and leads to better overall outcomes.

In the following, a case study for the design and test of customized knee implant is presented [47][48][49][50].

3.6.1 Customized knee prosthesis

In advanced stages of knee osteoarthritis, when conservative treatments are no longer effective, Total Knee Arthroplasty (TKA) is the most widely adopted surgical procedure. The operation replaces the damaged articular cartilage and portions of the underlying bone with artificial prosthetic components. Conventional TKA systems are typically manufactured in standardized sizes based on anthropometric datasets representing average anatomical dimensions [142][143]. Although these designs generally provide acceptable outcomes for many patients, they do not always account for the wide variability in knee morphology observed across individuals.

Human knee anatomy shows considerable variation not only in overall size but also in several geometric characteristics, including the mediolateral to anteroposterior ratio of the distal femur, condylar curvature, joint-line orientation, and the morphology of the trochlear groove and tibial plateaus [144]. Population-based studies have also demonstrated relevant differences associated with sex and ethnicity [145]. As a consequence, the geometry of commercially available implants does not always match the patient's bony anatomy precisely [146]. This mismatch can result in overhang, where the implant extends beyond the bone surface and irritates surrounding soft tissues, or undercoverage, where the resected bone is not fully supported by the prosthetic component. Both situations may negatively influence postoperative outcomes.

To avoid implant overhang, surgeons sometimes select a smaller femoral component than the one suggested by the bone dimensions. However, downsizing the component may expose more cancellous bone and reduce the posterior condylar offset, which can affect joint stability and limit the flexion range of the knee. In addition, inadequate bone coverage may increase the risk of postoperative bleeding and compromise implant fixation [146]. These limitations have motivated the development of patient-specific prosthetic components designed to better reproduce individual joint anatomy [147].

Customized knee implants are generated using anatomical information obtained from preoperative medical imaging, typically computed tomography or magnetic resonance imaging [144]. Through image segmentation, three-dimensional models of the distal femur, proximal tibia, and patella are reconstructed. These models enable detailed evaluation of joint alignment and bone wear, allowing surgeons to simulate the surgical procedure virtually. During this planning phase, the native alignment of the joint can be reproduced, bone resections can be optimized, and prosthetic components can be designed to match the patient's anatomy. Once the design is validated, the implants and associated surgical guides can be manufactured using advanced production techniques such as additive manufacturing.

Patient-specific implants aim to restore joint anatomy more accurately than conventional prostheses, improving bone coverage and reducing the likelihood of implant overhang or undercoverage. Improved conformity between the implant and the bone surface may reduce postoperative swelling and bleeding from exposed bone surfaces, potentially accelerating recovery [148]. Furthermore, by reproducing the natural geometry of the knee, customized prostheses may allow more physiological joint kinematics and improved patient satisfaction compared with standard implants [147].

Several biomechanical studies have investigated the performance of customized knee prostheses [142][147]. Computational analyses have shown that patient-specific implants can reduce contact stresses on polyethylene tibial inserts when compared with conventional off-the-shelf components. Lower contact stresses are associated with reduced wear of the polyethylene insert, which is a major factor influencing the long-term durability of knee prostheses [149]. Additional studies have also reported that customized implants may reproduce joint kinematics more closely to those observed in healthy knees, which may contribute to improved functional outcomes [150].

Despite these advantages, the design of customized implants remains challenging. Many of the existing approaches rely on manual intervention during the design process, which increases both development time and cost [151][152][153]. Some methods extract morphological parameters from three-dimensional models of the knee to guide implant design [152], while others employ rapid prototyping techniques to manufacture prosthetic components [153]. However, these workflows often require the use of multiple software platforms and extensive manual adjustments. Moreover, several published studies have validated their design procedures on a single case, limiting the generalizability of their results [154].

Another important factor influencing the success of TKA is the alignment strategy adopted during surgery [155]. Traditionally, mechanical alignment has been the standard approach. In this technique, the distal femur and proximal tibia are resected perpendicular to the mechanical axis of the lower limb, aiming to achieve a neutral hip-knee-ankle alignment [156]. However, recent research has shown that many individuals naturally exhibit slight deviations from this theoretical alignment even before the onset of osteoarthritis [157]. As a result, restoring the patient’s original joint orientation may be more physiologically appropriate than forcing a neutral mechanical alignment.

This concept has led to increasing interest in kinematic alignment, a surgical technique that attempts to preserve the patient’s natural joint-line orientation and ligament balance [156]. By reproducing the original anatomical alignment, kinematic techniques aim to restore knee motion more closely to the native joint. Clinical and biomechanical studies have suggested that kinematically aligned TKA may provide improved gait characteristics and reduced joint loading compared with mechanically aligned procedures [158] [159] [160].

Material selection also plays a critical role in implant performance. In conventional TKA systems, femoral components are typically manufactured from cobalt-chromium alloys, while tibial components are commonly made from titanium alloys. The tibial insert, which acts as the articulating surface between the femoral and tibial components, is usually produced from ultra-high molecular weight polyethylene (UHMWPE). Although UHMWPE has demonstrated excellent clinical performance, wear of the polyethylene insert remains a major factor limiting implant longevity [161]. For this reason, alternative materials such as poly-ether-ether-ketone (PEEK) and carbon-fiber-reinforced PEEK have been investigated due to their favorable mechanical properties and biocompatibility [162] [163].

The present study proposes an automated framework for the design and evaluation of customized knee implants, as shown in Figure 22. The workflow begins with the generation of a Statistical Shape Model of the femur, which serves as the anatomical reference for defining the design procedure. The distal femoral region of the SSM is analyzed in detail in order to identify the typical spatial distribution of the articular cartilage and to reconstruct the original joint surface that may have been altered by degenerative processes.

Figure 22. Procedure to design and test customized implant.

To approximate the natural cartilage boundary, a reference curve is traced along the femoral surface following the anatomical region normally occupied by the cartilage layer. This curve defines the area where cartilage reconstruction is required. The selected surface region is then extruded outward along the local surface normal vectors to recreate the missing cartilage volume. The extrusion thickness is generally set to approximately 1.5 mm, corresponding to the average cartilage thickness of the distal femur, although this parameter can be adjusted if patient-specific measurements are available. The reconstructed cartilage volume is subsequently merged with the femoral geometry through a Boolean union operation, producing a continuous model representing the restored joint surface.

Because osteoarthritic knees frequently present osteophytes, which are abnormal bony outgrowths at the joint margins, an additional surface processing step is performed. A median smoothing filter with a kernel size of 3 mm is applied to reduce surface irregularities and obtain a more homogeneous anatomical surface while preserving the overall geometry of the femoral condyles.

In the subsequent stage, cutting planes are defined on the processed model according to clinically relevant surgical parameters. These parameters include the alignment strategy, the configuration of femoral resections, and the material used for the tibial insert. Two alignment strategies are investigated: a horizontal alignment and a physiological alignment that preserves the natural orientation of the joint line. In addition, two configurations of femoral resections are considered: a conventional design based on five resection planes and an alternative configuration including an additional posterior facet. The influence of two different tibial insert materials, UHMWPE and PEEK, is also evaluated.

Finite Element Analysis is then employed to assess the biomechanical performance of the different implant configurations. Each model is subjected to identical boundary conditions and loading scenarios representing physiological weight-bearing conditions. A vertical compressive load of 1150N is applied to the femur while the tibia is constrained, enabling simulation of contact interactions between the prosthetic components. Stress distribution and deformation patterns are analyzed to evaluate the mechanical behavior of the implant under load.

Following the design phase, anatomical landmarks defined on the reference SSM are transferred automatically to the patient-specific femoral model. This operation ensures that the customized implant geometry is accurately aligned with the patient’s anatomy. The accuracy of the landmark transfer process is quantitatively evaluated using similarity metrics such as the Dice Similarity Coefficient and the Hausdorff Distance, which measure the geometric correspondence between the automatically generated model and reference solutions.

To validate the effectiveness of the proposed approach, a comparative biomechanical analysis is performed. A baseline model representing the healthy knee condition is reconstructed by generating three-dimensional models of the femur, tibia, femoral cartilage, tibial cartilage, and menisci. In parallel, a model of a standard off-the-shelf prosthesis is obtained through three-dimensional scanning and aligned with the patient’s anatomy. Finite element simulations are then conducted for three different scenarios: the reconstructed healthy knee, the standard prosthetic configuration, and the customized implant.

The comparative analysis focuses on key biomechanical indicators, including contact pressure at the tibiofemoral interface, stress distribution within the implant components, and displacement behavior. The results show that implant material has the most significant influence on stress levels within the tibial insert, followed by the alignment strategy, whereas the number of femoral resection facets has a smaller effect. Among the evaluated configurations, the combination of physiological alignment, six femoral resection facets, and a UHMWPE tibial insert produced the lowest peak stress values (6.43 MPa) and a more uniform stress distribution between the medial and lateral compartments.

Additional analyses of displacement patterns confirm that implant material strongly influences deformation behavior. Stiffer materials such as PEEK exhibit lower deformation but higher stress concentrations, whereas UHMWPE allows greater elastic deformation while maintaining lower stress levels.

The automated design procedure was also compared with a conventional manual workflow. Quantitative similarity metrics demonstrated a strong geometric correspondence between the two approaches (DSC = 0.77), while the automated method significantly reduced the time required to generate the implant model (from 31 to 8 min). Moreover, the automated pipeline resulted in slightly reduced bone resection volumes, preserving a larger portion of the patient's native bone structure, which may be advantageous in potential revision surgeries.

Finally, the customized implant was compared with the standard off-the-shelf prosthesis and the reconstructed healthy knee model. The patient-specific solution produced a more homogeneous stress distribution across the tibial insert, whereas the standard implant showed more localized stress concentrations. Since excessive localized loading can accelerate polyethylene wear and reduce implant longevity, a more uniform stress distribution is considered beneficial for long-term prosthesis performance.

Overall, the proposed automated pipeline demonstrates the feasibility of rapidly generating patient-specific knee implants while simultaneously evaluating their biomechanical performance through finite element simulation. By integrating anatomical modeling, computational biomechanics, and automated design strategies, this approach may support the development of prosthetic components that more closely replicate individual anatomy and improve functional outcomes following total knee arthroplasty.

3.7 Treatment impact

Measuring the impact of surgery using MoCap technology involves the detailed analysis of a patient's movement patterns before and after the procedure to assess changes in gait, posture, and overall mobility. A case study related to total hip arthroplasty is reported [51].

3.7.1 The impact of THA

Total hip arthroplasty (THA) is widely recognized as one of the most effective surgical interventions for the treatment of advanced hip osteoarthritis. Several operative techniques have been developed to access the hip joint, the most common being the posterior, lateral, and anterior approaches, each of which involves different anatomical structures [164][165]. Current trends reported in national joint registries indicate that the posterior approach is the most frequently adopted technique, followed by the lateral and the anterior approaches.

The posterior approach allows preservation of the hip abductor muscles and flexors; however, the external rotator muscles must be detached to expose the joint, and particular care is required to avoid injury to the sciatic nerve. The lateral approach provides direct visualization of the joint but requires partial detachment of the gluteal musculature and a proximal portion of the vastus lateralis, which may contribute to postoperative gait alterations such as limping. In contrast, the direct anterior approach has gained increasing attention because it exploits an intermuscular plane between the sartorius, rectus femoris, iliopsoas, and tensor fasciae latae, allowing access to the joint while minimizing muscle disruption [166][167][168]. Despite these technical differences, the relative advantages of each approach remain debated, particularly with respect to surgical complexity, complication rates, rehabilitation time, and patient-reported outcomes. Since each technique affects specific soft-tissue structures, it has been hypothesized that the surgical approach may influence the early recovery process and postoperative gait patterns [169].

Clinical outcomes following THA are commonly evaluated using patient-reported questionnaires that assess pain relief, functional recovery, and quality of life. Among the most frequently used instruments are the Western Ontario and McMaster Universities Osteoarthritis Index (WOMAC), the Harris Hip Score, the Short Form-36 (SF-36), the PROM-10 questionnaire, and the Hip disability and Osteoarthritis Outcome Score (HOOS) [170][171]. Although these tools provide valuable information on patient perception and functional status, they remain subjective and may not capture subtle functional changes [172][173]. For this reason, growing attention has been directed toward objective biomechanical assessments of gait following THA [174][175][176][177].

Gait analysis provides quantitative measurements of locomotor performance and offers detailed insight into the biomechanical adaptations occurring after surgery [176]. By examining temporal and spatial characteristics of walking, this technique allows researchers to investigate the mechanisms underlying gait alterations and to evaluate the effectiveness of surgical and rehabilitation strategies. Moreover, quantitative gait metrics may assist clinicians in predicting the duration of postoperative hospitalization and in optimizing rehabilitation protocols. Most previous investigations have examined gait at medium- and long-term follow-up intervals, typically three, six, or twelve months after surgery [178] [179]. Consequently, limited information is available regarding the very early phase of recovery immediately after the procedure. This aspect has become increasingly relevant because the length of hospital stay after THA has progressively decreased over time, often lasting only a few days. Assessing gait performance within the first postoperative week may therefore provide useful information for designing timely rehabilitation strategies.

To explore the short-term biomechanical effects of THA, patients were assessed both before surgery and seven days afterward. This short follow-up interval was selected to capture the immediate functional consequences of the procedure. The initial dataset included a series of spatiotemporal gait parameters measured for both the affected and unaffected limbs, together with indices describing gait symmetry. These parameters characterized walking features such as gait cycle duration, stance and swing phase percentages, step and stride lengths, step width, and peak swing velocity. The collected gait measurements were subsequently processed using multivariate statistical techniques to identify the underlying patterns in the dataset. Exploratory factor analysis (EFA) is a multivariate statistical method designed to uncover hidden relationships within a set of observed variables.

The factor analysis identified four principal domains that explained most of the variability in the dataset. These domains corresponded to well-established components of human gait and were interpreted as pace, phases, rhythm, and postural control [180]. The pace domain describes overall walking speed and stride characteristics, while the phases domain represents the temporal distribution of stance and swing intervals during the gait cycle. Rhythm reflects the temporal organization and consistency of stepping patterns, and postural control is associated with balance-related parameters and the spatial configuration of foot placement.

The analysis revealed substantial modifications in gait patterns one week after surgery. The most pronounced variation was observed in the rhythm domain, indicating significant alterations in the temporal structure of walking. Postural control also showed a marked change, suggesting that patients adopted compensatory strategies to maintain stability during the early postoperative phase. In contrast, the pace domain decreased, reflecting the reduction in walking speed typically observed shortly after surgery. Changes in the phases domain were present but less pronounced compared with the other domains.

An examination of the dominant variables associated with each domain highlighted several characteristic modifications in postoperative gait. Patients required more time to complete each gait cycle, indicating slower walking patterns. In addition, the distance between successive foot placements increased, resulting in a wider base of support likely adopted to improve balance. The proportion of the gait cycle spent in the stance phase also increased, meaning that the foot remained in contact with the ground for longer periods. At the same time, stride length decreased, reflecting shorter steps and a more cautious walking strategy.

Although these general trends were observed across all surgical approaches, differences emerged when comparing the groups. In particular, the duration of the stance phase differed among approaches. Patients who underwent the posterior approach exhibited shorter relative stance times compared with those treated with the lateral or anterior techniques. Interestingly, the stance phase duration observed in the posterior approach group deviated from values typically associated with healthy walking patterns, whereas the lateral and anterior approach groups showed values closer to physiological references.

The findings of this study demonstrate that measurable alterations in gait biomechanics are already present during the first postoperative week following total hip arthroplasty. The use of exploratory factor analysis provided a systematic framework for interpreting the complex dataset obtained from gait measurements by reducing numerous variables to a smaller number of meaningful domains. This dimensionality reduction approach also minimizes the risk of statistical errors that may arise when a large number of parameters are analyzed independently.

Through this approach, it was possible to identify the principal aspects of locomotor function that are affected during the early stages of postoperative recovery. The observed changes in rhythm, postural control, and pace indicate that patients modify their walking behavior shortly after surgery, likely adopting protective strategies aimed at maintaining stability and reducing mechanical stress on the operated joint.

Chapter 4: Discussion

This research presents the development of a patient digital twin framework designed to support orthopedic assessment and treatment across a wide range of musculoskeletal conditions. The proposed system integrates several advanced technologies, including three-dimensional modeling, deep learning algorithms, statistical shape modeling, finite element analysis, and motion capture within a unified analytical environment.

Through the evaluation of multiple clinical scenarios, the work demonstrates the flexibility and reliability of the proposed methodology in addressing different orthopedic pathologies. The results emphasize the relevance of morphological analysis for identifying potential risk factors and improving diagnostic procedures. Furthermore, the framework proved effective for investigating the biomechanical consequences of pathological conditions, evaluating personalized therapeutic strategies, and objectively assessing surgical outcomes through gait analysis.

Although three-dimensional anatomical models are widely recognized for providing more detailed and accurate representations of bone structures, morphological investigations in clinical practice still rely largely on traditional two-dimensional measurements. This limitation is mainly related to the complexity of 3D reconstruction workflows, which often require specialized expertise and considerable processing time. To address this issue, the present work introduces an integrated framework that combines automated image segmentation using deep learning techniques with automated morphological analysis of the reconstructed anatomical models. In particular, the SegResNet architecture was evaluated as a tool for the automated segmentation of femoral structures from medical images. The performance of the segmentation algorithm was influenced by the size of the training dataset. In this study, a dataset consisting of 50 patients was employed. Despite being smaller than those used in many large-scale investigations, the model achieved satisfactory results, reaching a Dice Similarity Coefficient of up to 0.94. This level of accuracy is generally considered adequate for most orthopedic applications. Expanding the dataset with additional annotated images would likely further improve the robustness and generalizability of the segmentation model.

To facilitate morphological analysis, dedicated software tools were developed to support the identification of anatomical risk factors and the diagnosis of orthopedic conditions. These tools were designed to be accessible to clinicians without advanced experience in 3D modeling. The workflow requires the user to identify a limited number of anatomical landmarks on the bone surface, after which the software performs the analysis in a semi-automated manner. This approach simplifies the evaluation process while reducing the subjectivity associated with manual measurements.

The implementation of statistical shape modeling also played a key role in the proposed framework. SSM was employed both for automated landmark placement and for performing morphological measurements. This approach enabled the investigation of anatomical variability and pathological alterations while also facilitating the design of patient-specific prosthetic components. In particular, the methodology proved effective for analyzing complex anatomical structures such as the femur. By examining shape variations across the population, it becomes possible to identify correlations between different anatomical features and to better characterize morphological patterns associated with conditions such as anterior cruciate ligament injuries.

In addition to morphological analysis, this work proposes a novel automated pipeline for the design of customized implant components. Because each patient exhibits unique anatomical characteristics, three-dimensional modeling techniques allow the creation of prosthetic components tailored to individual anatomy. Automation of the design process was achieved through the use of template-based landmark registration. Automating this procedure offers several advantages, including significant reductions in design time and the possibility for clinicians without specialized modeling expertise to generate customized implant geometries within seconds. Nevertheless, the precision achieved by the automated procedure does not yet fully match the level attainable by experienced engineers. Furthermore, the current validation of the pipeline is limited to computational analyses, as the study did not include the production of physical implant prototypes or clinical trials. Consequently, the translation of this automated design pipeline into clinical practice would require additional experimental validation and would likely face regulatory considerations.

Finite element analysis was also incorporated into the framework to investigate biomechanical alterations associated with orthopedic pathologies, including meniscal injuries. Integrating biomechanical simulations with clinical data may provide valuable support for surgical decision-making. Through computational modeling, FEA enables the evaluation of mechanical changes induced by specific pathological conditions and may help surgeons assess whether surgical intervention is necessary by simulating the biomechanical consequences of meniscal tears. In the present study, simulations were performed using linear elastic material models for the menisci and articular cartilage under static loading conditions at full knee extension. Future work will aim to develop more advanced models that incorporate the viscoelastic properties of biological tissues and the contribution of major knee ligaments, allowing the simulation of more realistic and dynamic joint behavior.

Motion capture technology was another essential component of the proposed digital twin framework, particularly for analyzing locomotor function and evaluating the effects of surgical procedures. A dedicated gait analysis model was developed for patients undergoing total hip arthroplasty. The model identified several characteristic changes in walking patterns during the early postoperative phase, including an increase in gait cycle duration, a reduction in stride length, an enlargement of the base of support, and longer ground contact times. The analysis also revealed differences among surgical approaches: patients treated with the posterior approach exhibited significantly shorter stance times compared with those who underwent lateral or anterior procedures. Additionally, individuals operated using the posterior approach appeared to show a greater tendency toward Trendelenburg gait patterns. In this investigation, gait data were collected using markerless motion capture systems, which represented the most suitable option considering the fragility of the patient population. However, it should be noted that markerless systems may present some limitations in measurement accuracy under certain conditions, even though precautions were taken during data acquisition to minimize potential errors.

Future developments of this research will involve testing the framework on larger and more diverse patient populations, as well as extending its application to additional orthopedic conditions in order to improve the generalizability of the methodology. The generation of highly accurate 3D anatomical models and the analysis of large datasets derived from medical imaging and motion capture systems require considerable computational resources. Continuous validation of the models will therefore be essential to ensure accuracy and reliability. Moreover, although the proposed approach shows considerable potential, its implementation in routine clinical practice would require appropriate training for healthcare professionals and substantial investment in technological infrastructure.

The successful adoption of digital twin technologies in orthopedics also depends on close collaboration among multiple professional figures, including orthopedic surgeons, biomedical engineers, data scientists, and clinicians. Each discipline contributes essential expertise for the development and application of such complex systems. Importantly, the proposed framework is not intended to replace the role of clinicians but rather to provide decision-support tools that enhance clinical evaluation and treatment planning. In this context, ethical concerns regarding the use of artificial intelligence are mitigated because the final responsibility for clinical decisions remains with the physician. In addition, the integration of complementary technologies, such as predictive artificial intelligence models capable of estimating treatment outcomes, may further improve the performance and clinical relevance of the system.

In summary, this work establishes a methodological basis for the development of patient digital twins in orthopedic medicine. The proposed framework provides an integrated platform capable of supporting prevention, diagnosis, treatment planning, and outcome evaluation across different musculoskeletal disorders. By combining advanced imaging analysis, biomechanical simulation, and motion analysis, the approach offers a comprehensive and patient-specific perspective on orthopedic care, paving the way for future advancements in personalized medicine.

List of figures

References

[1] R. P. Fischer, A. Volpert, P. Antonino, and T. D. Ahrens, “Digital patient twins for personalized therapeutics and pharmaceutical manufacturing,” *Front. Digit. Health*, vol. 5, p. 1302338, Jan. 2023, doi: 10.3389/FDGTH.2023.1302338/BIBTEX.

[2] Y. Toritsuka and Y. Yamada, “A View of Predisposing Factors by Novel 3D Imaging Techniques for the PF Joint,” *Advances in Knee Ligament and Knee Preservation Surgery*, pp. 249–263, Jan. 2022, doi: 10.1007/978-3-030-84748-7_21.

[3] O. Ronneberger, P. Fischer, and T. Brox, “U-Net: Convolutional Networks for Biomedical Image Segmentation,” *Lecture Notes in Computer Science (including subseries Lecture Notes in Artificial Intelligence and Lecture Notes in Bioinformatics)*, vol. 9351, pp. 234–241, 2015, doi: 10.1007/978-3-319-24574-4_28.

[4] L. Wade, L. Needham, P. McGuigan, and J. Bilzon, “Applications and limitations of current markerless motion capture methods for clinical gait biomechanics,” *PeerJ*, vol. 10, Feb. 2022, doi: 10.7717/PEERJ.12995.

[5] A. Vallée, “Digital twin for healthcare systems,” *Front. Digit. Health*, vol. 5, p. 1253050, 2023, doi: 10.3389/FDGTH.2023.1253050.

[6] E. Katsoulakis *et al.*, “Digital twins for health: a scoping review,” *npj Digital Medicine 2024 7:1*, vol. 7, no. 1, pp. 1–11, Mar. 2024, doi: 10.1038/s41746-024-01073-0.

[7] K. Aubert *et al.*, “Development of Digital Twins to Optimize Trauma Surgery and Postoperative Management. A Case Study Focusing on Tibial Plateau Fracture,” *Front. Bioeng. Biotechnol.*, vol. 9, p. 722275, Oct. 2021, doi: 10.3389/FBIOE.2021.722275/BIBTEX.

[8] S. Banik, R. M. Rangayyan, and G. S. Boag, “Landmarking and Segmentation of 3D CT Images,” *Synthesis Lectures on Biomedical Engineering*, vol. 30, pp. 1–148, Mar. 2009, doi: 10.2200/S00185ED1V01Y200903BME030.

[9] G. Dougherty, “Applications of Medical Image Processing in the Diagnosis and Treatment of Spinal Deformity”, doi: 10.1007/978-1-4419-9779-1_10.

[10] F. Auricchio and S. Marconi, “3D printing: clinical applications in orthopaedics and traumatology,” *EFORT Open Rev.*, vol. 1, no. 5, p. 121, May 2016, doi: 10.1302/2058-5241.1.000012.

[11] T. Falk *et al.*, “U-Net: deep learning for cell counting, detection, and morphometry,” *Nature Methods 2018 16:1*, vol. 16, no. 1, pp. 67–70, Dec. 2018, doi: 10.1038/s41592-018-0261-2.

[12] G. Colombo, G. Facoetti, and C. Rizzi, “A digital patient for computer-aided prosthesis design,” *Interface Focus*, vol. 3, no. 2, Apr. 2013, doi: 10.1098/RSFS.2012.0082.

[13] M. Yahya, J. A. Shah, K. A. Kadir, Z. M. Yusof, S. Khan, and A. Warsi, “Motion capture sensing techniques used in human upper limb motion: a review,” *Sensor Review*, vol. 39, no. 4, pp. 504–511, Jul. 2019, doi: 10.1108/SR-10-2018-0270.

[14] “Review on Motion Capture Technology | Enhanced Reader.”

[15] W. W. T. Lam, Y. M. Tang, and K. N. K. Fong, “A systematic review of the applications of markerless motion capture (MMC) technology for clinical measurement in rehabilitation,” *J. Neuroeng. Rehabil.*, vol. 20, no. 1, pp. 1–26, Dec. 2023, doi: 10.1186/S12984-023-01186-9/TABLES/2.

[16] K. Das, T. de Paula Oliveira, and J. Newell, “Comparison of markerless and marker-based motion capture systems using 95% functional limits of agreement in a linear mixed-effects modelling framework,” *Scientific Reports 2023 13:1*, vol. 13, no. 1, pp. 1–15, Dec. 2023, doi: 10.1038/s41598-023-49360-2.

[17] “Scientific Image and Illustration Software | BioRender.” Accessed: May 30, 2025. [Online]. Available: https://www.biorender.com/

[18] H. Madry *et al.*, “Early osteoarthritis of the knee,” *Knee Surg. Sports Traumatol. Arthrosc.*, vol. 24, no. 6, pp. 1753–1762, Jun. 2016, doi: 10.1007/S00167-016-4068-3.

[19] D. Primorac *et al.*, “Knee Osteoarthritis: A Review of Pathogenesis and State-Of-The-Art Non-Operative Therapeutic Considerations,” *Genes 2020, Vol. 11, Page 854*, vol. 11, no. 8, p. 854, Jul. 2020, doi: 10.3390/GENES11080854.

[20] C. F. van Eck, C. A. Q. Martins, S. M. Vyas, U. Celentano, C. N. van Dijk, and F. H. Fu, “Femoral intercondylar notch shape and dimensions in ACL-injured patients,” *Knee Surg. Sports Traumatol. Arthrosc.*, vol. 18, no. 9, pp. 1257–1262, 2010, doi: 10.1007/S00167-010-1135-Z.

[21] S. Takahashi, Y. Nagano, W. Ito, Y. Kido, and T. Okuwaki, “A retrospective study of mechanisms of anterior cruciate ligament injuries in high school basketball, handball, judo, soccer, and volleyball,” *Medicine*, vol. 98, no. 26, p. e16030, Jun. 2019, doi: 10.1097/MD.0000000000016030.

[22] J. Evans, A. Mabrouk, and J. l. Nielson, “Anterior Cruciate Ligament Knee Injury,” *StatPearls*, Nov. 2023, Accessed: Sep. 26, 2024. [Online]. Available: https://www.ncbi.nlm.nih.gov/books/NBK499848/

[23] M. Shemesh *et al.*, "Effects of a novel medial meniscus implant on the knee compartments: imaging and biomechanical aspects," *Biomech. Model. Mechanobiol.*, vol. 19, no. 6, pp. 2049–2059, Dec. 2020, doi: 10.1007/S10237-020-01323-6.

[24] K. T. Boyd and P. T. Myers, "Meniscus preservation; rationale, repair techniques and results," *Knee*, vol. 10, no. 1, pp. 1–11, 2003, doi: 10.1016/S0968-0160(02)00147-3.

[25] S. Kopf *et al.*, "Management of traumatic meniscus tears: the 2019 ESSKA meniscus consensus," *Knee Surgery, Sports Traumatology, Arthroscopy*, vol. 28, no. 4, pp. 1177–1194, Apr. 2020, doi: 10.1007/S00167-020-05847-3/TABLES/2.

[26] M. A. Miniato, P. Anand, and M. Varacallo, "Anatomy, Shoulder and Upper Limb, Shoulder," *StatPearls*, Jul. 2023, Accessed: Sep. 26, 2024. [Online]. Available: https://www.ncbi.nlm.nih.gov/books/NBK536933/

[27] C. Mitchell, A. Adebajo, E. Hay, and A. Carr, "Shoulder pain: diagnosis and management in primary care," *BMJ*, vol. 331, no. 7525, pp. 1124–1128, Nov. 2005, doi: 10.1136/BMJ.331.7525.1124.

[28] S. N. Sambandam, V. Khanna, A. Gul, and V. Mounasamy, "Rotator cuff tears: An evidence based approach," *World J. Orthop.*, vol. 6, no. 11, p. 902, Dec. 2015, doi: 10.5312/WJO.V6.I11.902.

[29] L. Laudicina and R. D'Ambrosia, "Management of irreparable rotator cuff tears and glenohumeral arthritis," *Orthopedics*, vol. 28, no. 4, pp. 382–388, 2005, doi: 10.3928/0147-7447-20050401-13.

[30] M. Tsutsumi, A. Nimura, and K. Akita, "Clinical anatomy of the musculoskeletal system in the hip region," *Anat. Sci. Int.*, vol. 97, no. 2, pp. 157–164, Mar. 2022, doi: 10.1007/S12565-021-00638-3/FIGURES/5.

[31] J. Runhaar, Ö. Özbulut, M. Kloppenburg, M. Boers, J. W. J. Bijlsma, and S. M. A. Bierma-Zeinstra, "Diagnostic criteria for early hip osteoarthritis: first steps, based on the CHECK study," *Rheumatology (Oxford)*, vol. 60, no. 11, p. 5158, Nov. 2021, doi: 10.1093/RHEUMATOLOGY/KEAB111.

[32] K. S. Sim, M. E. Nia, C. P. Tso, and T. K. Kho, "Brain Ventricle Detection Using Hausdorff Distance," *Emerging Trends in Applications and Infrastructures for Computational Biology, Bioinformatics, and Systems Biology: Systems and Applications*, pp. 523–531, Mar. 2016, doi: 10.1016/B978-0-12-804203-8.00034-1.

[33] C. P. S. Kulseng, V. Nainamalai, E. Grøvik, J. T. Geitung, A. Årøen, and K. I. Gjesdal, "Automatic segmentation of human knee anatomy by a convolutional neural network applying

a 3D MRI protocol," *BMC Musculoskelet. Disord.*, vol. 24, no. 1, pp. 1–12, Dec. 2023, doi: 10.1186/S12891-023-06153-Y/FIGURES/6.

[34] "MONAI - Home." Accessed: Jun. 27, 2024. [Online]. Available: https://monai.io/

[35] "MONAI Label - Product Page." Accessed: Jun. 27, 2024. [Online]. Available: https://monai.io/label.html

[36] "3D Slicer image computing platform | 3D Slicer." Accessed: Jun. 27, 2024. [Online]. Available: https://www.slicer.org/

[37] A. Van Haver *et al.*, "A statistical shape model of trochlear dysplasia of the knee," *Knee*, vol. 21, no. 2, pp. 518–523, 2014, doi: 10.1016/J.KNEE.2013.11.016.

[38] L. Quintens *et al.*, "Anatomical Variation of the Tibia – a Principal Component Analysis," *Scientific Reports 2019 9:1*, vol. 9, no. 1, pp. 1–10, May 2019, doi: 10.1038/s41598-019-44092-8.

[39] A. Ghidotti, A. Vitali, D. Regazzoni, M. W. Cohen, and C. Rizzi, "Comparative Analysis of Convolutional Neural Network Architectures for Automated Knee Segmentation in Medical Imaging: A Performance Evaluation," *J. Comput. Inf. Sci. Eng.*, vol. 24, no. 5, May 2024, doi: 10.1115/1.4064450/1193886.

[40] A. Ghidotti, D. Regazzoni, M. W. Cohen, and V. Condello, "A Statistical Shape Model of Femur of ACL-Injured Knee," *Proceedings of the ASME Design Engineering Technical Conference*, vol. 2A-2024, Nov. 2024, doi: 10.1115/DETC2024-142809.

[41] A. Ghidotti, A. Cattaneo, A. Vitali, and D. Regazzoni, "A Morphological Evaluation Tool in 3D Slicer," 2022, doi: 10.14733/cadconfP.2022.225-229.

[42] A. Ghidotti, A. Cattaneo, A. Vitali, D. Regazzoni, and C. Rizzi, "ACL Morsky: Semi-automatic Tool for Assessing the Risk of Developing an Anterior Cruciate Ligament Injury," *Comput. Aided. Des. Appl.*, vol. 20, no. 4, pp. 731–748, 2023, doi: 10.14733/cadaps.2023.736-748.

[43] A. Ghidotti and C. Rizzi, "Morphological Evaluation of Shoulder Instability: A Customized Module Title: Morphological evaluation of shoulder instability: a customized module," pp. 313–317, doi: 10.14733/cadconfP.2023.313-317.

[44] A. Ghidotti, F. Locatelli, N. Belotti, D. Regazzoni, and C. Rizzi, "A Morphological Evaluation of Shoulder Parameters: A Medical Support Tool for the Diagnosis," *Proceedings of the ASME Design Engineering Technical Conference*, vol. 2, Nov. 2022, doi: 10.1115/DETC2022-89974.

[45] A. Ghidotti, A. Cattaneo, A. Vitali, D. Regazzoni, C. Rizzi, and G. Fiorentino, "Towards Kinematic Assessment of Trendelenburg Gait After Total Hip Arthroplasty Using Mocap Systems," *Lecture Notes in Mechanical Engineering*, pp. 224–232, 2024, doi: 10.1007/978-3-031-52075-4_26.

[46] A. Ghidotti, A. Vitali, D. Regazzoni, and C. Rizzi, "An Investigation of Innovative 3D Modelling Procedures for Patient-specific Total Knee Arthroplasty," *Comput. Aided. Des. Appl.*, vol. 19, no. 2, pp. 306–319, 2022, doi: 10.14733/cadaps.2022.306-319.

[47] A. Ghidotti, D. Landi, D. Regazzoni, and C. Rizzi, "A 3D Modeling Approach to Realize and Test Customized Knee Implants," *Lecture Notes in Mechanical Engineering*, pp. 242–252, 2023, doi: 10.1007/978-3-031-15928-2_21.

[48] A. Ghidotti, D. Landi, D. Regazzoni, and C. Rizzi, "Evaluation of Clinical and Technical Parameters to Customize Total Knee Arthroplasty Implants," *J. Comput. Inf. Sci. Eng.*, vol. 22, no. 6, Dec. 2022, doi: 10.1115/1.4055427/1145938.

[49] A. Ghidotti, A. Vitali, D. Regazzoni, and C. Rizzi, "Human Modelling and Design of Custom-Made Knee Implants: Definition of an Automatic Procedure," *ASME International Mechanical Engineering Congress and Exposition, Proceedings (IMECE)*, vol. 2, Feb. 2024, doi: 10.1115/IMECE2023-112550.

[50] A. Cattaneo *et al.*, "Motion acquisition of gait characteristics one week after total hip arthroplasty: a factor analysis," *Arch. Orthop. Trauma Surg.*, vol. 144, no. 5, pp. 2347–2356, May 2024, doi: 10.1007/S00402-024-05245-1/FIGURES/4.

[51] F. Ambellan, A. Tack, M. Ehlke, and S. Zachow, "Automated segmentation of knee bone and cartilage combining statistical shape knowledge and convolutional neural networks: Data from the Osteoarthritis Initiative," *Med. Image Anal.*, vol. 52, pp. 109–118, Feb. 2019, doi: 10.1016/J.MEDIA.2018.11.009.

[52] Z. Zhou, G. Zhao, R. Kijowski, and F. Liu, "Deep convolutional neural network for segmentation of knee joint anatomy," *Magn. Reson. Med.*, vol. 80, no. 6, p. 2759, Dec. 2018, doi: 10.1002/MRM.27229.

[53] H. Chen *et al.*, "Knee Bone and Cartilage Segmentation Based on a 3D Deep Neural Network Using Adversarial Loss for Prior Shape Constraint," *Front. Med. (Lausanne).*, vol. 9, p. 792900, May 2022, doi: 10.3389/FMED.2022.792900/BIBTEX.

[54] P. L. Pröve *et al.*, "Automated segmentation of the knee for age assessment in 3D MR images using convolutional neural networks," *Int. J. Legal Med.*, vol. 133, no. 4, pp. 1191–1205, Jul. 2019, doi: 10.1007/S00414-018-1953-Y.

[55] B. Robert and P. Boulanger, “Automatic Bone Segmentation from MRI for Real-Time Knee Tracking in Fluoroscopic Imaging,” *Diagnostics 2022, Vol. 12, Page 2228*, vol. 12, no. 9, p. 2228, Sep. 2022, doi: 10.3390/DIAGNOSTICS12092228.

[56] M. Perslev, A. Pai, J. Runhaar, C. Igel, and E. B. Dam, “Cross-Cohort Automatic Knee MRI Segmentation With Multi-Planar U-Nets,” *Journal of Magnetic Resonance Imaging*, vol. 55, no. 6, pp. 1650–1663, Jun. 2022, doi: 10.1002/JMRI.27978.

[57] X. Tang *et al.*, “Fully Automatic Knee Joint Segmentation and Quantitative Analysis for Osteoarthritis from Magnetic Resonance (MR) Images Using a Deep Learning Model,” *Med. Sci. Monit.*, vol. 28, pp. e936733-1, Jun. 2022, doi: 10.12659/MSM.936733.

[58] M. Li *et al.*, “Automatic segmentation model of intercondylar fossa based on deep learning: a novel and effective assessment method for the notch volume,” *BMC Musculoskelet. Disord.*, vol. 23, no. 1, pp. 1–10, Dec. 2022, doi: 10.1186/S12891-022-05378-7/TABLES/4.

[59] J. H. Cueva, D. Castillo, H. Espinós-Morató, D. Durán, P. Díaz, and V. Lakshminarayanan, “Detection and Classification of Knee Osteoarthritis,” *Diagnostics*, vol. 12, no. 10, Oct. 2022, doi: 10.3390/DIAGNOSTICS12102362.

[60] W. Liu *et al.*, “A Novel Focal Ordinal Loss for Assessment of Knee Osteoarthritis Severity,” *Neural Process. Lett.*, vol. 54, no. 6, pp. 5199–5224, Dec. 2022, doi: 10.1007/S11063-022-10857-Y.

[61] S. A. Revathi, B. Sathish Babu, and K. N. Subramanya, “Deep Learning Approach for Segmenting and Classifying Knee Osteoarthritis Using MR Images,” pp. 209–221, 2023, doi: 10.1007/978-981-19-7041-2_16.

[62] A. Myronenko, “3D MRI brain tumor segmentation using autoencoder regularization,” *Lecture Notes in Computer Science (including subseries Lecture Notes in Artificial Intelligence and Lecture Notes in Bioinformatics)*, vol. 11384 LNCS, pp. 311–320, 2019, doi: 10.1007/978-3-030-11726-9_28.

[63] Y. Kamkova, E. Pelanis, A. Bjørnerud, B. Edwin, O. J. Elle, and R. P. Kumar, “A Fast Method for Whole Liver- and Colorectal Liver Metastasis Segmentations from MRI Using 3D FCNN Networks,” *Applied Sciences 2022, Vol. 12, Page 5145*, vol. 12, no. 10, p. 5145, May 2022, doi: 10.3390/APP12105145.

[64] A. Van Haver *et al.*, “A statistical shape model of trochlear dysplasia of the knee,” *Knee*, vol. 21, no. 2, pp. 518–523, Mar. 2014, doi: 10.1016/J.KNEE.2013.11.016.

[65] L. Quintens *et al.*, "Anatomical Variation of the Tibia – a Principal Component Analysis," *Scientific Reports 2019 9:1*, vol. 9, no. 1, pp. 1–10, May 2019, doi: 10.1038/s41598-019-44092-8.

[66] V. Eggerding *et al.*, "Knee shape might predict clinical outcome after an anterior cruciate ligament rupture," *Bone Joint J.*, vol. 96-B, no. 6, pp. 737–742, 2014, doi: 10.1302/0301-620X.96B6.32975.

[67] V. Pedoia *et al.*, "Three-dimensional MRI-based statistical shape model and application to a cohort of knees with acute ACL injury," *Osteoarthritis Cartilage*, vol. 23, no. 10, pp. 1695–1703, Oct. 2015, doi: 10.1016/J.JOCA.2015.05.027.

[68] S. K. Polamalu, V. Musahl, and R. E. Debski, "Tibiofemoral bony morphology features associated with ACL injury and sex utilizing three-dimensional statistical shape modeling," 2020, doi: 10.1002/jor.24952.

[69] M. A. Bowes, L. S. Lohmander, C. B. H. Wolstenholme, G. R. Vincent, P. G. Conaghan, and R. B. Frobell, "Marked and rapid change of bone shape in acutely ACL injured knees - an exploratory analysis of the Kanon trial," *Osteoarthritis Cartilage*, vol. 27, no. 4, pp. 638–645, Apr. 2019, doi: 10.1016/J.JOCA.2018.12.021.

[70] C. Phombut, S. Rooppakhun, and B. Sindhupakorn, "Morphometric Analysis and Three-Dimensional Computed Tomography Reconstruction of Thai Distal Femur," *Applied Sciences 2021, Vol. 11, Page 1052*, vol. 11, no. 3, p. 1052, Jan. 2021, doi: 10.3390/APP11031052.

[71] Z. Chen, Y. Wang, X. Li, K. Wang, Z. Li, and P. Yang, "An automatic measurement system of distal femur morphological parameters using 3D slicer software," *Bone*, vol. 156, p. 116300, Mar. 2022, doi: 10.1016/J.BONE.2021.116300.

[72] J. L. Yellin, R. L. Parisien, N. S. Talathi, A. S. Farooqi, M. S. Kocher, and T. J. Ganley, "Narrow Notch Width is a Risk Factor for Anterior Cruciate Ligament Injury in the Pediatric Population: A Multicenter Study," *Arthrosc. Sports Med. Rehabil.*, vol. 3, no. 3, p. e823, Jun. 2021, doi: 10.1016/J.ASMR.2021.01.024.

[73] M. Tuca *et al.*, "Stenotic Intercondylar Notch as a Risk Factor for Physeal-Sparing ACL Reconstruction Failure: A Case-Control Study," *JAAOS Global Research & Reviews*, vol. 5, no. 7, Jul. 2021, doi: 10.5435/JAAOSGLOBAL-D-21-00143.

[74] R. Andrade *et al.*, "Notch morphology is a risk factor for ACL injury: a systematic review and meta-analysis," *Journal of ISAKOS*, vol. 1, no. 2, pp. 70–81, Mar. 2016, doi: 10.1136/JISAKOS-2015-000030.

[75] K. Suprasanna, T. Chamala, and A. Kumar, “Comparison of anatomical risk factors for noncontact anterior cruciate ligament injury using magnetic resonance imaging,” *J. Clin. Orthop. Trauma*, vol. 10, no. 1, pp. 143–148, Jan. 2019, doi: 10.1016/J.JCOT.2017.08.002.

[76] B. Raja, N. Marathe, J. Desai, A. Dahapute, S. Shah, and A. Chavan, “Evaluation of anatomic risk factors using magnetic resonance imaging in non-contact anterior cruciate ligament injury,” *J. Clin. Orthop. Trauma*, vol. 10, no. 4, p. 710, Jul. 2019, doi: 10.1016/J.JCOT.2019.02.013.

[77] J. Grammens, A. Van Haver, F. Danckaers, B. Booth, J. Sijbers, and P. Verdonk, “Small medial femoral condyle morphotype is associated with medial compartment degeneration and distinct morphological characteristics: a comparative pilot study,” *Knee Surg. Sports Traumatol. Arthrosc.*, vol. 29, no. 6, pp. 1777–1789, Jun. 2021, doi: 10.1007/S00167-020-06218-8.

[78] V. Kızılgöz, A. K. Sivrioğlu, G. R. Ulusoy, H. Aydın, S. S. Karayol, and U. Menderes, “Analysis of the risk factors for anterior cruciate ligament injury: an investigation of structural tendencies,” *Clin. Imaging*, vol. 50, pp. 20–30, Jul. 2018, doi: 10.1016/J.CLINIMAG.2017.12.004.

[79] E. A. Audenaert, C. Pattyn, G. Steenackers, J. De Roeck, D. Vandermeulen, and P. Claes, “Statistical Shape Modeling of Skeletal Anatomy for Sex Discrimination: Their Training Size, Sexual Dimorphism, and Asymmetry,” *Front. Bioeng. Biotechnol.*, vol. 7, p. 494182, Nov. 2019, doi: 10.3389/FBIOE.2019.00302/BIBTEX.

[80] F. Liu *et al.*, “Stenotic intercondylar notch is not a risk factor for posterior cruciate ligament rupture: a morphological analyses using magnetic resonance imaging,” *Knee Surg. Sports Traumatol. Arthrosc.*, vol. 30, no. 5, pp. 1711–1717, May 2022, doi: 10.1007/S00167-021-06724-3.

[81] A. Misir, G. Sayer, E. Uzun, B. Guney, and A. Guney, “Individual and Combined Anatomic Risk Factors for the Development of an Anterior Cruciate Ligament Rupture in Men: A Multiple Factor Analysis Case-Control Study,” *Am. J. Sports Med.*, vol. 50, no. 2, pp. 433–440, Feb. 2022, doi: 10.1177/03635465211062594.

[82] O. Al-Saeed, M. Brown, R. Athyal, and M. Sheikh, “Association of femoral intercondylar notch morphology, width index and the risk of anterior cruciate ligament injury,” *Knee Surg. Sports Traumatol. Arthrosc.*, vol. 21, no. 3, pp. 678–682, Mar. 2013, doi: 10.1007/S00167-012-2038-Y.

[83] B. Basukala, A. Joshi, and I. Pradhan, “The Effect of the Intercondylar Notch Shape and Notch Width Index on Anterior Cruciate Ligament Injuries,” *J. Nepal Health Res. Counc.*, vol. 17, no. 4, pp. 532–536, Jan. 2020, doi: 10.33314/JNHRC.V17I4.1858.

[84] R. A. Simon, J. S. Everhart, H. N. Nagaraja, and A. M. Chaudhari, “A case-control study of anterior cruciate ligament volume, tibial plateau slopes and intercondylar notch dimensions in ACL-injured knees,” *J. Biomech.*, vol. 43, no. 9, pp. 1702–1707, Jun. 2010, doi: 10.1016/J.JBIOMECH.2010.02.033.

[85] T. Bouras, P. Fennema, S. Burke, and H. Bosman, “Stenotic intercondylar notch type is correlated with anterior cruciate ligament injury in female patients using magnetic resonance imaging,” *Knee Surg. Sports Traumatol. Arthrosc.*, vol. 26, no. 4, pp. 1252–1257, Apr. 2018, doi: 10.1007/S00167-017-4625-4.

[86] S. M. Fahim, T. Dhawan, N. Jagadeesh, and Y. P. Ashwathnarayan, “The relationship of anterior cruciate ligament injuries with MRI based calculation of femoral notch width, notch width index, notch shape - A randomized control study,” *J. Clin. Orthop. Trauma*, vol. 17, pp. 5–10, Jun. 2021, doi: 10.1016/J.JCOT.2021.01.006.

[87] C. A. Görmeli, G. Görmeli, Y. B. Öztürk, Z. Özdemir, and A. Kahraman, “The effect of the intercondyler notch width index on anterior cruciate ligament injuries: A study on groups with unilateral and bilateral ACL injury,” *Orthop. J. Sports Med.*, vol. 2, no. 11, Nov. 2014, doi: 10.1177/2325967114S00204.

[88] K. Hoteya *et al.*, “Association between intercondylar notch narrowing and bilateral anterior cruciate ligament injuries in athletes,” *Arch. Orthop. Trauma Surg.*, vol. 131, no. 3, pp. 371–376, Mar. 2011, doi: 10.1007/S00402-010-1254-5.

[89] L. Shen, Z. G. Jin, Q. R. Dong, and L. B. Li, “Anatomical risk factors of anterior cruciate ligament injury,” *Chin. Med. J. (Engl).*, vol. 131, no. 24, pp. 2960–2967, Dec. 2018, doi: 10.4103/0366-6999.247207/ASSET/FEE04AC2-319E-44A9-B65C-5945DB715DFF/ASSETS/GRAPHIC/0366-6999-131-24-110-F010.PNG.

[90] M. Jagodzinski, G. M. Richter, and H. H. Pässler, “Biomechanical analysis of knee hyperextension and of the impingement of the anterior cruciate ligament: a cinematographic MRI study with impact on tibial tunnel positioning in anterior cruciate ligament reconstruction,” *Knee Surg. Sports Traumatol. Arthrosc.*, vol. 8, no. 1, pp. 11–19, 2000, doi: 10.1007/S001670050004.

[91] H. M. Wang, S. J. Shultz, and R. J. Schmitz, “Association of Anterior Cruciate Ligament Width With Anterior Knee Laxity,” *J. Athl. Train.*, vol. 51, no. 6, pp. 460–465, Jun. 2016, doi: 10.4085/1062-6050-51.7.07.

[92] E. Alentorn-Geli *et al.*, “An Evaluation of the Association Between Radiographic Intercondylar Notch Narrowing and Anterior Cruciate Ligament Injury in Men: The Notch Angle Is a Better Parameter Than Notch Width,” *Arthroscopy*, vol. 31, no. 10, pp. 2004–2013, Oct. 2015, doi: 10.1016/J.ARTHRO.2015.04.088.

[93] M. S. Barnum, E. D. Boyd, P. Vacek, J. R. Slauterbeck, and B. D. Beynnon, “Association of Geometric Characteristics of Knee Anatomy (Alpha Angle and Intercondylar Notch Type) With Noncontact ACL Injury,” *Am. J. Sports Med.*, vol. 49, no. 10, pp. 2624–2630, Aug. 2021, doi: 10.1177/03635465211023750.

[94] H. Gollwitzer *et al.*, “The natural alpha angle of the femoral head-neck junction: a cross-sectional CT study in 1312 femurs,” *Bone Joint J.*, vol. 100-B, no. 5, pp. 570–578, May 2018, doi: 10.1302/0301-620X.100B5.BJJ-2017-0249.R3.

[95] O. V. Lopes *et al.*, “Assessment of the alpha angle and mobility of the hip in patients with noncontact anterior cruciate ligament injury,” *Int. Orthop.*, vol. 41, no. 8, pp. 1601–1605, Aug. 2017, doi: 10.1007/S00264-017-3482-6.

[96] M. Philippon, C. Dewing, K. Briggs, and J. R. Steadman, “Decreased femoral head–neck offset: a possible risk factor for ACL injury,” *Knee Surgery, Sports Traumatology, Arthroscopy*, vol. 20, no. 12, p. 2585, Dec. 2012, doi: 10.1007/S00167-012-1881-1.

[97] P. G. T. De Sousa Filho, A. C. Marques, L. S. Pereira, B. A. Pigozzo, and R. S. P. E Albuquerque, “Analysis of Posterior Tibial Slope as Risk Factor to Anterior Cruciate Ligament Tear,” *Rev. Bras. Ortop. (Sao. Paulo).*, vol. 56, no. 1, pp. 47–52, Feb. 2021, doi: 10.1055/S-0040-1712495.

[98] P. Di Benedetto, M. M. Buttironi, F. Mancuso, A. Beltrame, R. Gisonni, and A. Causero, “Anterior cruciate ligament reconstruction: the role of lateral posterior tibial slope as a potential risk factor for failure,” *Acta Bio Medica : Atenei Parmensis*, vol. 91, no. Suppl 14, pp. 1–9, 2020, doi: 10.23750/ABM.V91I14-S.10996.

[99] T. Kumar Panigrahi, A. Das, T. Mohanty, S. Samanta, and S. Kumar Mohapatra, “Study of relationship of posterior tibial slope in anterior cruciate ligament injury,” *J. Orthop.*, vol. 21, pp. 487–490, Sep. 2020, doi: 10.1016/J.JOR.2020.08.032.

[100] F. E. USTABAŞIOĞLU, C. Samanci, and D. ALİŞ, “Evaluation of Intercondylar Notch, Condylar Morphology and Tibial Slope on Magnetic Resonance Imaging and their Influence

on Rupture of the Anterior Cruciate Ligament," *Haydarpaşa Numune Medical Journal*, vol. 60, no. 2, pp. 116–122, 2020, doi: 10.14744/HNHJ.2018.48344.

[101] L. Hirtler, K. Tschematschar, F. Kainberger, and S. Röhrich, "Applicability of Semi-Quantitative Evaluation of the Intercondylar Notch," *Applied Sciences 2021, Vol. 11, Page 5921*, vol. 11, no. 13, p. 5921, Jun. 2021, doi: 10.3390/APP11135921.

[102] G. Ghosh, "Effects of posterior tibial slopes on noncontact anterior cruciate ligament injury," *Saudi Journal of Sports Medicine*, vol. 15, no. 3, p. 214, 2015, doi: 10.4103/1319-6308.164275.

[103] Q. Zhao, D. Jin, and H. Yuan, "Correlation between glenoid bone structure and recurrent anterior dislocation of the shoulder joint," *Folia Morphol. (Warsz).*, vol. 82, no. 3, pp. 712–720, 2023, doi: 10.5603/FM.A2022.0067.

[104] M. R. Cohn *et al.*, "Does native glenoid anatomy predispose to shoulder instability? An MRI analysis," *J. Shoulder Elbow Surg.*, vol. 31, no. 6S, pp. S110–S116, Jun. 2022, doi: 10.1016/J.JSE.2022.03.002.

[105] N. W. Willigenburg, R. A. Bouma, V. A. B. Scholtes, V. P. M. van der Hulst, D. F. P. van Deurzen, and M. P. J. van den Bekerom, "Does the innate relative size of the humeral head and glenoid affect the risk of anterior shoulder instability?," *Shoulder Elbow*, vol. 11, no. 6, pp. 424–429, Dec. 2019, doi: 10.1177/1758573218805099.

[106] J. Hong *et al.*, "Risk factors for anterior shoulder instability: a matched case-control study," *J. Shoulder Elbow Surg.*, vol. 28, no. 5, pp. 869–874, May 2019, doi: 10.1016/J.JSE.2018.09.014.

[107] C. D. Peltz, R. Zauel, N. Ramo, N. Mehran, V. Moutzouros, and M. J. Bey, "Differences in glenohumeral joint morphology between patients with anterior shoulder instability and healthy, uninjured volunteers," *J. Shoulder Elbow Surg.*, vol. 24, no. 7, pp. 1014–1020, Jul. 2015, doi: 10.1016/J.JSE.2015.03.024.

[108] M. Jacxsens, S. Y. Elhabian, S. E. Brady, P. N. Chalmers, R. Z. Tashjian, and H. B. Henninger, "Coracoacromial Morphology: A Contributor to Recurrent Traumatic Anterior Glenohumeral Instability?," *J. Shoulder Elbow Surg.*, vol. 28, no. 7, p. 1316, Jul. 2019, doi: 10.1016/J.JSE.2019.01.009.

[109] Ü. Aygün, Y. Çalik, C. Işik, H. Şahin, R. Şahin, and D. Ö. Aygün, "The importance of glenoid version in patients with anterior dislocation of the shoulder," *J. Shoulder Elbow Surg.*, vol. 25, no. 12, pp. 1930–1936, Dec. 2016, doi: 10.1016/J.JSE.2016.09.018.

[110] E. Hohmann and K. Tetsworth, “Glenoid version and inclination are risk factors for anterior shoulder dislocation,” *J. Shoulder Elbow Surg.*, vol. 24, no. 8, pp. 1268–1273, Aug. 2015, doi: 10.1016/J.JSE.2015.03.032.

[111] B. Saygi, N. Karahan, O. Karakus, A. I. Demir, O. C. Ozkan, and F. N. Soylu-Boy, “Analysis of glenohumeral morphological factors for anterior shoulder instability and rotator cuff tear by magnetic resonance imaging,” *J. Orthop. Surg. (Hong Kong)*, vol. 26, no. 2, May 2018, doi: 10.1177/2309499018768100.

[112] N. Paopongthong, P. Atthakomol, and C. Phornphutkul, “The relationship of glenoid version and severity of glenoid bone loss in anterior shoulder instability patients: A retrospective cohort study,” *Asia. Pac. J. Sports Med. Arthrosc. Rehabil. Technol.*, vol. 28, pp. 25–30, Apr. 2022, doi: 10.1016/J.ASMART.2022.03.001.

[113] J. Rayes, J. Xu, S. Sparavalo, J. Ma, L. Jonah, and I. Wong, “Calculating glenoid bone loss based on glenoid height using ipsilateral three-dimensional computed tomography,” *Knee Surg. Sports Traumatol. Arthrosc.*, vol. 31, no. 1, pp. 169–176, Jan. 2023, doi: 10.1007/S00167-022-07020-4.

[114] M. Haas *et al.*, “Glenoid morphology is associated with the development of instability arthropathy,” *J. Shoulder Elbow Surg.*, vol. 28, no. 5, pp. 893–899, May 2019, doi: 10.1016/J.JSE.2018.09.010.

[115] H. Graichen, J. Jakob, R. von Eisenhart-Rothe, K. H. Englmeier, M. Reiser, and F. Eckstein, “Validation of cartilage volume and thickness measurements in the human shoulder with quantitative magnetic resonance imaging,” *Osteoarthritis Cartilage*, vol. 11, no. 7, pp. 475–482, Jul. 2003, doi: 10.1016/S1063-4584(03)00077-3.

[116] U. M, Q. I, and A. M, “Subacromial impingement syndrome,” *Orthop. Rev. (Pavia).*, vol. 4, no. 2, May 2012, doi: 10.4081/OR.2012.E18.

[117] F. de Oliveira França, A. C. Godinho, E. J. S. Ribeiro, L. Falster, L. E. G. Búrigo, and R. B. Nunes, “Evaluation of the acromiohumeral distance by means of magnetic resonance imaging umerus,” *Rev. Bras. Ortop. (Sao. Paulo).*, vol. 51, no. 2, pp. 169–174, Mar. 2016, doi: 10.1016/J.RBOE.2016.01.008.

[118] D. Goutallier, P. Le Guilloux, J. M. Postel, C. Radier, J. Bernageau, and S. Zilber, “Acromio humeral distance less than six millimeter: Its meaning in full-thickness rotator cuff tear,” *Orthopaedics & Traumatology: Surgery & Research*, vol. 97, no. 3, pp. 246–251, May 2011, doi: 10.1016/J.OTSR.2011.01.010.

[119] L. U. Bigliani, J. B. Ticker, E. L. Flatow, L. J. Soslowsky, and V. C. Mow, “The relationship of acromial architecture to rotator cuff disease.,” *Clin. Sports Med.*, vol. 10, no. 4, pp. 823–838, Oct. 1991, doi: 10.1016/s0278-5919(20)30586-x.

[120] A. McLean and F. Taylor, “Classifications in Brief: Bigliani Classification of Acromial Morphology,” *Clin. Orthop. Relat. Res.*, vol. 477, no. 8, pp. 1958–1961, Aug. 2019, doi: 10.1097/CORR.0000000000000770.

[121] R. W. Nyffeler and D. C. Meyer, “Acromion and glenoid shape: Why are they important predictive factors for the future of our shoulders?,” *EFORT Open Rev.*, vol. 2, no. 5, p. 141, May 2017, doi: 10.1302/2058-5241.2.160076.

[122] R. W. Nyffeler, C. M. L. Werner, A. Sukthankar, M. R. Schmid, and C. Gerber, “Association of a large lateral extension of the acromion with rotator cuff tears,” *Journal of Bone and Joint Surgery*, vol. 88, no. 4, pp. 800–805, 2006, doi: 10.2106/JBJS.D.03042.

[123] M. P. Banas, R. J. Miller, and S. Totterman, “Relationship between the lateral acromion angle and rotator cuff disease,” *J. Shoulder Elbow Surg.*, vol. 4, no. 6, pp. 454–461, 1995, doi: 10.1016/S1058-2746(05)80038-2.

[124] A. Sharifi, M. J. Siebert, and A. Chhabra, “How to Measure Glenoid Bone Stock and Version and Why It Is Important: A Practical Guide,” *Radiographics*, vol. 40, no. 6, pp. 1671–1683, Oct. 2020, doi: 10.1148/RG.2020200008.

[125] P. N. Chalmers, L. Beck, E. Granger, H. Henninger, and R. Z. Tashjian, “Superior glenoid inclination and rotator cuff tears,” *J. Shoulder Elbow Surg.*, vol. 27, no. 8, pp. 1444–1450, Aug. 2018, doi: 10.1016/J.JSE.2018.02.043.

[126] P. Hattam, A. Smeatham, and L. Funk, “Handbook of special tests in musculoskeletal examination : An evidence-based guide for clinicians,” p. 324.

[127] L. C. V. Ferreira, A. G. Rabelo, M. F. Vieira, A. A. Pereira, and A. de O. Andrade, “Gait variability and symmetry assessment with inertial sensors for quantitative discrimination of Trendelenburg sign in total hip arthroplasty patients: a pilot study based on convenience sampling,” *Research on Biomedical Engineering*, vol. 34, no. 1, pp. 65–72, Mar. 2018, doi: 10.1590/2446-4740.07017.

[128] R. Zügner, R. Tranberg, V. Lisovskaja, and J. Kärrholm, “Different reliability of instrumented gait analysis between patients with unilateral hip osteoarthritis, unilateral hip prosthesis and healthy controls,” *BMC Musculoskelet. Disord.*, vol. 19, no. 1, Jul. 2018, doi: 10.1186/S12891-018-2145-0.

[129] B. Westhoff, A. Petermann, M. A. Hirsch, R. Willers, and R. Krauspe, “Computerized gait analysis in Legg Calvé Perthes disease--analysis of the frontal plane,” *Gait Posture*, vol. 24, no. 2, pp. 196–202, Oct. 2006, doi: 10.1016/J.GAITPOST.2005.08.008.

[130] Y. Zhang, X. Zhou, M. Pijnappels, and S. M. Bruijn, “Differences in Gait Stability and Acceleration Characteristics Between Healthy Young and Older Females,” *Frontiers in Rehabilitation Sciences*, vol. 2, p. 763309, Nov. 2021, doi: 10.3389/FRESC.2021.763309/BIBTEX.

[131] A. Ghidotti, M. Penzo, D. Landi, D. Regazzoni, and C. Rizzi, “The Effect of Meniscal Tears on Knee Biomechanics: a Finite Element Analysis Investigation,” *Volume 1: Acoustics, Vibration, and Phononics; Advanced Design and Information Technologies*, Nov. 2024, doi: 10.1115/IMECE2024-145299.

[132] V. Wadhwa, H. Omar, K. Coyner, M. Khazzam, W. Robertson, and A. Chhabra, “ISAKOS classification of meniscal tears-illustration on 2D and 3D isotropic spin echo MR imaging,” *Eur. J. Radiol.*, vol. 85, no. 1, pp. 15–24, Jan. 2016, doi: 10.1016/J.EJRAD.2015.10.022.

[133] S. D. Masouros, I. D. McDermott, A. A. Amis, and A. M. J. Bull, “Biomechanics of the meniscus-meniscal ligament construct of the knee,” *Knee Surg. Sports Traumatol. Arthrosc.*, vol. 16, no. 12, pp. 1121–1132, Dec. 2008, doi: 10.1007/S00167-008-0616-9.

[134] K. Zhang *et al.*, “The biomechanical changes of load distribution with longitudinal tears of meniscal horns on knee joint: A finite element analysis,” *J. Orthop. Surg. Res.*, vol. 14, no. 1, pp. 1–12, Jul. 2019, doi: 10.1186/S13018-019-1255-1/FIGURES/8.

[135] N. Özkaya, M. Nordin, D. Goldsheyder, and D. Leger, “Fundamentals of biomechanics: Equilibrium, motion, and deformation: Third edition,” *Fundamentals of Biomechanics: Equilibrium, Motion, and Deformation: Third Edition*, pp. 1–275, Jan. 2012, doi: 10.1007/978-1-4614-1150-5/COVER.

[136] E. S. Mameri *et al.*, “Review of Meniscus Anatomy and Biomechanics,” *Curr. Rev. Musculoskelet. Med.*, vol. 15, no. 5, pp. 323–335, Oct. 2022, doi: 10.1007/S12178-022-09768-1.

[137] H. R. C. Bao, D. Zhu, H. Gong, and G. S. Gu, “The effect of complete radial lateral meniscus posterior root tear on the knee contact mechanics: a finite element analysis,” *J. Orthop. Sci.*, vol. 18, no. 2, pp. 256–263, 2013, doi: 10.1007/S00776-012-0334-5.

[138] Y. Dong, G. Hu, Y. Dong, Y. Hu, and Q. Xu, “The effect of meniscal tears and resultant partial meniscectomies on the knee contact stresses: a finite element analysis,” *Comput. Methods*

Biomech. Biomed. Engin., vol. 17, no. 13, pp. 1452–1463, 2014, doi: 10.1080/10255842.2012.753063.

[139] S. Wang, K. Hase, S. Kita, and S. Ogaya, “Biomechanical effects of medial meniscus radial tears on the knee joint during gait: A concurrent finite element musculoskeletal framework investigation,” *Front. Bioeng. Biotechnol.*, vol. 10, Oct. 2022, doi: 10.3389/FBIOE.2022.957435.

[140] L. Li *et al.*, “Biomechanical analysis of the effect of medial meniscus degenerative and traumatic lesions on the knee joint,” *Am. J. Transl. Res.*, vol. 11, no. 2, p. 542, 2019, Accessed: Jun. 27, 2023. [Online]. Available: /pmc/articles/PMC6413253/

[141] S. M. Gajjar, K. P. Solanki, S. Shanmugasundaram, and S. B. S. Kambhampati, “Meniscal Extrusion: A Narrative Review,” *Orthop. J. Sports Med.*, vol. 9, no. 11, 2021, doi: 10.1177/23259671211043797.

[142] J. A. Lee, Y. G. Koh, and K. T. Kang, “Biomechanical and Clinical Effect of Patient-Specific or Customized Knee Implants: A Review,” *Journal of Clinical Medicine 2020, Vol. 9, Page 1559*, vol. 9, no. 5, p. 1559, May 2020, doi: 10.3390/JCM9051559.

[143] E. Sappey-Marinier, C. Tibesku, T. A. S. Selmi, and M. Bonnin, “Custom Total Knee Arthroplasty,” *Personalized Hip and Knee Joint Replacement*, pp. 255–264, Jan. 2020, doi: 10.1007/978-3-030-24243-5_22.

[144] N. O. Sarpong, D. Chen, and H. J. Cooper, “Custom/Patient-Specific Total Knee Arthroplasty,” *Essentials of Cemented Knee Arthroplasty*, pp. 377–384, Jan. 2022, doi: 10.1007/978-3-662-63113-3_33.

[145] C. W. Ha and S. E. Na, “The correctness of fit of current total knee prostheses compared with intra-operative anthropometric measurements in Korean knees,” *J. Bone Joint Surg. Br.*, vol. 94, no. 5, pp. 638–641, May 2012, doi: 10.1302/0301-620X.94B5.28824.

[146] M. Meier, S. Zingde, A. Steinert, W. Kurtz, F. Koeck, and J. Beckmann, “What Is the Possible Impact of High Variability of Distal Femoral Geometry on TKA? A CT Data Analysis of 24,042 Knees,” *Clin. Orthop. Relat. Res.*, vol. 477, no. 3, p. 561, Mar. 2019, doi: 10.1097/CORR.0000000000000611.

[147] V. Neginhal, W. Kurtz, and L. Schroeder, “Patient Satisfaction, Functional Outcomes, and Survivorship in Patients with a Customized Posterior-Stabilized Total Knee Replacement,” *JBJS Rev.*, vol. 8, no. 7, 2020, doi: 10.2106/JBJS.RVW.19.00104.

[148] A. T. Namin *et al.*, “Adoption of New Medical Technologies: The Case of Customized Individually Made Knee Implants,” *Value in Health*, vol. 22, no. 4, pp. 423–430, Apr. 2019, doi: 10.1016/J.JVAL.2019.01.008.

[149] Y. G. Koh, J. A. Lee, P. K. Chung, and K. T. Kang, “Computational analysis of customized cruciate retaining total knee arthroplasty restoration of native knee joint biomechanics,” *Artif. Organs*, vol. 43, no. 5, pp. 504–514, May 2019, doi: 10.1111/AOR.13382.

[150] I. M. Zeller, A. Sharma, W. B. Kurtz, M. R. Anderle, and R. D. Komistek, “Customized versus Patient-Sized Cruciate-Retaining Total Knee Arthroplasty: An In Vivo Kinematics Study Using Mobile Fluoroscopy,” *J. Arthroplasty*, vol. 32, no. 4, pp. 1344–1350, Apr. 2017, doi: 10.1016/J.ARTH.2016.09.034.

[151] I. H. Korkmaz, I. Kaymaz, Ö. S. Ylldlrlm, F. Murat, and H. Kovacl, “Designing and in vitro testing of a novel patient-specific total knee prosthesis using the probabilistic approach,” *Biomedizinische Technik*, vol. 67, no. 4, pp. 295–305, Aug. 2022, doi: 10.1515/BMT-2021-0136/ASSET/GRAPHIC/J_BMT-2021-0136_FIG_008.JPG.

[152] Y. Jun, “Morphological analysis of the human knee joint for creating custom-made implant models”, doi: 10.1007/s00170-010-2785-1.

[153] A. R. Balwan and V. D. Shinde, “Development of patient specific knee joint implant,” *Mater. Today Proc.*, vol. 27, pp. 288–293, Jan. 2020, doi: 10.1016/J.MATPR.2019.11.032.

[154] M. S. Utomo, M. I. Amal, S. Supriadi, D. Malau, D. Annur, and A. W. Pramono, “Design of modular femoral implant based on anthropometry of eastern asian,” *AIP Conf. Proc.*, vol. 2088, no. 1, p. 20033, Mar. 2019, doi: 10.1063/1.5095285/798359.

[155] Z. Mou *et al.*, “Optimization of parameters for femoral component implantation during TKA using finite element analysis and orthogonal array testing,” *J. Orthop. Surg. Res.*, vol. 13, no. 1, pp. 1–12, Jul. 2018, doi: 10.1186/S13018-018-0891-1/FIGURES/7.

[156] P. Moewis, S. Checa, I. Kutzner, H. Hommel, and G. N. Duda, “Physiological joint line total knee arthroplasty designs are especially sensitive to rotational placement – A finite element analysis,” *PLoS One*, vol. 13, no. 2, p. e0192225, Feb. 2018, doi: 10.1371/JOURNAL.PONE.0192225.

[157] A. J. Nedopil, S. M. Howell, and M. L. Hull, “Kinematically Aligned Total Knee Arthroplasty Using Calipered Measurements, Manual Instruments, and Verification Checks,” *Personalized Hip and Knee Joint Replacement*, pp. 279–300, Jan. 2020, doi: 10.1007/978-3-030-24243-5_24.

[158] J. H. Yeo, J. K. Seon, D. H. Lee, and E. K. Song, "No difference in outcomes and gait analysis between mechanical and kinematic knee alignment methods using robotic total knee arthroplasty," *Knee Surg. Sports Traumatol. Arthrosc.*, vol. 27, no. 4, pp. 1142–1147, Apr. 2019, doi: 10.1007/S00167-018-5133-X.

[159] A. Lübbeke *et al.*, "A randomised controlled trial of kinematically and mechanically aligned total knee replacements: two-year clinical results," *Bone Joint J.*, vol. 96-B, no. 7, pp. 868–875, 2014, doi: 10.1302/0301-620X.96B7.32812.

[160] W. Blakeney, J. Clément, F. Desmeules, N. Hagemeister, C. Rivière, and P. A. Vendittoli, "Kinematic alignment in total knee arthroplasty better reproduces normal gait than mechanical alignment," *Knee Surg. Sports Traumatol. Arthrosc.*, vol. 27, no. 5, pp. 1410–1417, May 2019, doi: 10.1007/S00167-018-5174-1.

[161] C. L. Brockett, S. Carbone, J. Fisher, and L. M. Jennings, "PEEK and CFR-PEEK as alternative bearing materials to UHMWPE in a fixed bearing total knee replacement: An experimental wear study," *Wear*, vol. 374–375, pp. 86–91, Mar. 2017, doi: 10.1016/J.WEAR.2016.12.010.

[162] K. T. Kang, J. Son, S. K. Kwon, O. R. Kwon, J. H. Park, and Y. G. Koh, "Finite element analysis for the biomechanical effect of tibial insert materials in total knee arthroplasty," *Compos. Struct.*, vol. 201, pp. 141–150, Oct. 2018, doi: 10.1016/J.COMPSTRUCT.2018.06.036.

[163] Y. G. Koh, J. A. Lee, and K. T. Kang, "Prediction of Wear on Tibial Inserts Made of UHMWPE, PEEK, and CFR-PEEK in Total Knee Arthroplasty Using Finite-Element Analysis," *Lubricants 2019, Vol. 7, Page 30*, vol. 7, no. 4, p. 30, Apr. 2019, doi: 10.3390/LUBRICANTS7040030.

[164] G. R. Galakatos, "Direct Anterior Total Hip Arthroplasty," *Mo. Med.*, vol. 115, no. 6, p. 537, Nov. 2018, doi: 10.2106/jbjs.st.k.00015.

[165] S. Petis, J. Howard, B. Lanting, I. Jones, T. Birmingham, and E. Vasarhelyi, "Comparing the anterior, posterior and lateral approach: gait analysis in total hip arthroplasty," *Can. J. Surg.*, vol. 61, no. 1, pp. 50–57, 2018, doi: 10.1503/CJS.003217.

[166] T. Ilchmann, "Approaches for primary total hip replacement," *HIP International*, vol. 24, pp. S2–S6, Jul. 2014, doi: 10.5301/HIPINT.5000163/ASSET/IMAGES/LARGE/10.5301_HIPINT.5000163-FIG1.JPEG.

[167] R. M. Meneghini, S. A. Smits, R. R. Swinford, and R. E. Bahamonde, "A Randomized, Prospective Study of 3 Minimally Invasive Surgical Approaches in Total Hip Arthroplasty:

Comprehensive Gait Analysis," *J. Arthroplasty*, vol. 23, no. 6, pp. 68–73, Sep. 2008, doi: 10.1016/J.ARTH.2008.05.014.

[168] U. S. Sibia, T. R. Turner, J. H. MacDonald, and P. J. King, "The Impact of Surgical Technique on Patient Reported Outcome Measures and Early Complications After Total Hip Arthroplasty," *J. Arthroplasty*, vol. 32, no. 4, pp. 1171–1175, Apr. 2017, doi: 10.1016/J.ARTH.2016.10.031.

[169] G. Mantovani, M. Lamontagne, D. Varin, G. G. Cerulli, and P. E. Beaulé, "Comparison of total hip arthroplasty surgical approaches by Principal Component Analysis," *J. Biomech.*, vol. 45, no. 12, pp. 2109–2115, Aug. 2012, doi: 10.1016/J.JBIOMECH.2012.05.041.

[170] S. Lyman, Y. Y. Lee, P. D. Franklin, W. Li, D. J. Mayman, and D. E. Padgett, "Validation of the HOOS, JR: A Short-form Hip Replacement Survey," *Clin. Orthop. Relat. Res.*, vol. 474, no. 6, pp. 1472–1482, Jun. 2016, doi: 10.1007/S11999-016-4718-2.

[171] R. R. Martin and A. Disantis, "Editorial Commentary: Patient-Reported Outcome Measures With Established Clinically Important Outcome Values Should Be Used for Hip Arthroscopy Patients: Sifting Through the White Noise," *Arthroscopy*, vol. 37, no. 10, pp. 3122–3124, Oct. 2021, doi: 10.1016/J.ARTHRO.2021.05.036.

[172] M. Gavrilović and D. B. Popović, "A principal component analysis (PCA) based assessment of the gait performance," *Biomed. Tech. (Berl).*, vol. 66, no. 5, pp. 449–457, Oct. 2021, doi: 10.1515/BMT-2020-0307.

[173] R. J. Boekesteijn, J. M. H. Smolders, V. J. J. F. Busch, A. C. H. Geurts, and K. Smulders, "Independent and sensitive gait parameters for objective evaluation in knee and hip osteoarthritis using wearable sensors," *BMC Musculoskelet. Disord.*, vol. 22, no. 1, Dec. 2021, doi: 10.1186/S12891-021-04074-2.

[174] R. Moyer *et al.*, "Postoperative Gait Mechanics After Total Hip Arthroplasty: A Systematic Review and Meta-Analysis," *JBJS Rev.*, vol. 6, no. 11, p. E1, Nov. 2018, doi: 10.2106/JBJS.RVW.17.00133.

[175] A. Bertaux *et al.*, "Gait analysis dataset of healthy volunteers and patients before and 6 months after total hip arthroplasty," *Sci. Data*, vol. 9, no. 1, Dec. 2022, doi: 10.1038/S41597-022-01483-3.

[176] W. S. Kim, H. Choi, J. W. Jung, J. S. Yoon, and J. H. Jeoung, "Asymmetry and Variability Should Be Included in the Assessment of Gait Function in Poststroke Hemiplegia With Independent Ambulation During Early Rehabilitation," *Arch. Phys. Med. Rehabil.*, vol. 102, no. 4, pp. 611–618, Apr. 2021, doi: 10.1016/J.APMR.2020.10.115.

[177] R. M. Queen, R. J. Butler, T. S. Watters, S. S. Kelley, D. E. Attarian, and M. P. Bolognesi, "The effect of total hip arthroplasty surgical approach on postoperative gait mechanics," *J. Arthroplasty*, vol. 26, no. 6 Suppl, pp. 66–71, 2011, doi: 10.1016/J.ARTH.2011.04.033.

[178] J. S. Bahl, M. J. Nelson, M. Taylor, L. B. Solomon, J. B. Arnold, and D. Thewlis, "Biomechanical changes and recovery of gait function after total hip arthroplasty for osteoarthritis: a systematic review and meta-analysis," *Osteoarthritis Cartilage*, vol. 26, no. 7, pp. 847–863, Jul. 2018, doi: 10.1016/J.JOCA.2018.02.897.

[179] L. Mendiolagoitia, M. Á. Rodríguez, I. Crespo, M. del Valle, and H. Olmedillas, "Kinematic Gait Analysis After Primary Total Hip Replacement: A Systematic Review: Gait After Total Hip Replacement: A Systematic Review," *Indian J. Orthop.*, vol. 54, no. 6, pp. 767–775, Nov. 2020, doi: 10.1007/S43465-020-00101-X.

[180] A. Gouelle, F. Mégrot, A. Gouelle, and F. Mégrot, "Interpreting Spatiotemporal Parameters, Symmetry, and Variability in Clinical Gait Analysis," *Handbook of Human Motion*, pp. 1–20, 2016, doi: 10.1007/978-3-319-30808-1_35-1.